Alma Mater Studiorum · Università di Bologna

Scuola di Scienze
Corso di Laurea Magistrale in Fisica del Sistema Terra

Development of a relationship between physical parameters of tsunami waves and tsunami intensity based on macroscopic effects and its application to the Italian tsunami database

Relatore:
Prof. Jacopo Selva

Correlatore:
Dott.ssa Laura Graziani

Presentata da:
Giovanni Zanaboni

Sessione IV
Anno Accademico 2021/2022

Abstract

The frequency of occurrence of tsunamis is lower than that of other natural disasters, which is why they are considered rare events. However, it must be considered that their impact can be devastating and it may extend to large geographical areas. Consequently, for low-probability high-impact events like tsunamis, it is crucial to implement all possible actions to mitigate the risk.

The tsunami hazard assessment is the result of a scientific process that integrates traditional geological methods, the analysis of the instrumental and the historical record, the statistical analysis of the tsunami sources and numerical modelling. For this reason, precise analyses of near past events and understanding how historical tsunamis interacted with the land, to the best of capabilities, is the only way to inform tsunami source and propagation models, as well as forecast models like hazard analyses and to quantitatively test such models againsts data.

The primary objective of this thesis is to establish an explicit relationship between the macroscopic intensity, derived from the description of historical tsunamis, and the quantitative measure of the size of a tsunami, expressed through physical parameters that describe the tsunami waves and inundations. This is done first by defining an approximate estimation method based on the estimate of the local effects and a simplified 1D physical onshore propagation model to convert the available observation assessments into one predefined reference physical metrics. Among the physical parameters, wave height at the coast was chosen as the reference due to its stability and independence of inland effects. This method was then implemented for a set of well-known past events to build a homogeneous dataset with both the macroscopic intensity and the reference physical measure of tsunami explicitly estimated. This dataset is finally analysed to establish a statistical relationship between macroscopic intensity and wave height. The resulting empirical regression is obtained by performing an orthogonal regression, allowing to establish a direct and invertible relationship between the two parameters, accounting for their relevant uncertainties.

The target relationship is extensively tested and finally applied to all data contained in the Italian Tsunami Effect Database (ITED), providing a homogeneous estimation of the wave height for all existing tsunami observations in Italy. This can provide meaningful comparative data for models and simulations, as well as the opportunity for quantitatively testing tsunami hazard models for the Italian coasts and informing tsunami risk management initiatives.

Sommario

La frequenza di accadimento degli tsunami è più bassa rispetto a quella di altre calamità naturali, per questo sono considerati eventi rari. Tuttavia, bisogna considerare che il loro impatto può essere devastante e può estendersi a vaste aree geografiche. Di conseguenza, per eventi a bassa probabilità ed alto impatto come gli tsunami, è fondamentale mettere in atto tutte le azioni possibili per mitigare il rischio.

La valutazione del rischio di tsunami è il risultato di un processo scientifico che integra i metodi geologici tradizionali, l'analisi delle misure strumentali e della documentazione storica, l'analisi statistica delle sorgenti di tsunami e la modellazione numerica. Per questo motivo, l'analisi dettagliata degli eventi del passato recente e la comprensione, per quanto possibile, di come gli tsunami storici hanno interagito con il territorio è l'unico modo per informare i modelli di sorgente e di propagazione degli tsunami, così come i modelli di forecast come gli studi di pericolosità. Questi dati sono fondamentali per definire test statistici per verificare quantitativamente la consistenza di tali modelli coi dati, verificandone l'accuratezza.

L'obiettivo primario di questa tesi è stabilire una relazione esplicita tra la valutazione degli tsunami storici fatta attraverso le intensità macroscopiche e la grandezza in termini quantitativi di uno tsunami, espressa attraverso i parametri fisici che descrivono le onde e l'inondazione dello tsunami. Al fine di ottenere questa relazione, è stato innanzitutto definito un semplice metodo basato sulla stima degli effetti locali ed un modello 1D semplificato per la propagazione sulla costa, per convertire la stima delle osservazioni esistenti in un'unica misura di riferimento. Tra i parametri fisici, è stata scelta l'altezza d'onda lungo la linea di costa come riferimento poiché risulta stabile ed è indipendente dagli effetti topografici dell'entroterra. Attraverso l'applicazione di questo modello ad una selezione di eventi passati, è stato prodotto un dataset omogeneo contenente sia la valutazione delle intensità macroscopiche, sia l'altezza stimata dell'onda sulla costa. Infine, questo dataset è stato analizzato statisticamente per stabilire una correlazione tra l'altezza d'onda e l'intensità macroscopica al sito. Questa relazione empirica, che fornisce le stime quantitative, è ottenuta eseguendo una regressione ortogonale che permette di stabilire una relazione diretta e invertibile tra i parametri, tenendo conto delle significative incertezze presenti nella loro stima.

La relazione target ottenuta è stata prima testata, per verificarne la robustezza. Infine, è stata applicata a tutti i dati esistenti nel database italiano

degli effetti di tsunami (ITED), fornendo una stima omogenea dell'altezza d'onda per tutte le osservazioni di tsunami esistenti lungo le coste dell'Italia. In questo modo è possibile ottenere dati comparativi significativi per modelli e simulazioni, oltre che fornire informazioni utili per la pianificazione di azioni di mitigazioni del rischio tsunami e per la verifica della pericolosità da tsunami, permettendo la realizzazione di test statistici quantitativi per verificarne l'accuratezza.

Contents

Introduction **1**

1 Tsunamis and their impact on coastal environments **3**

1.1 Generation and propagation *3*

1.2 Impact on coasts and physical parameters *9*

1.3 Tsunami intensity scales *13*

1.4 Relations between physical parameters and intensity in seismology *19*

2 Existing datasets for the impact of historical tsunamis **22**

3 Dataset preparation **29**

3.1 Criteria for transects creation *35*

3.2 Events selection *37*

3.2.1 The 1908 Messina and Reggio Calabria tsunami 38

3.2.2 The 2002 Stromboli tsunami 43

3.2.3 The 2020 Aegean Sea tsunami 45

3.3 Results *46*

4 Developing and testing a relationship between wave height and macroscopic tsunami intensity **53**

4.1 Regression analysis and relative uncertainties – Orthogonal Distance Regression *53*

4.2 Stability of the regression to alternative variance ratios *65*

5 Application to the Italian dataset **67**

6 Conclusions **76**

Bibliography **81**

Appendix A **90**

Appendix B **98**

Introduction

Over the past two decades, global awareness of tsunamis and research efforts on them have increased significantly, due to the consequences of two of the biggest earthquakes ever recorded: the 2004 Indian Ocean earthquake and the 2011 Tōhoku earthquake generated two enormous tsunamis that affected the Indian and the Pacific Oceans, respectively.

Tsunamis are events rarer than earthquakes and for this reason the databases for storing information and measurements are much smaller. Detailed knowledge of their impact on the coast is limited to a few events, unevenly distributed over time. Since 2000 BC, the Global Historical Tsunami Database (NCEI/WDS) reports 2797 events. Unfortunately, only about 35% have the highest reliability value (4, Tsunami Defined) and about half of these are concentrated since the 1960s and constitute the majority of recorded events. The small number of available observations is the reason for the high uncertainty in the description of the source (Behrens & Dias, 2015).

To extend over time and enrich databases of observations, tsunami catalogues have been developed collecting information on the effects produced by historical tsunamis and estimates their impact (Papadopoulos et al., 2014 and reference therein). In the Mediterranean, the main catalogues of this type are the Euro-Mediterranean tsunami catalogue (EMTC) and the database of the effects that tsunamis have had on Italian coasts (ITED) (Maramai et al., 2019a, 2019b). Such catalogues mainly collect description of the events, summarising such information with macroscopic tsunami intensity scales (Sieberg 1927; Ambraseys, 1962; Soloviev et al., 2000; Papadopoulos & Imamura, 2001; Papadopoulos et al., 2007; Maramai et al. 2019a, 2019b; Baptista and Miranda, 2009; Papadopoulos et al., 2020a, 2020b).

A relationship between tsunami parameters and tsunami intensity does not exist, and its development is the main goal of this thesis. The application of this relationship will allow significantly extending the existing database for the Euro-Mediterranean coasts, associating each estimated macroscopic intensity to a physical parameter describing tsunami waves. A similar process has been developed for macroseismic intensity data (Faccioli & Cauzzi, 2006; Gomez-Capera et al., 2007; Faenza & Michelini, 2010; Gomez-Capera et al., 2020),

allowing, for example, for a quantitative test of the most recent national hazard model (Meletti et al., 2021; Visini et al., 2021). Similarly, this relationship for tsunamis will allow the evaluation of the most recent tsunami hazard model applicable to the Italian coasts (NEAMTHM18, Basili et al., 2021), presently adopted by the Italian legislation to define evacuation areas (DPC 2018; Tonini et al., 2021; Selva et al., 2021).

In the followings, Chapter 1 introduces the physical phenomenon of tsunamis, briefly describing their generation and propagation modelling, and the impact they can have on the coast, both illustrating the main quantitative and qualitative methods to describe impact. Chapter 2 describes the main existing databases, focusing on the ones available for Italy. Chapter 3 describes, tests and applies to a set of past events a simple method to relate to each other the different physical parameters describing tsunami waves, producing an extended homogeneous dataset containing both tsunami intensity and wave height. Chapter 4 describes the development and the testing of the empirical regression that relates wave height to tsunami intensity, also considering the errors that are present on both variables. In Chapter 5, this relationship is applied to the entire database referring to the Italian coasts (ITED), in order to obtain an estimate of the wave heights that have characterised the historical events.

1 Tsunamis and their impact on coastal environments

The translation of the Japanese word 'tsunami' is 'wave in harbour', so it is the description of the arrival of abnormal waves into human settlements. The study of these natural threats is extremely complex, and it includes both the analytical aspect and the phenomenological impact. Macroscopically, tsunami science can be divided into the analysis of three phases of the phenomenon evolution: generation, propagation and impact of the waves on the coasts.

Tsunamis are generated by an external forcing that perturbs the initial equilibrium of fluids. For most fluids, gravity is the main restoring force for hydrostatic equilibrium after an external forcing. Tsunamis are gravity waves, distinguished by extremely long periods and wavelengths up to tens of kilometres (Lay & Wallace, 1995). Many natural and non-natural sources may generate the initial perturbation, including earthquakes, landslides, volcanoes, and many others.

The occurrence of tsunamis is simulated by modelling the source and the propagation up to inundation. This is made through models of the sources described by a long list of parameters, and models of the generation and propagation of the tsunami, through the bathymetry of the portion of ocean in which tsunami waves propagate, the bathymetry near the shoreline and the topography of the land where the tsunami inundates.

The distribution of tsunami around the globe is dominated by the Pacific Ocean, with a large number of events generated by the Pacific Ring of Fire, the plate boundaries that surround the Pacific Ocean.This system of sources generate up to 70% of the events in the Pacific Ocean. The remaining percentages are distributed roughly similarly between the Mediterranean (15%), Caribbean Sea and Atlantic Oceans (9%) and Indian Ocean (6%) (NCEI/WDS, IOC-UNESCO, 2019).

1.1 Generation and propagation

Tsunamis are a disturbance of the surface of a water body generated by impulsive sources. In nature, they are often caused by earthquakes, but may be

generated also by landslides, volcanic eruptions, atmospheric disturbances and even meteorite impacts (Figure 1.2). They are commonly called seismic sea waves because most of them are a consequence of earthquakes, especially along the subduction zones: around 70-81% of them were a consequence of great shallow earthquakes (Levin & Nosov, 2016; NCEI/WDS; IOC-UNESCO, 2019). This uncertainty on the percentage arises because not all historical events do have an identified origin and some events presented a combined generation mechanism.

Considering a seismic dislocation as an impulsive source, the initial tsunami displacement is assumed to be triggered by a coseismic ocean bottom deformation, which is transmitted to the sea surface. The displacement is usually considered vertical (Figure 1.1), thus mainly generated by dip-slip (thrust or normal) earthquakes like the ones occurring on the subduction interface, but tsunami generation can exceptionally occur by horizontal displacement of the ocean bottom, like in strike-slip faulting, as analysed by Tanioka & Satake (1996) and Elbanna et al. (2021).

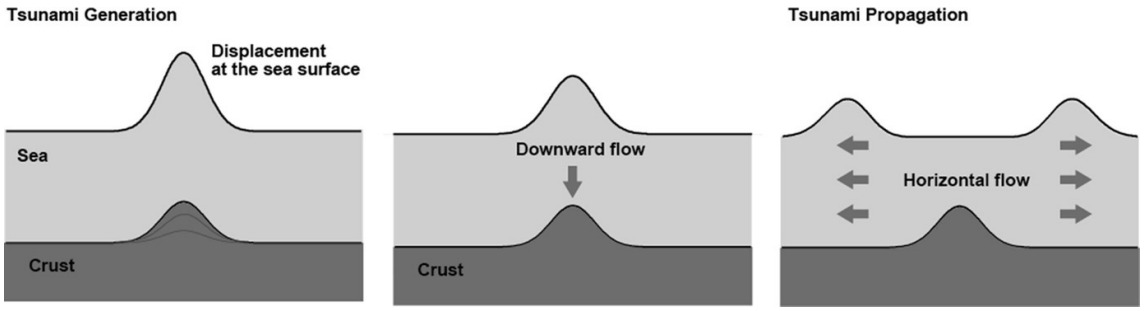

Figure 1.1 - Tsunami Generation. From Saito (2019).

In scientific literature, many attempts were made to study the influence of the seismic source parameters on the consequent tsunami. In the simplest case, the source of a tsunamigenic earthquake can be assumed as a rectangular fault with a uniform slip distribution and the initial tsunami height can roughly be displayed as a large seabed displacement. For tsunami generation simulations, the initial displacement distribution at the sea surface is considered smoother than the one at the sea bottom and it is commonly calculated from a spatial low-pass filter, known as Kajiura filter (Kajiura, 1963; Saito, 2019). In general, the intensity of a tsunami is proportional to the magnitude of the earthquake that caused it, but this dependence is not absolute and has a strong variability. Given the same magnitude of two events, the differences are mainly related to the physical and geographical characteristics of the earthquakes: water depth around the epicentre, focal mechanisms and depths of the seismic source, slip distribution, and other characteristics of the source area, like for example the presence of sediments (e.g. Gusiakov, 2011; Lorito et al., 2011; Scala et al., 2020).

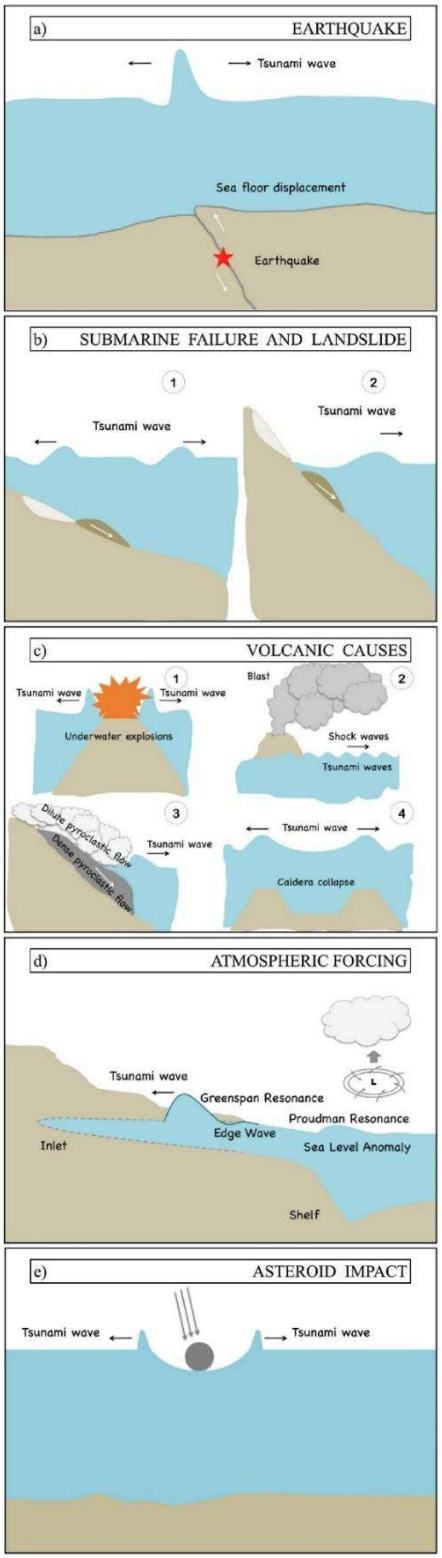

Figure 1.2 – Sources of tsunami waves: (a) earthquakes; (b) submarine (1) and subaerial (2) mass failures; (c) volcanic activity including (1) underwater explosion, (2) blast exciting free waves in the atmosphere which transfers energy to water, (3) pyroclastic flows, and (4) rapid ground deformations or caldera collapses; (d) resonances occurring after atmospheric; and (e) oceanic impacts of asteroids and comets. From Grezio et al. (2017).

Non-seismic sources are less common phenomena than earthquakes and their characterisation is even more complex, as the manifestation of these phenomena can occur in many ways. Tsunami warning systems, with very few exceptions like the Stromboli island system (DPC & Regione Sicilia, 2015), are basically designed for events triggered by earthquakes and have as their primary aim the location of the epicentre and/or the detection of the waves offshore (Paris, 2015; IOC-UNESCO, 2019).

Landslide tsunamis present a great variability, also in terms of the time duration of the source, and several parameters related to the kinematics, the size and the rheology of the falling landslide must be considered, making modelling of such sources more challenging (Piatanesi et al., 2008; Løvholt et al., 2015; Selva et al., 2021). The effects of tsunamis generated by landslides are usually more limited to a local or regional geographical area than for seismic sources, but they can be very severe as in the case of Lituya Bay events in Alaska in 1936 and 1958, reaching hundreds of metres in height (NCEI/WDS; Levin & Nosov, 2016). Landslides tsunamis are extremely dangerous in fjords, closed basins and bays, and have a heterogeneous distribution because they can interest lakes and rivers. Landslides triggered by seismic waves can also give a relevant contribution to the potential tsunami energy of an earthquake, increasing the hazard (Levin & Nosov, 2016).

Volcanogenic tsunamis can be a result of many different physical mechanisms. Usually, the discharge into water of a large volume of material is at low velocities with lava flows, but can also be faster with explosive eruption, giving an impulsive perturbation to the water basin. Large pyroclastic flows can also produce water perturbation, as well as subaerial and underwater landslides caused by the volcanic activity. Indeed, volcanic edifices are particularly unstable and subject to earthquakes, deformations, and gas discharges, all potential triggers of landslides. Probably, the most dangerous phenomena are related to large explosive eruptions and caldera forming eruptions near or in water basins. The interaction between water and magma and the shockwaves generated by the explosion could also create non-linear effects, capable of having comparable waves and effects of earthquake tsunamis (Paris, 2015; Levin & Nosov, 2016; Selva et al., 2021). The best events to exemplify these complex interactions are the explosion of the Krakatau volcano in 1883 and the recent 2022 Hunga Tonga–Hunga Ha'apai event at Tonga islands.

As shown in Figure 1.2, tsunamis may be generated also by other phenomena, other than earthquakes, landslides and volcanic events, like the impact of asteroids or atmospheric perturbations, like for meteo-tsunamis.

Notably, different sources may be active also simultaneously, like for the Hunga Tonga–Hunga Ha'apai eruptions, in which tsunami waves were triggered by both the volcanic explosion and its atmospheric perturbation (Omira et al. 2022), or even the 1908 Messina earthquake, during which probably a seismically-induced submarine landslide generate part of the observed tsunami signal (Selva et al., 2021 and references therein).

Tsunamis have different characteristics in the near-field and far-field due to the initial amplitude and length of the waves and the position and the type of the source. Tsunami waves produced by earthquakes are long waves characterised by long periods and wavelengths (tens to hundreds of kilometres), involving not only the surface of the basin, but the entire thickness of water (Levin & Nosov, 2016). The equations that describe the motion of a fluid in the most general way are the Navier-Stokes equations. The first approximation, which considers the fluid inviscid, are the Euler equations which can be written in the linearized form thanks to the assumption that amplitude of the waves is much smaller than water depth:

$$\frac{\partial v}{\partial t} = g - \frac{1}{\rho}\nabla p \qquad (1.1)$$

where **v** is the velocity of water particles, g is the gravitational acceleration, ρ is the density and p is the pressure. Further assumptions for the fluid are homogeneity (ρ is constant) and incompressibility ($\nabla \cdot v = 0$) and the motion is irrotational ($\nabla \times v = 0$).

The motion solutions describe a prograde elliptical orbit, which decreases with depth. From by the dynamic boundary conditions, it is possible to derive the dispersion relation for gravity waves, which is the relation between the angular frequency and the wavenumber:

$$\omega^2 = gk\ tanh\ (kh) \qquad (1.2)$$

where ω is the angular frequency, k is the wavenumber and h is the depth of the water basin. In general, it is not linear, so there is dispersion.

The propagation of long wavelength dominated sources can be approached with the *shallow-water approximation* because the wavelengths are much greater than water depth ($\lambda \gg h$):

$$tanh\ (kh)\ \approx kh \qquad (1.3)$$

so, the dispersion relation become linear:

$$\omega^2 = gk^2h \tag{1.4}$$

$$\omega^2 = c^2k^2 \tag{1.5}$$

since

$$c = \sqrt{gh} \tag{1.6}$$

where c is the waves' propagation speed, not influenced by wavelength but dependent on water depth.

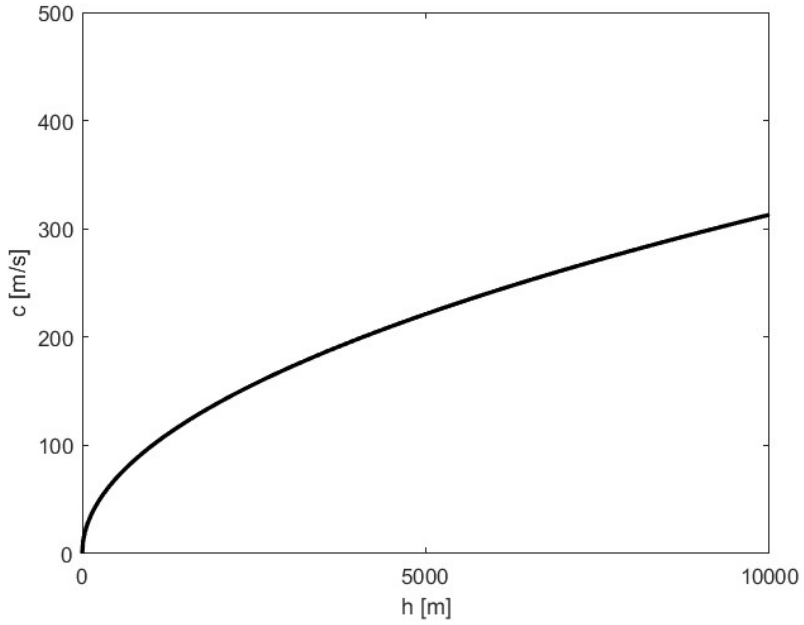

Figure 1.3 – Velocity of tsunami waves in shallow-water approximation.

This approximation is adequate for tsunamis that present large wavelengths, explaining the phenomenon of *teletsunamis*, which are transoceanic waves that propagate for thousands of kilometres from one side of the oceans to the other, essentially without dispersion of energy.

Landslides and volcanic activity usually produce tsunamis that present short wavelengths ($\lambda \ll h$) and the wave velocity is given by:

$$c = \sqrt{\lambda g/2\pi} \tag{1.7}$$

so:

$$\lambda = \frac{2\pi c}{\omega} \tag{1.8}$$

and present a greater dispersion behaviour with motion that decay exponentially with depth from the surface (Lay & Wallace, 1995). Compared to the waves produced by large earthquakes, these sources mostly produce localised tsunamis and their effects on the far-field are often limited (Paris, 2015; Selva et al., 2021).

Differences in propagation are essential to understand which areas may be affected after a tsunamigenic event, but what most determines the danger to humans is how the wave approaches the coastline and how it impacts on it.

1.2 Impact on coasts and physical parameters

When tsunami waves are approaching to the coastline:

- The water depth h decreases,
- Their velocity decreases following the relation $c = \sqrt{gh}$ (in shallow-water approximation, see eq. 1.7),
- Their wavelength decreases following the relation $\lambda = \frac{2\pi}{\omega}$ (eq. 1.8),
- Their height increases because their energy is concentrated in a decreasing volume.

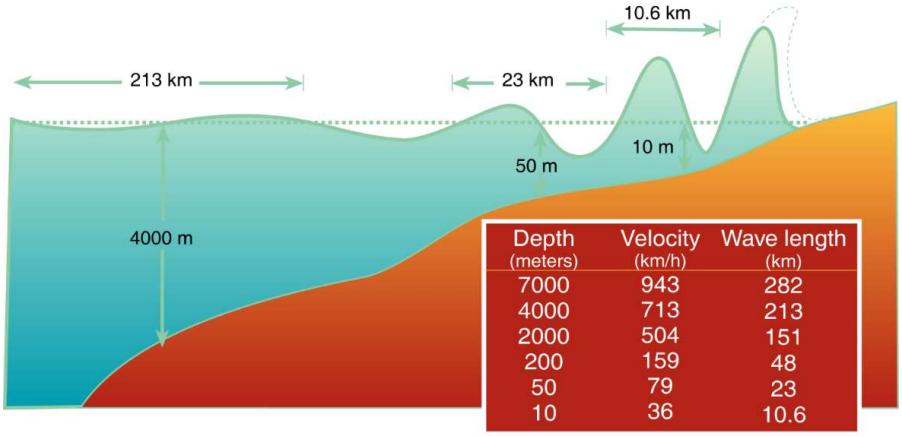

Figure 1.4 - Ocean and offshore waves parameters. From Centro Allerta Tsunami INGV.

At this stage, with the same incoming waves, what most influences the impact on the coast is the bathymetry of the seafloor. Tsunami propagation simulations are implemented with grids that approximate, at various scales of accuracy, the seabed in the target area. In the open ocean, a global approximation such as GEBCO (with a resolution of 30 arcseconds ~1 km) is sufficient, while for reliable simulations of the impact on the coast, resolutions in the order of tens of metres to few metres are required.

The wave collision with the coast (also called the run-up problem) is, among all the tsunami phases, probably the most complicated to describe and to

model. As described in the previous paragraph, while the propagation in deep sea is, in most cases, a linear problem, in the interaction with the coast, many assumptions made previously lose their validity.

- Wave amplitude is no longer shorter than the wavelength,
- Wave amplitude of the tsunami may be comparable to the depth,
- The wavelength is not larger than water depth.

Therefore, the non-linear term in the Euler equation is no longer neglectable, wave velocity depends on position, with the result that the shape of the waves is modified (Levin & Nosov, 2016).

The impact of water beyond the coastline and its propagation can lead to a severe impact depending also on the topographical and land cover characteristics of the affected area. As summarised by Levin & Nosov (2016), the scientific community has studied the run-up problem for many decades, proposing many mathematical models for simulations, targeting specific areas but almost always considering the coastline as a uniform flat escarpment. Numerical simulations use both nonlinear shallow-water equations (in the case of long-period tsunamis) and Boussinesq equations (in the case of shorter wave tsunamis, such as those of landslide origin).

A further issue related to tsunami inundation modelling is that, as the water pours over land, it brings with it more and more debris and suspended particles, as well as boulders and any man-made objects, constantly changing density and abrasion capacity on structures. This aspect is twofold: it increases the danger and difficulty of modelling; however, the debris inside may be the only sign that a past tsunami may have left in the form of sediment. Paleo-tsunamis are discovered and studied precisely because of this.

The physical parameters usually adopted to characterise the tsunami waves describe the size of the wave and its ability to permeate the land (Figure 1.5):

- **Height of the wave along the shoreline**. Elevation reached by the water above the shoreline at the moment of impact. It is not easy to measure as it leaves no physical evidence.
- Elevation reached by water when onshore measured as **Tsunami elevation** (from sea level reference) or **flow depth** (from the ground).
- **Run-up**, maximum tsunami run-up value observed or measured, in metres.

- **Inundation (Ingression) or inundation length.** Maximum water intrusion that can be linear (in m) as in Figure 1.5 or in relation to an inundated area (in m^2).
- **Wave drawdown or withdrawn shoreline**. Vertical or horizontal water retreat.

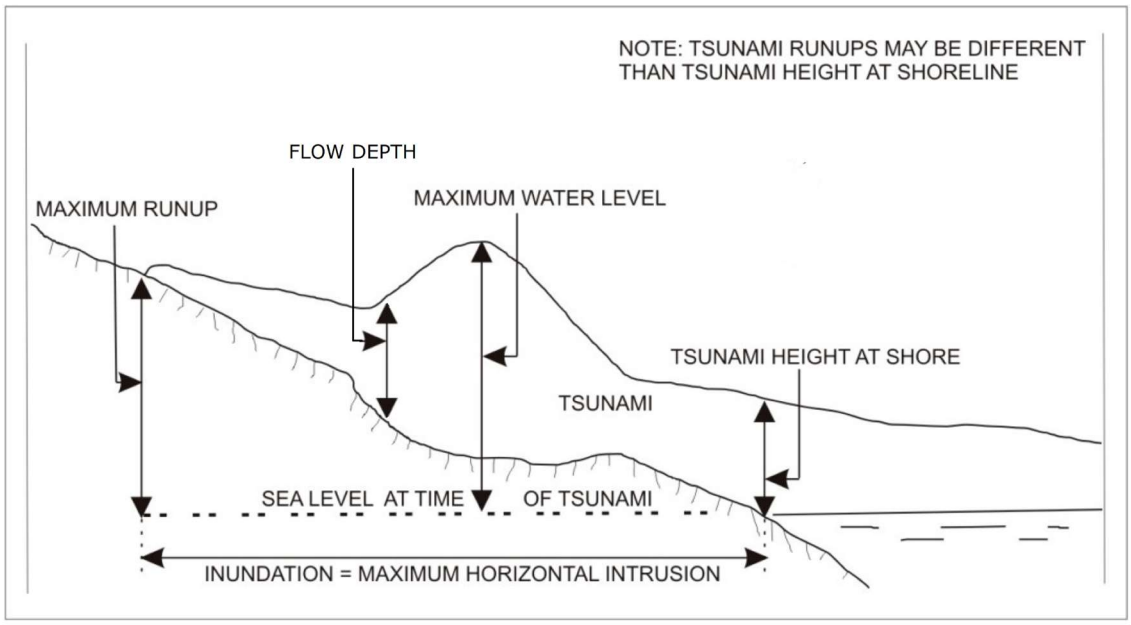

Figure 1.5 - Physics measures for the quantitative description of a tsunami. Modified from Triantafyllou et al. (2021).

Run-up and inundation length are the two main and most frequently used parameters for the description, as they can also be observed for some time after the event. Nowadays, the inundation area can be accurately measured even shortly after the tsunami has occurred, thanks to satellite imagery and remote sensing techniques.

Another important parameter is the maximum inundation height (MIH), which is the maximum wave elevation inland and it corresponds to the Maximum Water Level in Figure 1.5. The MIH is the tsunami intensity adopted in some probabilistic tsunami hazard assessment and wave propagation modelling studies (e.g. Glimsdal et al., 2019; Basili et al., 2021).

All these parameters may be explicitly estimated by modelling the tsunami inundation for each individual tsunami. When explicit modelling is not possible, approximated methods are often adopted. A typical example is when probabilistic tsunami hazard analysis is evaluated at regional or national scales, for which explicit inundation modelling at all target points for all the considered sources is impossible. Such methods estimate inundation from off-shore tsunami parameters, similarly to the seismic analogue in which seismic wave parameters

at the site are evaluated from the wave parameters on the underlying hard rock layer. In this sense, such approximated models treat local inundation like 'site effects'. Thus, here with site effects we mean the local variability and relationship among the different quantitative parameters, and the name derives from the seismic analogue, where seismic waves are modelled on hard-rock, separating the effect of the heterogeneous medium close to a target point. Such site effects are produced by geological, topographical and bathymetric spatial variability that influence the waves of hazardous events such as earthquakes and tsunamis, attenuating or amplifying them. In seismology, the surface geology and the geotechnical characteristics of soil deposits are recognised to influence local ground shaking. Concerning tsunamis, the following can be considered as site effects:

- Bathymetry in the last tens of metres from the coast,
- Topography,
- The type of ground cover, expressed as roughness.

The simplest methods to treat site amplification for tsunamis is using an empirical approach that considers the dissipation process of the wave energy as it travels over land: 200 metres on dry land and 400 metres in the riverbed are expected for each metre of wave height on the coast (Leonard et al., 2008; Smart et al., 2016; TSUMAPS-NEAM, 2022). This empirical model is very approximate and does not consider local differences in the variables but illustrates an average to obtain preliminary estimates.

More advanced models of this type also exist. Recent studies have shown that onshore roughness (Gayer et al., 2010), land cover roughness (Kaiser et al., 2011), energetic and hydraulic properties in flows (Energy Grade Line Analysis - EGLA, Chock, 2016), as well as the offshore bathymetric profile (Glimsdal et al., 2019) have considerable influence on run-up and inundation distances.

When possible, inundation parameters are instead estimated by explicitly modelling tsunami inundation. Recent models for shoaling and inundation are based on high-resolution bathymetric and topographic data, also considering an approximation for the bottom friction specifying land cover characteristics using, for example, the Manning factor (Selva et al., 2021). Smart et al. (2016) proposed a new method for evaluating the resistance of water on the ground. This model is described in Chapter 3, because inversion is applied to obtain an extension of the chosen event data.

1.3 Tsunami intensity scales

Quantifying the size of a tsunami is still being studied today, since there are no internationally recognised and normed standards to indicate the magnitude of a tsunami event and often intensity is used as a measure (Papadopoulos et al., 2020). Before presenting the main scales and equations proposed over the years, it is necessary to define the substantial difference between an intensity and a magnitude. Magnitude is a physical metric of the energy released by an event. It is possible to indicate more than one relying on different physical magnitudes, but they refer to the whole event and should indicate the overall size of it. Intensity, on the other hand, is a classification of the severity of the phenomenon on the basis of the observed effects, so it has a qualitative nature and not a quantitative one like a magnitude.

The first tsunami intensity scale was proposed by Sieberg (1927), in analogy to the work done for the macroseismic intensity scale, where macroscopic descriptions of the tsunami wave effects on the coast were presented. This 6-degree scale was later modified by Ambraseys (1962) with a more detailed description of the effects of the wave, arriving at the Sieberg-Ambraseys intensity scale used in the literature, also in the tsunami catalogue of the Euro-Mediterranean region (e.g. Maramai et al. 2019a, 2019b; Papadopoulos et al., 2007; Baptista and Miranda, 2009; Soloviev et al., 2000) .

The Sieberg-Ambraseys tsunami intensity scale

1. **Very light**. Wave so weak as to be perceptible only on tide-gauge records.
2. **Light**. Waves noticed by those living along the shore and familiar with the sea. On very flat shores generally noticed.
3. **Rather strong**. Generally noticed. Flooding of gently sloping coasts. Light sailing vessels carried away on shore. Slight damage to light structures situated near the coasts. In estuaries, reversal of the river flow for some distance upstream.
4. **Strong**. Flooding of the shore to some depth. Light scouring on man-made ground. Embankments and dikes damaged. Light structures near the coast damaged. Solid structures on the coast injured. Big sailing vessels and small ships drifted inland or carried out to sea. Coasts littered with floating debris.
5. **Very strong**. General flooding of the shore to some depth. Quay-walls and solid structures near the sea damaged. Light structures destroyed. Severe scouring of cultivated land and littering of the coast

with floating items and sea animals. With the exception of big ships, all other type of vessels carried inland or out to sea. Big bores in estuary rivers. Harbour works damaged. People drowned. Wave accompanied by strong roar.

6. **Disastrous**. Partial or complete destruction of man-made structures for some distance from the shore. Flooding of coasts to great depths. Big ships severely damaged. Trees uprooted or broken. Many casualties.

The first attempts towards the introduction of the tsunami magnitude concept was noted in the Japanese literature from the 1940s to the 1960s, with the publications by Imamura and later by Iida, where the maximum tsunami height was adopted as the reference, H_{max} (in m), observed at the coast or measured in tide-gauge records, and was considered as a metric of tsunami magnitude, m:

$$m = log_2 H_{max} \tag{1.9}$$

These proposals led to the definition of the Imamura-Iida magnitude scale consisting of 6 points ranging from -1 to 4 (Papadopoulos & Imamura, 2001; Papadopoulos, 2003; Lekkas et al., 2013; IOC-UNESCO, 2019; Papadopoulos et al., 2020).

In the following decades, there were modifications and attempts to improve the Imamura-Iida magnitude. The proposal of Soloviev & Go (1974) defined a formulation for an intensity:

$$I = log_2 (H \sqrt{2}) \tag{1.10}$$

where H is the mean wave height measured at the coast closest to the source and the valid values are from -5 to 10. But as Papadopoulos & Imamura (2001) remarked, this is a magnitude rather than an intensity scale since it is also based on a physical quantity. Despite this observation, it remains the only 'intensity' listed in the Global Historical Tsunami Database NCEI/WDS (2022).

A similar case proposed for an intensity, but based on a physical magnitude, was published by Shuto (1993):

$$i_s = log_2 H \tag{1.11}$$

Differently from the formulation of Soloviev & Go (1974), H is defined as a local wave height that varies according to the anthropogenic elements on which the prediction of a possible impact is made: fishing boat, individual house or

aquaculture (Papadopoulos & Imamura, 2001). It is a mixture of magnitude and intensity (Papadopoulos, 2003).

The historical evolution proposed by multiple articles (Papadopoulos & Imamura, 2001; Levin & Nosov, 2016; Lekkas et al., 2013; IOC-UNESCO, 2019; Papadopoulos et al, 2020) explains that, after the seismological research on magnitudes, inspired by the concept of magnitude of surface waves for earthquakes, the multiple articles by Abe and Hatori in the 1980s tried to formulate magnitudes based on multiple physical parameters: not only the amplitude of the wave but also the distance from the epicentre of the tsunamigenic earthquake.

With the aim of approaching source strength rather than wave characteristics, Murty & Loomis (1980), still in analogy with progress in seismology, proposed a new objective tsunami magnitude scale:

$$M_L = 2\,(log_{10}\,E\, - 19) \qquad (1.12)$$

based on the total energy of the tsunami E.

In analogy with official macroseismic scales, the intensity scale proposed by Papadopoulos and Imamura (2001) is a 12-degree scale based on the following basic principles:

- *Independence* from any physical parameter,
- *Sensitivity*, with an adequate number of divisions (or grades) in order to describe even small differences in tsunami effects,
- *A detailed description of* (a) the effects on humans; (b) the effects on objects, including vessels of variable size, and on nature; (c) damage to buildings.

The Papadopoulos-Imamura tsunami intensity scale

I. Not felt

(a) Not felt even under the most favorable circumstances.
(b) No effect.
(c) No damage.

II. Scarcely felt

(a) Felt by few people onboard small vessels. Not observed on the coast.
(b) No effect.
(c) No damage.

III. Weak

(a) Felt by most people onboard small vessels. Observed by few people on the coast.
(b) No effect.
(c) No damage.

IV. Largely observed

(a) Felt by all onboard small vessels and by few people onboard large vessels. Observed by most people on the coast.
(b) Few small vessels move slightly onshore.
(c) No damage.

V. Strong

(a) Felt by all onboard large vessels and observed by all on the coast. Few people are frightened and run to higher ground.
(b) Many small vessels move strongly onshore, few of them crash into each other or overturn. Traces of sand layer are left behind on ground with favorable conditions. Limited flooding of cultivated land.
(c) Limited flooding of outdoor facilities (e.g., gardens) of near-shore structures.

VI. Slightly damaging

(a) Many people are frightened and run to higher ground.
(b) Most small vessels move violently onshore, crash strongly into each other, or overturn.
(c) Damage and flooding in a few wooden structures. Most masonry buildings withstand.

VII. Damaging

(a) Most people are frightened and try to run to higher ground.
(b) Many small vessels damaged. Few large vessels oscillate violently. Objects of variable size and stability overturn and drift. Sand layer and accumulations of pebbles are left behind. Few aquaculture rafts washed away.
(c) Many wooden structures damaged, few are demolished or washed away. Damage of grade 1 and flooding in a few masonry buildings.

VIII. Heavily damaging

(a) All people escape to higher ground, a few are washed away.

(b) Most of the small vessels are damaged, many are washed away. Few large vessels are moved ashore or crash into each other. Big objects are drifted away. Erosion and littering in the beach. Extensive flooding. Slight damage in tsunami control forest, stop drifts. Many aquaculture rafts washed away, few partially damaged.
(c) Most wooden structures are washed away or demolished. Damage of grade 2 in a few masonry buildings. Most RC buildings sustain damage, in a few damage of grade 1 and flooding is observed.

IX. Destructive

(a) Many people are washed away.
(b) Most small vessels are destroyed or washed away. Many large vessels are moved violently ashore, few are destroyed. Extensive erosion and littering of the beach. Local ground subsidence. Partial destruction in tsunami control forest, stop drifts. Most aquaculture rafts washed away, many partially damaged.
(c) Damage of grade 3 in many masonry buildings, few RC buildings suffer from damage grade 2.

X. Very destructive

(a) General panic. Most people are washed away.
(b) Most large vessels are moved violently ashore, many are destroyed or collide with buildings. Small boulders from the sea bottom are moved inland. Cars overturned and drifted. Oil spills, fires start. Extensive ground subsidence.
(c) Damage of grade 4 in many masonry buildings, few RC buildings suffer from damage grade 3. Artificial embankments collapse, port water breaks damaged.

XI. Devastating

(b) Lifelines interrupted. Extensive fires. Water backwash drifts cars and other objects in the sea. Big boulders from the sea bottom are moved inland.
(c) Damage of grade 5 in many masonry buildings. Few RC buildings suffer from damage grade 4, many suffer from damage grade 3.

XII. Completely devastating

(c) Practically all masonry buildings demolished. Most RC buildings suffer from at least damage grade 3.

Tsunami Scale	Type of Tsunami	Analogy to Earthquake Scales
Intensity Scales		
Sieberg (1923 ,1927)	primitive 6-point intensity scale	early intensity scales
Ambraseys (1962)	improved 6-point intensity scale	improved intensity scales
Shuto (1993)	developed 6-point intensity scale	developed intensity scales
Papadopoulos and Imamura (2001)	new 12-point intensity scale	new EMS '92 and '98 12-point intensity scale
Magnitude Scales		
Imamura –Iida (40's, 50's and 60's)	primitive magnitude scale	local Richter magnitude scale
Soloviev (1970)	primitive magnitude scale	local Richter magnitude
Abe (1979, 1981, 1985, 1989)	magnitude scale	surface-wave magnitude scale
Murty –Loomis (1980)	magnitude scale	moment – magnitude scale

Figure 1.6 – Time evolution of tsunami size scales proposed and their analogy to earthquake size scales. From Papadopoulos (2003).

In the catastrophic events of 2004 (Indian Ocean) and 2011 (Japan), it was possible to exploit a range of damage assessment technologies that were not available until a few decades ago. For this reason, a new intensity scale was proposed by Lekkas et al. (2013), this one as well with twelve grades (standard reference established with the Mercalli-Cancani-Sieberg scale and later with the European macroseismic scale, EMS-98) like that of Papadopoulos & Imamura (2001). What makes it innovative is an extremely detailed analysis of the damage suffered by buildings, based on the EMS-98, owing to a much larger database of damage information than in 2001. A first approximation of some physical parameters that could characterise a degree of the scale is also assumed, but without resorting to mathematical formulations. Another fundamental criterion involves an analysis of geoenvironmental effects. It is based on another - integrative- seismological scale, the Environmental Seismic Intensity Scale - ESI 2007, proposed by Michetti et al. (2007). It is important to point out that the impact on the environment is the only link between contemporary, historical, paleo-tsunami and future events.

More recent studies have emphasised that tsunami-induced currents must also be considered in the hazard assessment, because maritime assets are vulnerable to significant damage, even without inundation (Lynett et al., 2014; Boschetti & Ioualalen, 2021).

Assigning intensities may seem easy at first glance, but discrete scales do not allow for half-step and when evaluating through qualitative descriptions, perhaps dating back to historical times, doubts may arise. Uncertainties on intensities present a very large variability between past events and recent events. In past tsunamis, but in general in any natural event, the collected witnesses could lead to an exaggerated assessment of intensities. The evaluation of past natural phenomena has always been fundamental to their understanding, but it has always been accompanied by a metaphysical or religious view. In the case of geology, leading up to modern geological science, uniformitarianism has prevailed over the catastrophist view, meaning that past events reoccur with the same intensity in present times. Furthermore, the intensity of a natural phenomenon is also strongly characterised by the economic and social development of the affected area, requiring a comparative evaluation with human population density, the development of infrastructure and ports, as well as road and railway networks. A significant resource for the assessment of past intensities are historical photographs, which provide visual evidence of the description of events. In conclusion, the assignment of intensities is immediate and descriptive for contemporary events, but complicated and approximate for past events, depending on elapsed time and on the accuracy of the descriptions.

Likewise in the assignment of macroseismic intensities, the intensity of a tsunami is not unique. It is important to distinguish between the intensity representative of the entire event (Global Tsunami Intensity), which generally coincides with the highest assigned intensity, and the intensities relative to the individual observation site (Local Tsunami Intensity), which can differ widely from place to place, since local site conditions influence the impact of a tsunami on the coast.

1.4 Relations between physical parameters and intensity in seismology

A relationship between tsunami parameters and tsunami intensity does not exist, and its development is one of the main goals of this thesis. However, the selected approach is based on the vast literature available for the analog problem in seismology. In seismology, the analysis of earthquake effects and their link to the earthquake source is such a vast and studied topic that it has become a science of its own: macroseismic seismology or macroseismology.

Seismological research has long been oriented towards an attempt to correlate seismic intensities with physical parameters of earthquakes, such as

local ground shaking accelerations or earthquake magnitudes. Such associations are not included in the concept of seismic intensity by definition (Papadopoulos & Imamura, 2001). Apart from a few cases, all regressions in seismological studies adopt the same functional form: a linear regression between the seismic intensity and the logarithm of the peak ground motion (PGM) (Faenza & Michelini (2010); Gomez-Capera et al. (2007); Cataldi et al., 2021):

$$log_{10} PGM = \alpha + \beta I \tag{1.13}$$

where the PGM is usually the peak ground acceleration (PGA), α and β are the two parameters under statistical study and I is the intensity.

The purpose of correlation proposals in seismology is to provide a tool for immediate estimation of intensities from ground shaking data (Faccioli & Cauzzi, 2006; Faenza & Michelini, 2010), but the opposite procedure is also a fundamental tool, especially for associating a physical quantity with a past intensity value. As expressed by Gomez-Capera et al. (2007):

- These relationships do not have a very good statistical correlation, but they remain the only tool for making such comparisons,
- The proposed relationships have different scales of intensity and are often difficult to compare,
- When they are obtained by means of an ordinary least squares relationship, they do not consider the error on both variables and consequently cannot be inverted,
- In many cases, the value of σ is not known.

A more recent paper by Gomez-Capera et al. (2020), proposed a non-linear functional form between intensity and the logarithm of PGA:

$$log_{10} PGM = \alpha + \beta \, log_{10} I \tag{1.14}$$

Several further analyses have been produced to connect intensity data not only to local physical characteristics of the seismic waves, but also to the source parameters, like for example the Boxer calculation code (Gasperini et al., 1999). Starting from the geographical distribution of macroseismic intensities, allows, over a grid of trial source locations, the estimation of the epicentral location,

magnitude, orientation and physical dimensions of the seismogenic source (box), or like the approximation of the surface projection of the fault entirely based on intensity data (Bakun and Wentworth, 1997; Tarabusi et al., 2020).

2 Existing datasets for the impact of historical tsunamis

The infrequency of tsunami events, particularly when previous events have occurred long before human memory, makes tsunami hazard assessment a challenging task (Grezio et al., 2017). Databases collecting all the available information about the past events are a fundamental tool for research and researchers are constantly analysing every piece of data available for their extension. Usually, tsunami databases include information on the generating cause (i.e. earthquake magnitude, geographic coordinates etc.), information about the effects produced by the tsunami and, when possible, instrumental records.

The most frequently cited database in the literature is the Global Historical Tsunami Database, which brings together data from 2000 B.C. to the present in the Atlantic, Indian, and Pacific Oceans; and the Mediterranean and Caribbean Seas (NCEI/WDS). An overview of the localised tsunamis contained in the catalogue is shown in Figure 2.1.

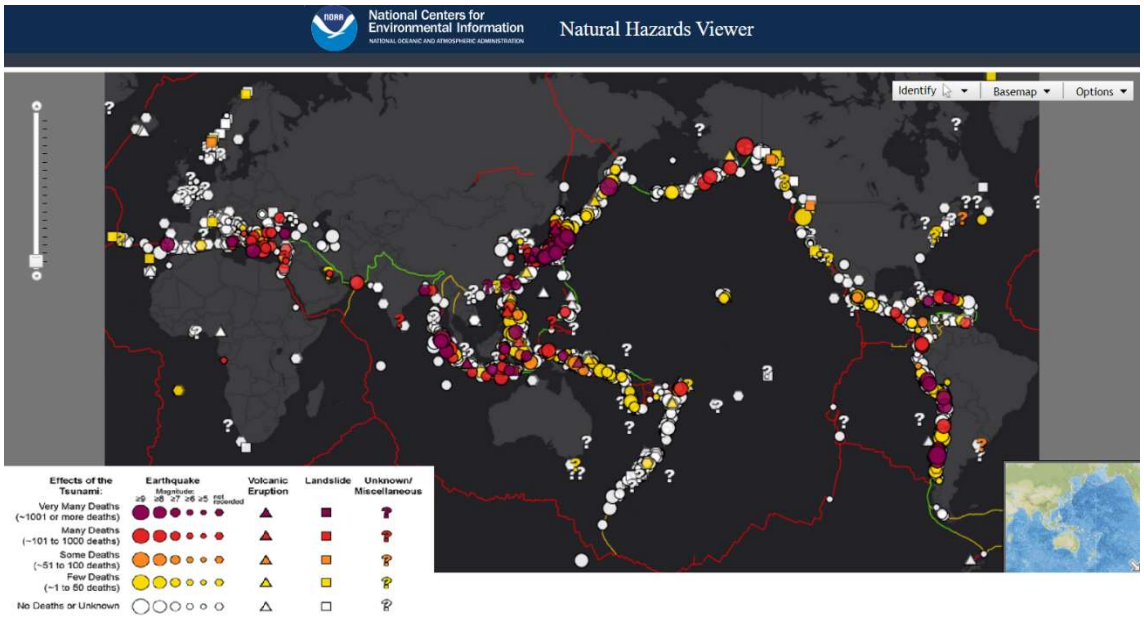

Figure 2.1 - Natural Hazards Map Viewer filtered for Tsunami events. From NCEI/WDS (2022).

National tsunami catalogues have gained significant importance on a regional scale around the world and have contributed to the world catalogue. One example is Japan, which provides a collection of all historical sources related

to tsunamis (Tsunami Digital Library - TDL) (https://tsunami-dl.jp/) with which is associated the Catalog of Tsunamis in Japan and Its Neighbouring Countries (https://tsunami-dl.jp/document/111), which describes all events that affected the Japanese area, notoriously the most tsunamigenic region in the world. Another example of a regional tsunami database is the New Zealand Tsunami database (https://tsunami.gns.cri.nz/) that is a collection of 128 tsunami events that affected the coasts of New Zealand including also events originating from distant sources (Chile, Mexico, etc.). For some regions, there are more detailed studies published as databases for individual countries: there is not always an interconnected network as for the European catalogue. NOAA, the National Oceanic and Atmospheric Administration provides posters detailing historical tsunamis that affected specific areas (Caribbean, Central America and Mexico, Hawaii, Tonga Trench, Papua New Guinea and the Solomon Islands and New Hebrides Trench) (https://www.ngdc.noaa.gov/hazard/tsu.shtml). The International Tsunami Information Centre also provides a series of historical catalogues converted to digital from paper form (http://itic.ioc-unesco.org/index.php?option=com_content&view=article&id=1502:225&catid=1333&Itemid=1333). These catalogues cover several areas of the world and different time windows. Among tsunami catalogues covering different geographical areas, it is worth mentioning the Central America (Molina, 1997), the Tonga-Fiji-New Hebrides region (Everingham, 1984), for some coasts of the Atlantic Ocean (Berninghausen, 1968) and for the Samoa Islands (Pararas-Carayannis & Dong, 1980).

Regarding the Euro-Mediterranean region, the current online databases are based on the precursor work called GITEC (Genesis and Impact of Tsunamis on the European Coasts) and the subsequent update by Tinti et al. (2001). The reference today is the Euro-Mediterranean Tsunami Catalogue (EMTC), proposed by Maramai et al. (2014), updated in 2019: Maramai et al. (2019a), which includes 294 tsunamis generated in the European and Mediterranean seas since 6150 B.C.. It is the result of a systematic review of all the regional catalogues available in literature covering the Euro-Mediterranean area allowing homogeneity of processing in the estimation of events that belong to different regions. The EMTC reports, for each tsunami, information on the main parameters of the event (date, region, subregion, reliability, tsunami intensity, run-up) and of the generating cause (i.e. geographical coordinates, earthquake magnitude, intensity, etc.) as well as detailed descriptions of the tsunami effects in the affected localities. As can be seen from the graph in Figure 2.2, most of the tsunamis in the catalogue were generated by earthquakes, mainly underwater earthquakes. When the tsunami is directly or indirectly generated by an

earthquake, the letter E is used: ER (submarine earthquake), EA (earthquake in land), EL (earthquake landslide -when the earthquake triggered a landslide), ES (earthquake marine slide - when the earthquake triggered a submarine slide). Analogously, letter V is used when the tsunami is directly or indirectly related to volcanic activity: VO (submarine eruption), VA (volcano associated – when the volcano is close to the coast), VL (volcanic landslide – subaerial avalanches on the volcano flanks), VS (volcanic marine slide – submarine avalanches on the volcano flanks). When the tsunami is caused by a gravitational instability not amenable to earthquakes or volcanic activity, the letter G is used: GL (gravitational landslide), GS (gravitational marine slide), GA (gravitational snow avalanche). The code UN (unknown cause) is used when the tsunami cause is unknown (Maramai et al., 2014, 2019a). To improve the quality of the data, the Italian section of EMTC is interoperable with the database of the Italian Archive of Historical Earthquake Data (ASMI). Archivio Storico Macrosismico Italiano (Rovida et al., 2017) and with the Italian Parametric Earthquake Catalogue (Rovida et al., 2022). Not all historical sources are reliable and not all events today are certain to have truly occurred or to have been real tsunamis or violent sea storms. The quality of a tsunami information is defined by a simple scale indicating a degree of reliability (Figure 2.3) that allows the users to evaluate the quality of the data.

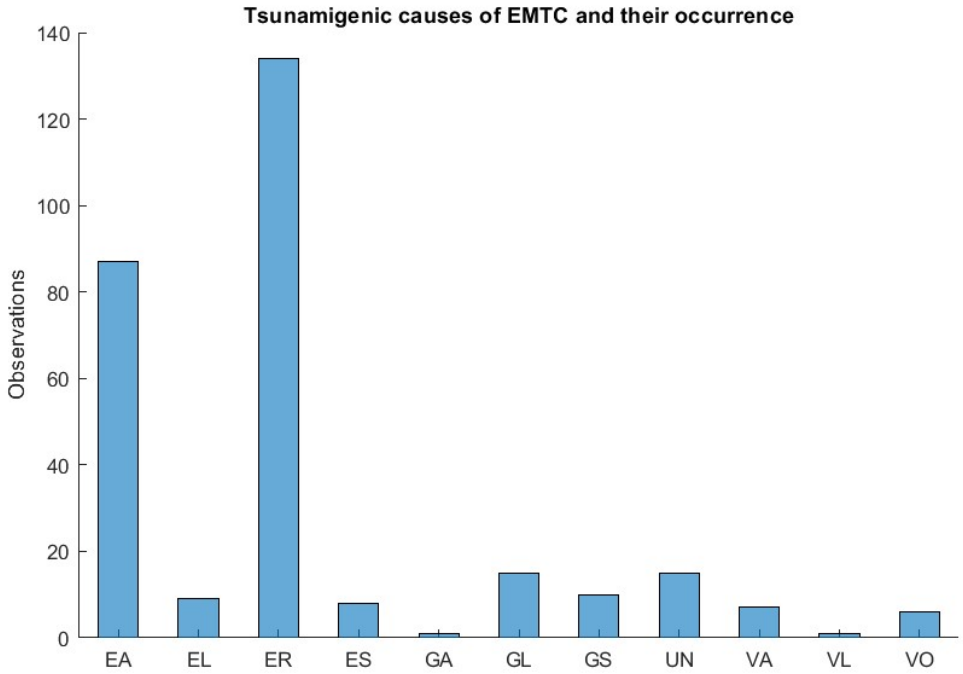

Figure 2.2 - Tsunamis in the Euro-Mediterranean area, divided according to the generating source. EA (earthquake in land), EL (earthquake landslide), ER (submarine earthquake), ES (earthquake marine slide). GA (gravitational snow avalanche), GL (gravitational landslide), GS (gravitational marine slide).

UN (unknown cause). VA (volcano associated), VL (volcanic landslide), VO (submarine eruption). Data from EMTC, Maramai et al. (2019).

Reliability	Description	Cause	Tsunami	Sources
4	Definite tsunami	×	×	×
3	Probable tsunami	×	×	/
2	Questionable tsunami	×	/	×
		/	×	×
		□	×	×
1	Improbable tsunami	×	/	/
		/	×	/
		□	×	/
0	Very improbable tsunami	/	/	×
		/	/	/
		□	/	×
No	No tsunami	All other combinations		

Figure 2.3 - Tsunami reliability, from Maramai et al. (2014) originally by Tinti et al. (2004).
× : fulfilled condition; / : partially fulfilled condition; □ : not fulfilled condition.

EMTC is searchable via a WebApp together with ITED (Italian Tsunami Effects Database) developed by Maramai et al. (2019b), a tool used to create the dataset used (Chapter 3). ITED is an ancillary database and provides information on the tsunami effects observed along the Italian coasts referring to Observation Points (OPs). OPs can be individual settlements, neighbourhoods or locations where there has been an eyewitness account, described by one of the many historical sources consulted for the production of ITED. Figure 2.4 displays an overview of the ITED-EMTC WebbApp with all the tsunamigenic sources in the Euro-Mediterranean area. The tsunamis that have affected the Italian coasts can be summarised in Figure 2.5, where the events are classified by reliability in each time interval. In order to quantify the severity of the effects produced by tsunamis, the authors of these two catalogues attributed the maximum tsunami intensity to each EMTC event according to both the Sieberg-Ambraseys and the Papadopoulos-Imamura scales. Tsunami effects at each site of ITED are also evaluated according to these two scales by assigning a local intensity. Consequently, each observation point has a local intensity, assessed on the basis of qualitative descriptions of the impact of the event at that location. For larger events, it is possible that more than one documentation is available, as many reports were produced, and therefore a cross- evaluation can be performed. In addition to the two evaluated intensities, ITED also provides, when available, a report on the time of arrival and the observed physical parameters and quantitative descriptions of the wave at a given location. The main quantitative items in the catalogue are: number of waves observed, the first movement of the sea (negative or positive), wave amplitude, observed wave height, run-up, sea

withdrawal, inundation (ingression), sea lowering, mean wave period. The database contains tsunami observations related to 77 tsunamis, 73 being originated within Italian territory and four triggered by sources located in neighbouring Mediterranean countries with effects along the Italian coasts (Maramai et al. 2021).

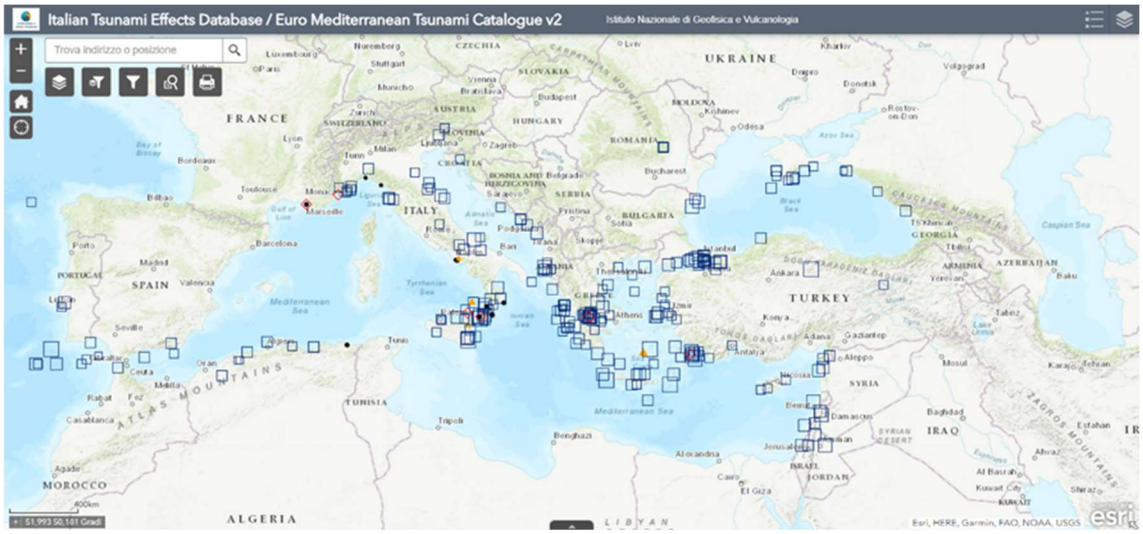

Figure 2.4 - Italian Tsunami Effects Database / Euro Mediterranean Tsunami Catalogue v2. WebApp which shows the sources of tsunami events in the Mediterranean. Blue squares represent earthquakes, red diamonds indicate landslides, yellow triangles volcanic eruptions and black dots indicate unknown causes. Maramai et al. (2019).

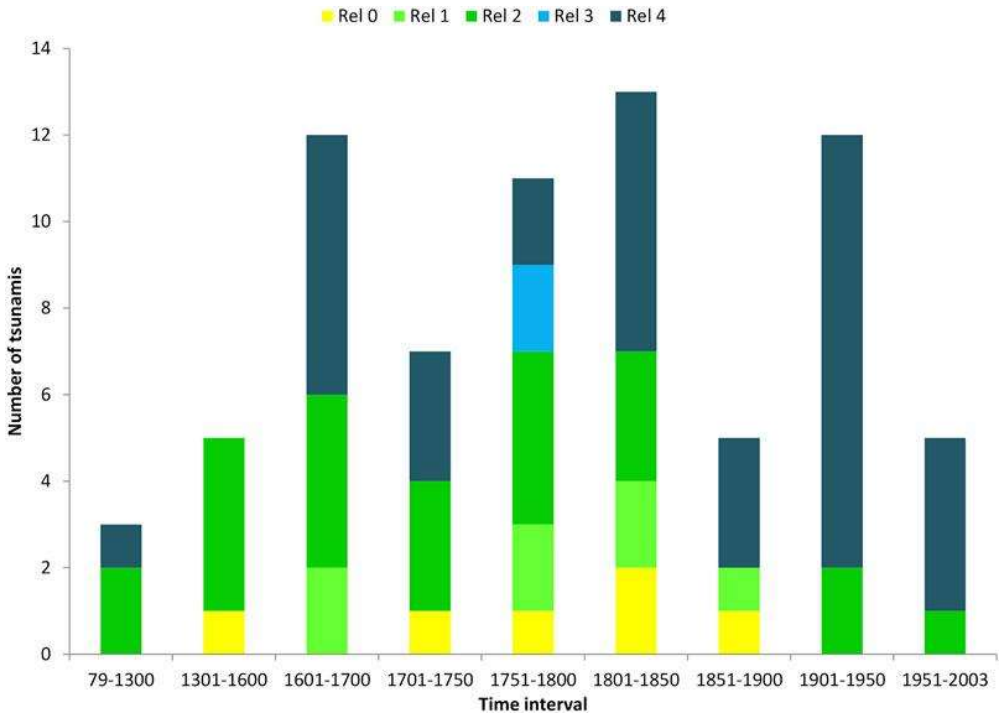

Figure 2.5 - Time distribution of the Italian tsunamis in EMTC2.0 per reliability classes, Rel 4: definite tsunami, Rel 3: probable tsunami, Rel 2: questionable tsunami, Rel 1: improbable tsunami, Rel 0: very improbable tsunami. From Maramai et al. (2021).

The total number of observation points (OP) in ITED is 318, for each OP a description of the effects with bibliographical references is provided together with local intensity value, when possible other parameters are displayed: for 91 OPs the run-up value is reported; for 70 OPs inundation distance is specified; for 7 OPs the wave heights is reported (Figure 2.6) (Maramai et al. 2021). For this reason, scientific research is continuously searching for new empirical relationships that can link physical parameters with each other with greater accuracy, as discussed in Chapter 1.

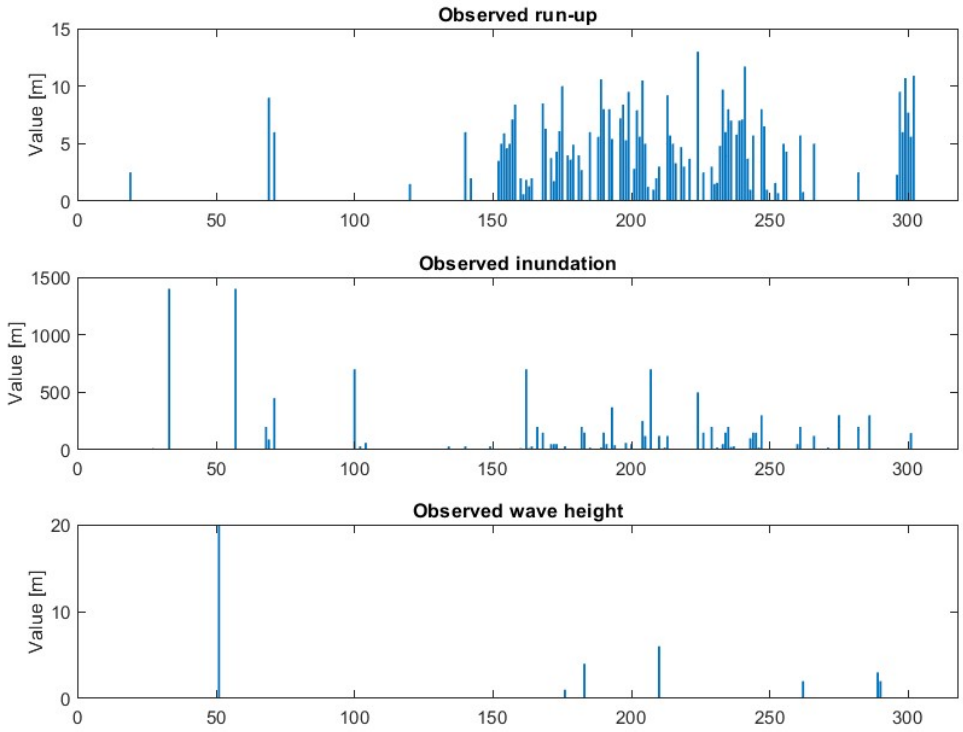

Figure 2.6 - Graphical summary of the main observed physical parameters included in ITED: run-up, inundation and wave height. The x-axis shows the total number of observation points. Data from Maramai et al. (2014, 2019b).

Individual country research has contributed to the expansion of increasingly comprehensive databases by digitally converting this information, which was more difficult to access when printed. The new digital archives often have direct support for geographical information, as in the case of all the catalogues mentioned so far. This allows for an immediate visualisation of the data in the area where it was obtained, making it even more immediate and easier for users to access.

In particular, ITED aims to highlight how exposed the Italian coasts are to tsunamis. It can provide an accurate reference for the validation of inundation

models. It is a fundamental tool for hazard assessment and for increasing awareness of this natural phenomenon, which is often unfamiliar to the population.

All catalogues are designed to store valuable information and describe it in the simplest form possible. The information contained therein documents events that occurred in the past in a synthetic form, which is why they are highly valuable. Such documentation is even more important in the field of geophysics, which studies events on a geological scale and therefore deals with phenomena that occur infrequently and tend to be forgotten by the population.

UNESCO, which has always been committed to culture, information and sensitivity to important issues, has also created a large-scale online information network, based on all possible information on an oceanic and regional scale: 'International Tsunami Information Centre | A UNESCO/IOC-NOAA Partnership' (http://itic.ioc-unesco.org/). This information centre heads the systems subdivided by macro-region, each of them engaged in awareness and system search and eventual warnings. The proposed web pages are divided geographically (Figure 2.7):

- International Tsunami Information Center (ITIC), mainly occupied with the Pacific Ocean, where most events occur,
- Caribbean Tsunami Information Center (CTIC),
- Indian Ocean Tsunami Information Center (IOTIC),
- North-Eastern Atlantic, Mediterranean and connected seas Tsunami Information Center (NEAMTIC).

Figure 2.7 - IOC Tsunami Information Centres.

3 Dataset preparation

Existing databases provide data acquired from available sources, without proposing any quantification of physical measurements other than those reported in historical documents or in the scientific literature, based on observations or direct measurements (mainly for recent events).

As described in Chapter 2, a variety of measurements of the physical parameters are available. However, to systematically correlate the macroscopic tsunami intensity with physical parameters, it is necessary to make reference to an homogeneous and standardised dataset of measures. To this end, it was necessary to decide a physical reference parameter for the purpose of developing this study and quantifying it, where it was lacking, from the other measurements reported by the dataset.

The simple relationship between the main physical parameters for measuring the effect of tsunamis on the coast can be obtained in the simplest possible way based on observations of historical phenomena. Such an approach is a 'rule-of-thumb' that can be used anywhere, without considering the resistance that different grounds may impose on the propagating wave or the morphology of the terrain, and is effective for determining evacuation areas as a first approximation. It was proposed by Leonard et al. (2008) for evacuation plans along the coasts of New Zealand but has also been adopted for the Italian Coasts (DPC, 2018) based on the results of the regional tsunami hazard model NEAMTHM18 (Basili et al., 2020) for the North Atlantic, Mediterranean and connected seas (NEAM). This empirical relationship is based on a simple attenuation law that only differentiates whether inundation occurred along a river or not and considers 1 m of maximum run-up for every 200 m of tsunami travel inland or 1 m for every 400 m up significant rivers, until a topographic obstacle is met (Leonard et al., 2008; Smart et al., 2016; Basili et al., 2021; Tonini et al., 2021).

The approximation mentioned above is particularly useful when there is no accurate information about the morphology of the area that may be affected by the wave, as well as there is not available any information about the tsunami ingression (e.g. inundation length or run-up, see Chapter 1). When it is possible to make an assessment, even an approximate one, of the average slope of the terrain, run-up and inundation length can be related by following:

$$R = L\,S_0 \tag{3.1}$$

where R is the run-up, L the inundation length and S_0 the mean slope. This relationship is very simple and intuitive, as run-up and ingression both indicate how far onshore the tsunami wave has penetrated, but in two different directions: horizontal and vertical. However, it is necessary to have a slope value that adequately characterises the affected location.

Run-up and inundation are the two main parameters for quantitatively describing the impact of tsunamis because they can be easily measured using the marks left by sediments and water, and databases allow almost exclusive access to these two data. However, these parameters implicitly contain a great variability as a function of topography and hydrography, whose exploration or analysis always require a significant effort in retrieving specific local topographic data. In addition, such parameters may reflect a very local situation, more than the general impact in an area that is generally referred to when macroscopic tsunami intensity is assigned. Moreover, they are subject to possible changes through time, due to both natural (e.g. coastal dynamics) and handmade (e.g. building of new infrastructures) reasons.

With the goal of retrieving a more stable and reproducible target parameter, the wave height along the coastline was chosen as the physical reference parameter, despite the fact that it is difficult to measure directly. This choice has not only the advantage of having a parameter that is more stable through time and representative of an entire area, more than a single point, but also is consistent with the tsunami parameter typically evaluated when inundation is not modelled.

Here, we follow the approach proposed by Smart et al. (2016) for run-up estimation from wave height, which is based on the concept of the *Roughness aperture* a.

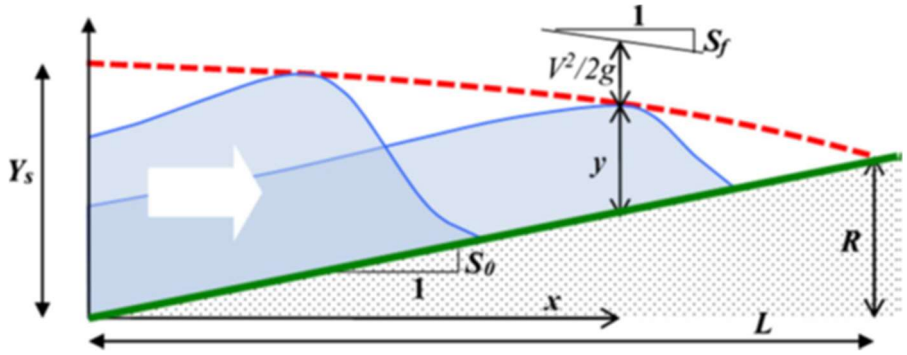

Figure 3.1 - Wave impact diagram on a land profile with constant slope S_0*. Wave-crest levels* Y_s*, onshore inundation distance* L*, run-up height* R*, total head friction gradient* S_f*, water depth* y *and the profile of wave-crest heights (dashed red line). From Smart et al. (2016).*

The model considers a tsunami wave, propagating onshore with a given velocity v over a uniform ground slope, from a one-dimensional perspective. The parameters involved are summarised in the diagram in Figure 3.1. Ground permeability is ignored and the wave is considered quasi-steady (Smart et al., 2016).

Bernoulli's equation for free-flowing currents (Henderson, 1966; Citrini & Noseda, 1987) provides:

$$H = z + y + \frac{v^2}{2g} \tag{3.2}$$

where v is the velocity, g is the gravitational acceleration, H is the hydraulic head, z is the bottom height and y is the flow depth. Differentiating along the direction of flow, since S_0 is the ground slope, S_f is the friction gradient or hydraulic head loss:

$$\frac{dH}{dx} = S_f \qquad\qquad \frac{dz}{dx} = S_0$$

the energy equation can be written as:

$$\frac{dy}{dx} = S_f - S_0 - \frac{1}{2g}\frac{d(v^2)}{dx} \tag{3.3}$$

In shallow water, the wave velocity is near constant throughout a vertical section and can be given by $v^2 = gy$ (Henderson, 1966), which coincides with the formulation expressed in equation (1.6) for the description of the *shallow-water approximation*, therefore substituting:

$$\frac{dy}{dx} = \frac{2}{3}(S_f - S_0) \tag{3.4}$$

For onshore tsunamis, the height of water flow resistance elements is usually comparable to or larger than the water depth and flow passes between these elements (Smart et al., 2016). For this reason, an appropriate flow resistance equation would be:

$$S_f = -\frac{f}{d}\frac{v^2}{2g} \tag{3.5}$$

where f is the local Darcy's friction factor and d is the distance between the flow protrusions such as trees or houses.

Darcy's friction factor is a dimensionless quantity used in the Darcy-Weisbach equation to describe frictional losses in the flow of a pipe or open channel (Barker, 2018). This factor is used precisely to express the passage of water, especially in built-up areas or through dense vegetation, such as in conduits or pipes and not over a uniform surface as in the case of Manning's coefficient.

Roughness aperture a, expressed in metres, can now be defined as the ratio of the distance between the protrusions to the local friction factor:

$$a = 2\frac{d}{f} \tag{3.6}$$

Flow resistance approximation can be written as:

$$S_f = -\frac{y}{a} \tag{3.7}$$

Equation (3.4) becomes, for the wave crest:

$$dy = -\frac{2}{3}\left(S_0 + \frac{y}{a}\right)dx \tag{3.8}$$

Separating the variables and integrating gives:

$$a\ ln(y + aS_0) = -\frac{2x}{3} + k \tag{3.9}$$

where k is a constant and can be assessed by setting conditions along the shoreline: y=Ys if x=0:

$$k = a\ ln(Y_S + aS_0) \tag{3.10}$$

By replacing the constant and making the water depth profile term explicit:

$$y = -aS_0 + (Y_S + aS_0)\ e^{-\frac{2x}{3a}} \tag{3.11}$$

If the maximum wave ingression conditions are set (y=0; x=L), the inundation distance estimation equation can be obtained:

$$L = \frac{3a}{2}\ ln\left(\frac{Y_S}{aS_0} + 1\right) \tag{3.12}$$

from which, under the assumption of a uniform slope (3.1), the estimate for the run-up height can be derived.

In addition to these equations, which are the main focus of the paper proposed by Smart et al. (2016), inverse equations were also derived, with the wave height along the shoreline predicted from the run-up or ingression variables:

$$Y_S = aS_0\ \left(e^{\frac{2L}{3a}} - 1\right) \tag{3.13}$$

$$Y_S = aS_0\ \left(e^{\frac{2R}{3aS_0}} - 1\right) \tag{3.14}$$

In order to be able to use equations (3.13) and (3.14) and relate the physical parameters to each other, it was necessary to study the two unknown parameters in detail for each observation point of the selected events:

- the *mean characteristic slope*, expressed as percentage [%],
- the ground cover expressed as *roughness aperture* [m].

Mean characteristic slope

The evaluation of a mean slope by using a constant criterion for all observations might be limiting for the purpose of an accurate description with regard to specific locations. For this reason, it was necessary to take into account

what was measured at that location, so that the slope of an area of similar size to that actually flooded by water during that event could be assessed. If, for example, a run-up value of 3.6 m was observed in a given OP, it was considered appropriate to assess the slope of a hillside up to an altitude above sea level of the same order of magnitude (e.g. 5 m). On the other hand, if a run-up value of 8.2 m was observed, it was considered more appropriate to assess the slope up to an altitude above sea level of at least 10 m.

Similarly, where an ingression of 20 m was observed, the slope was calculated along a consistent planimetric length (e.g. approximately 50 m). On the contrary, using a common criterion for all observations would have taken into account areas that were not certainly inundated by water, thus leading to a distortion of the slope quantification.

Roughness aperture

Within the relationship between the wave height at the coast and the physical parameters that describe the behaviour of a tsunami wave inland (run-up and ingression), a key role is represented by the friction that the ground and what stays above it affects the flowing water. In scientific literature, the reference usually used for high-resolution tsunami simulations is the Manning's coefficient, an empirically derived coefficient used in the Gauckler-Manning-Strickler equation for the description of friction losses (Gayer et al., 2010; Kaiser et al., 2011; Gibbons et al., 2022). This coefficient is tabulated for most materials and soils because the equation in which it appears describes the flow of liquids in free-flowing channels and it is usually used in engineering for civil and environmental applications. However, it is virtually impossible to define the appropriate coefficient in all points for historical events, since land-use changes significantly through time.

The *roughness aperture* proposed by Smart et al. (2016) is not used to describe a uniformly rough surface but rather to indicate how water is obstructed in its flow. It was therefore necessary to evaluate this new parameter for each observation, even though it is not calibrated for all ground covers because it is a 'novel parameter', as the authors themselves specify. With reference to the explicit form (3.6), it is reasonable to use a typical value for f of 0.05 for fully turbulent flow in rough conduits (Smart et al., 2016), as can be observed in Moody Diagram. What influences most is the distance between the obstacles, i.e. how dense the obstacles are on the ground that do not allow water to penetrate evenly. Smart et al. (2016) proposed a set of values for roughness aperture characterising

land cover types for the case study they considered (2009 South Pacific tsunami that mainly affected Samoa and South Java). Figure 3.2 shows the table suggested by Smart et al. (2016), where a value considered appropriate was added to characterise built-up areas rich in obstacles for the passage of water, to which corresponds a = 50 m, obtained assuming a distance between the flow protrusions d = 1.25 m.

Onshore roughness condition	Aperture value *a* (m)
Smooth open ground, beach	200
Undulating open ground	100
Light buildings, coconut plantations	80
Residential area with buildings and other obstacles	50
Dense vegetation, jungle	10

Figure 3.2 - Indication of suitable values for the roughness aperture parameter a, modified from Smart et al. (2016).

Even if the land-use at historical times cannot be always well characterised, the onshore roughness condition may be roughly estimated by knowing the local climate and the extension of villages at the time of the event.

3.1 Criteria for transects creation

To effectively evaluate *mean characteristic slope* and *roughness aperture*, transects of different lengths and heights were created for each OP. Transects are segments drawn on a map, which have the characteristic of being transverse to the coastline. In fact, all the transects analysed have one of their two ends resting in a small neighbourhood of the coastline, i.e. at an elevation of 0 m, and extend inland for a variable length depending on the data observed in that OP, as shown in Figure 3.3.

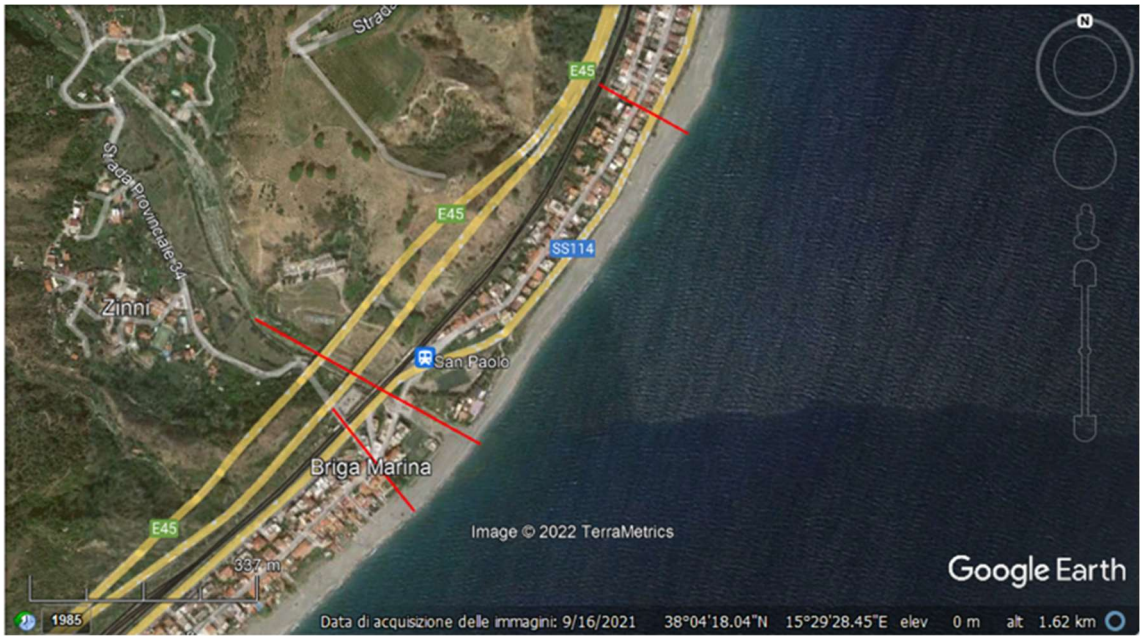

Figure 3.3 - From Google Earth. Example of transects drawn for the OPs of Briga Marina (San Paolo district) in the south and Malati district in the north, one of the areas of Sicily most severely affected by the 1908 Tsunami of Messina and Reggio Calabria. The central transect extends over the bed of the Briga stream, with a smaller slope than the residential areas.

As already mentioned in the previous section, run-up and ingression individually describe the effect at one precise point, which generally refers to the maximum measurement: run-up data generally refer to a built-up area, while ingression is measured along a less steep path, such as a rice field, valleys or streams. However, especially in the case of historical events, it is necessary to consider several sections for the characterisation of the affected area, since there is not always a precise benchmark and the OPs in the catalogues refer to entire localities or districts, mentioning several specific locations within them.

Generally speaking, transects were retrieved through the geographic information system (GIS) Google Earth Pro (https://www.google.it/intl/en/earth/). The choice of this GIS tool results from its immediate usability and the availability of a dataset not easily found on other platforms. The images together with distance and elevation data come from several sources together, allowing for greater global coverage.

The accuracy of the altimetry data can be considered sufficiently precise for the purpose of an approximate assessment of the slope. Despite Google Earth's lack of accurate data description and errors, there are many studies on the accuracy of the data shown on the software, enough that it can also be used for engineering design purposes. Some examples with the associated root mean square error (RMSE) are: Benker et al. (2011) 1.63 m; El-Ashmawy (2016) 1.85 m; Wang et al. (2017) 1.32 m.

The evaluation of the transects using a GIS system made it possible to assess the terrain elevation profile for each segment drawn on the map. Google Earth also provides a profile viewer, where the Digital Terrain Model (DTM) elevation values are shown at the points affected by the user-drawn section. Figure 3.4 shows the process used to evaluate the slope, considering the maximum elevation and linear length of the transect under consideration.

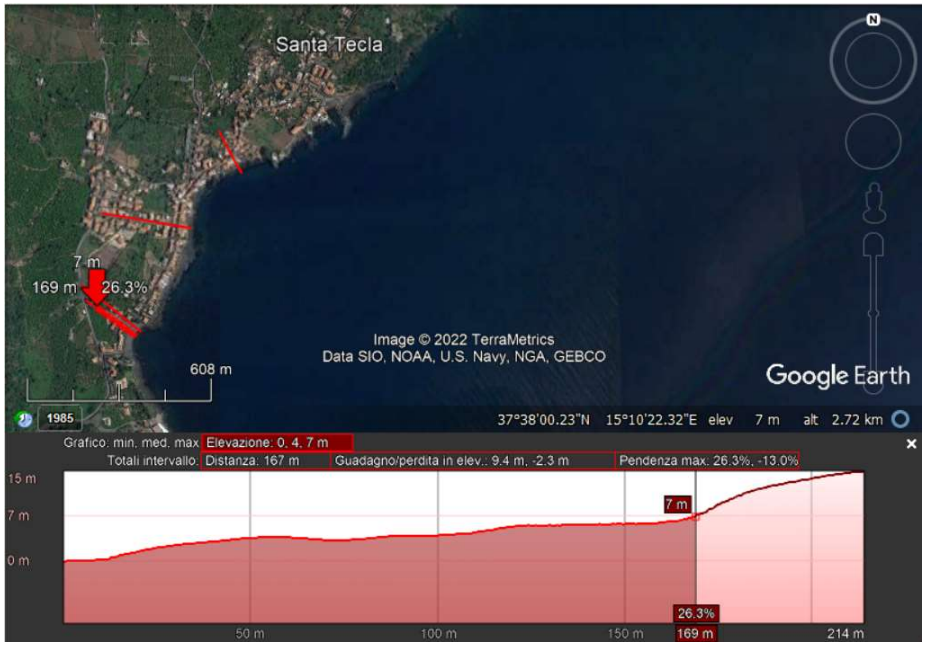

Figure 3.4 - From Google Earth. Example of transects plotted for the OP of Santa Tecla (Sicily). For one of the transects, the elevation profile from which the mean characteristic slope was calculated is displayed.

Google Earth was also useful for assigning a roughness aperture value (a), as it allowed us to assess which type of land cover was dominant among the three considered sufficiently descriptive (smooth open ground, beach a = 200 m; undulating open ground a = 100 m; residential area a = 50 m) (Values expanded from the table provided by Smart et al., 2016).

3.2 Events selection

In the ITED, the event with the most observation points is the tsunami that followed the Messina and Reggio Calabria earthquake of 1908. However, to implement the analysis for just one event may introduce an uncontrolled bias.

To extend the 1908 Messina tsunami datasets, the data analysis was implemented with two additional events: another tsunami significant for the Italian coasts, but with a different origin, which occurred following a volcanic landslide at Stromboli in 2002; and the tsunami that followed the Aegean Sea earthquake in 2020, which affected the coasts of Greece and Turkey. This allows

extending also the tsunami source typology, including one event with a purely seismic source and one with a purely non-seismic source. This is fundamental for a wider application of the relationships developed in Chapter 4, as existing datasets mix the different sources and the actual source is sometimes unknown for some historical event.

Considering the variety of OPs, many specific issues emerged when transets and roughness was to be estimated in all localities. For example, Figure 3.4, in the previous section, shows four transects plotted for the OP of Santa Tecla (Sicily), a location severely affected by the tsunami following the 1908 Messina and Reggio Calabria earthquake. This OP provides a very useful example to explain that some transects were incorrectly located. In Santa Tecla, the first two transects (north) were drawn in the centre of the locality, a place naturally protected by a steep cliff. Following consultation of the report by Baratta (1910) (visualised through CFTILab - Advanced Laboratory of Historical Seismology, Tarabusi et al., 2020), it was possible to identify the location of the run-up measured by (Platania, 1909a; 1909b; Baratta, 1910) at that locality, clearly indicated as the 'southern beach' (Baratta, 1910) and 'damages were particularly in the southern part of the village' (Platania, 1909b) (from ITED, Maramai et al., 2019b). Whenever similar situations occurred, that is when the precise location was not always identified, a flag was assigned to the relative data, marking observations potentially affected by large uncertainty. This occurs only for historical events like the Messina earthquake (see Section 3.2.1).

It has been noted that Google Earth's satellite image quality and the correspondence between elevation data and images (coastline elevation 0 m) varies greatly depending on the geographical area considered. In some cases, when the value at 0 m was too far from the coastline, it was not possible to assess the slope. In such cases, the transect(s) of the Observation Point were not considered.

3.2.1 The 1908 Messina and Reggio Calabria tsunami

The earthquake of 28 December 1908 of Messina and Reggio Calabria is one of the highest magnitude events in the Italian and Mediterranean seismic history, with a moment magnitude $M_w = 7.1$, according to the Italian catalogues (Mariotti, 2015; Rovida et al., 2017; Guidoboni et al., 2018; Guidoboni et al., 2019). The estimated total number of victims of the natural events was around 80.000. Most people perished as a consequence of the collapses caused by the earthquake, especially in the cities of Messina and Reggio, but the tsunami that hit the coasts of Sicily and Calabria a few minutes later aggravated the death toll

by hundreds, but it is thought up to 2000 (Boschi et al., 1995; Mariotti, 2015; NCEI/WDS).

During the months following the events, scholars at that time performed detailed surveys to document earthquake effects as well as tsunami effects. On the east coast of Sicily, tsunami wave run-up was between 6 and 9.50 m, with an extreme peak of 11.70 m at Sant'Alessio, on the southernmost coast of the province of Messina (Platania, 1909a; Platania 1909b; Baratta, 1910). Further south, beyond Catania, wave heights decreased progressively, but were still intense. On the northern coast of Sicily, the tsunami did not impact dramatically and the height was always less than 1 m.

On the Calabrian coast, wave run-ups were between about 6 and 11 m, with a maximum of about 13 m near Pellaro, south of Reggio Calabria (Platania, 1909a; Platania 1909b; Baratta, 1910). It was instead very reduced along the Tyrrhenian coast of Calabria. Even towards the south, and along the entire Ionian coast of Calabria, the waves were progressively less high and violent, with the exception of the possibly erroneous data measured in Roccella Ionica and Cirò Marina (Guidoboni & Mariotti, 2008). An overview of the main places affected can be seen in Figure 3.5 from one of the plates drawn by Baratta (1910).

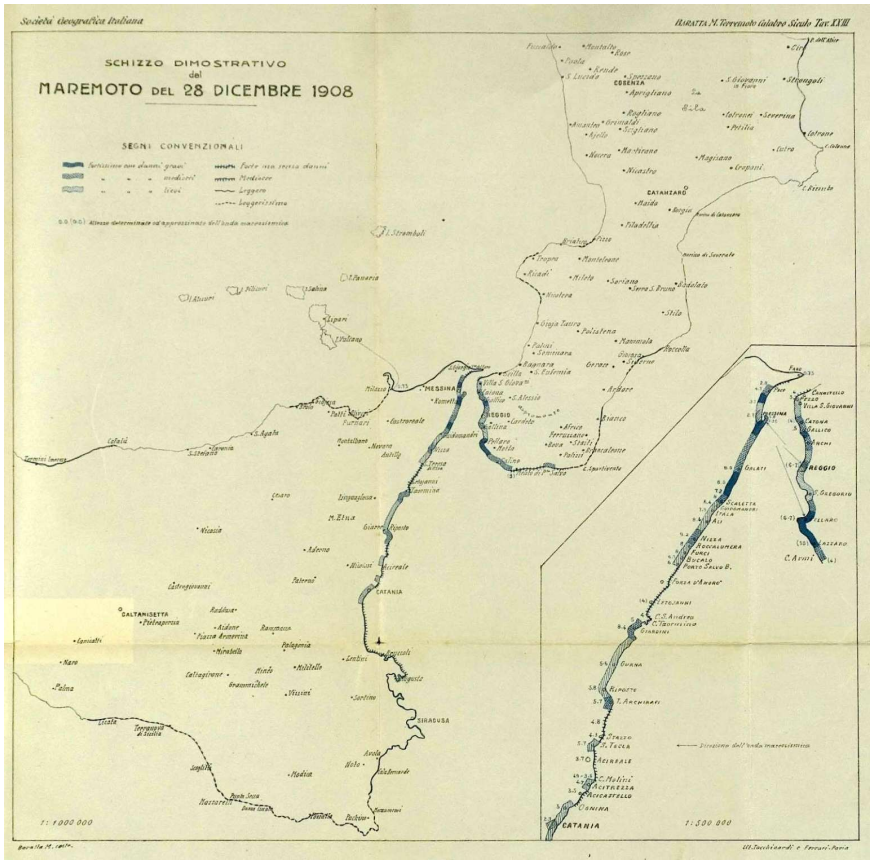

Figure 3.5 – Overview map of the 1908 Messina and Reggio Calabria tsunami. From Mariotti (2015). Produced by Baratta (1910).

This event was a milestone in the history of seismology and the study of tsunamis in Italy because the social and economic impact was very severe. Instrumental seismological data did not allow for an accurate analysis due to the technical limitations of the period, so the seismic source of this earthquake was mainly shaped by accurate macroseismic analysis. The source of the tsunami that followed this earthquake has been the topic of heated debate in the scientific community, leading to the publication of many articles and insightful papers. Even Omori (1909), after the months spent on expedition in the affected territories, had exposed that the differences in time and direction of the wave tracks 'determined chiefly from the observations of the trees bent or broken, and from displaced bodies' suggested a probable non-coincidence in the location of the earthquake and tsunami origin (Figure 3.6). As pointed out by Tinti & Armigliato (2003), the tsunami simulations, based on the assumed faults, showed a discrepancy between the wave distribution in the strait. Therefore, it is difficult to find a single source that can describe both tsunami effects and levelling data. To explain the very high run-ups recorded on the shores of the strait, the hypothesis that the tsunami may have been generated by an underwater landslide or a complex hybrid earthquake and underwater landslide system has also been considered by many researchers (NCEI/WDS; Piatanesi et al., 2008; Favalli et al., 2009; Billi et al., 2008; Schambach et al., 2020). Less decisive, but still significant, are the direct, hence subjective, testimonies of the observers: differences in the timing of arrival and the direction of first arrival of the wave, whether with a withdrawal or with a rise of the water.

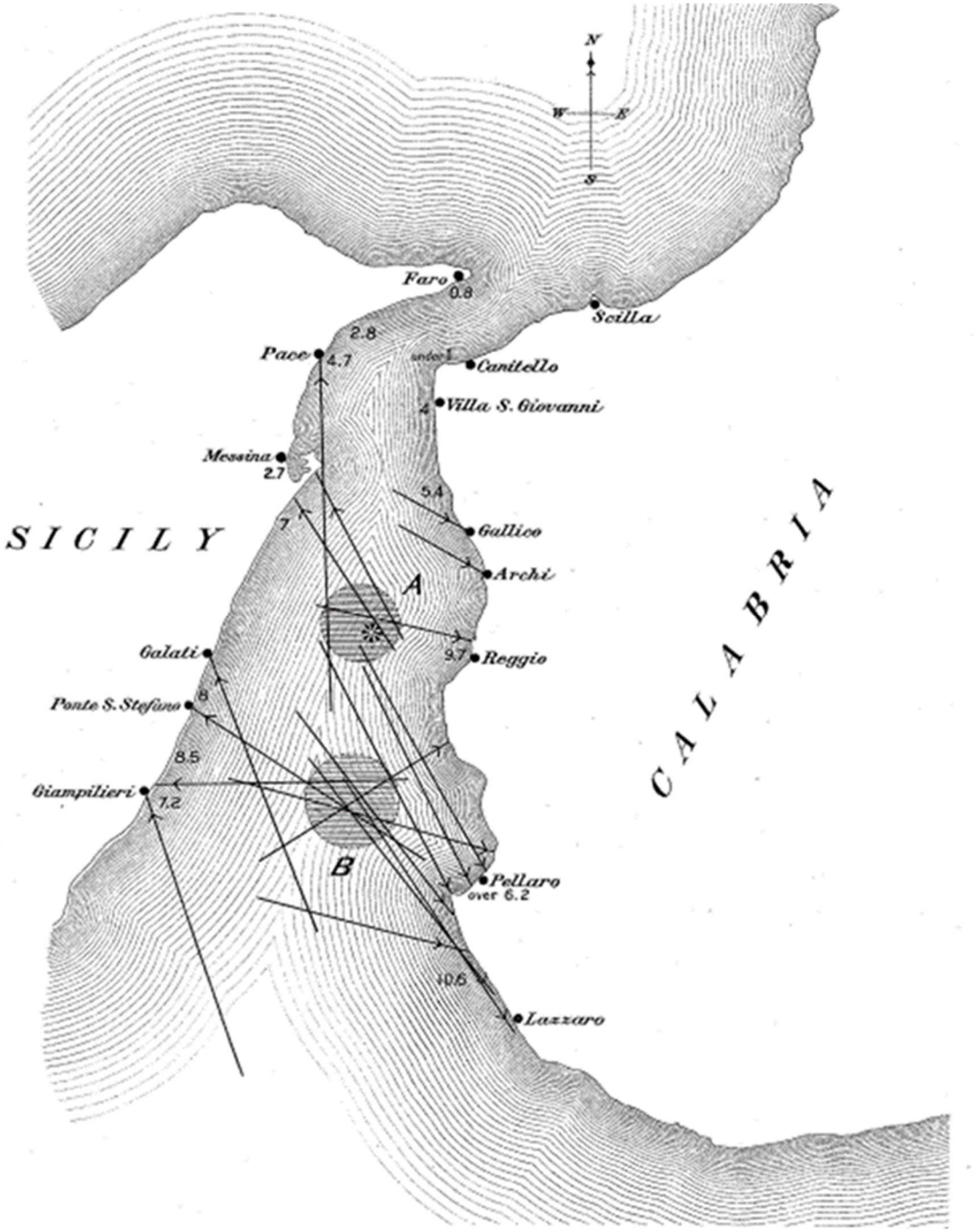

Figure 3.6 - Map showing the direction and the height of the tsunami at different places along the coast of the strait. B and A are the approximate positions of the main and secondary centres of origin of the tsunami, respectively.
From Omori (1909).

The data for this tsunami were retrieved from the Italian Tsunami Effect Database (ITED) proposed by Maramai et al. (2019). For this event, reference is made to historical sources of the scientists who went to most affected localities to analyse the affected villages (Mercalli, 1909; Omori, 1909; Platania, 1909a;

Platania 1909b; Baratta, 1910), but also takes into account localised sources that only describe provinces or municipalities. The synthetic data reported in the catalogue take into account both textual and photographic descriptions, in order to provide a report of as many physical parameters as possible, as well as a summary description of the effects. In the catalogue there are 119 OPs for this event, all of them with an assigned intensity, but only some include the observed values of the main physical parameters: wave height, run-up and inundation length. The OPs containing this data were considered useful and are categorised as follows: 43 with only run-up data; 15 with only inundation data; 35 with both run-up and inundation data; among these listed, 4 also provided wave height. The other observation points either only included data on the withdrawal before the arrival of the tsunami or did not have any physical data, so they were excluded from the study.

The creation of transects for this event was particularly challenging because the precise location of the data assigned to a location was not frequently specified. The reference catalogue (ITED) provides a summary effects report for each observation point and almost always this location is assigned to the coordinates of the centre of the municipality under investigation. The purpose of the analysis using GIS was to associate a slope with the measurement reported by the catalogues, therefore it was necessary to obtain coordinates that were as precise as possible. For this reason, it was necessary to extend the summary provided by ITED with in-depth research on the measurement site, trying to obtain pinpoint coordinates and not generic locations. This was sometimes possible thanks to the concise textual description provided by ITED itself (Maramai et al., 2019b), but on other occasions it was required to directly and extensively consult the historical reference sources themselves (Mercalli, 1909; Baratta, 1910, consulted via Tarabusi et al., 2020). Other information was acquired also from unofficial sources, such as newspaper articles, local websites, regional or municipal territorial planning documents, also helped, which helped localising observations and local conditions at the time of the event.

For each Observation Point, a detailed analysis was carried out and, based on how many input data were available, transects were created in order to assess the morphology of the area as accurately as possible. Appendix A contains the complete table with the notes that determined the distinction between the transects (1) indicated as Flags (all described in the table), i.e. those that did not have a good a priori correlation between textual description, geographical position and assigned data (2) excluded from the study, when no indication of the measurement location was provided or the GIS system presented strong inaccuracies between images and elevation, and (3) included in the study, when

by examining several sources it was possible to obtain a defined location or, preferably, coordinates, so as to obtain elevations compatible with the input data.

For this event, 208 transects were realised and considered in the analysis. Of these, 23 were flagged, allowing for a separate analysis of these more uncertain data, eventually producing results either including or excluding them.

3.2.2 The 2002 Stromboli tsunami

On 30 December 2002, the Stromboli volcano was affected by a mass collapse resulting from an intense volcanic activity. There were two main landslides that also involved part of the volcanic edifice, for a total volume of about 2-3×10^7 m^3 (Chiocci et al., 2008).

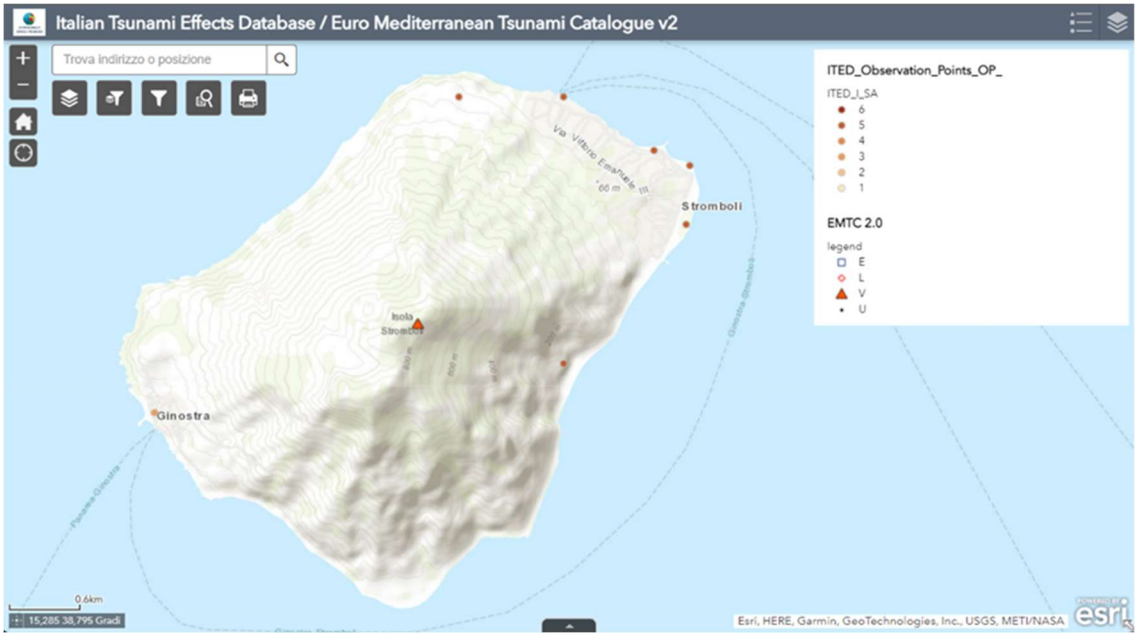

Figure 3.7 - Stromboli Island with the intensities referred to the areas and districts of the island expressed on the Sieberg-Ambraseys scale. From ITED (Maramai et al., 2019).

Observations conducted immediately after the tsunami for the quantitative description of the effects revealed a more violent effect in the northern and north-eastern coastline, between Punta Frontone and the village of Scari, with maximum runup heights of about 11 m (Tinti et al., 2006). The effects were the injury of three people and serious damage to buildings and structures. Fortunately, the landslide and subsequent tsunami occurred in winter, so the number of people was considerably smaller than during tourism periods: many of the damaged houses were uninhabited or belonged to tourist villages, especially in Ficogrande (Tinti et al., 2006). On the other Aeolian Islands and in

the far-field, the effects of the sea wave were documented only through eyewitness accounts.

Information and data on this event are available mainly from two survey articles on the effects of the tsunami on the island of Stromboli and observations on the other islands of the Aeolian archipelago: Maramai et al. (2005) and Tinti et al. (2006). From the ITED WebApp (Maramai et al., 2019b) it is possible to directly retrieve an overview of the locations (Figure 3.7) and the intensities associated with them.

A portion of this coastal stretch is shown in Figure 3.8. For some transects, the slope value was obtained from the sections reported, also graphically, in the survey article produced by Tinti et al. (2006).

For this event, 16 transects were taken into account from observations in the area. Among these 16, 3 are represented graphically by Tinti et al. (2006) and the characteristic slope was calculated using these detailed elevation profiles.

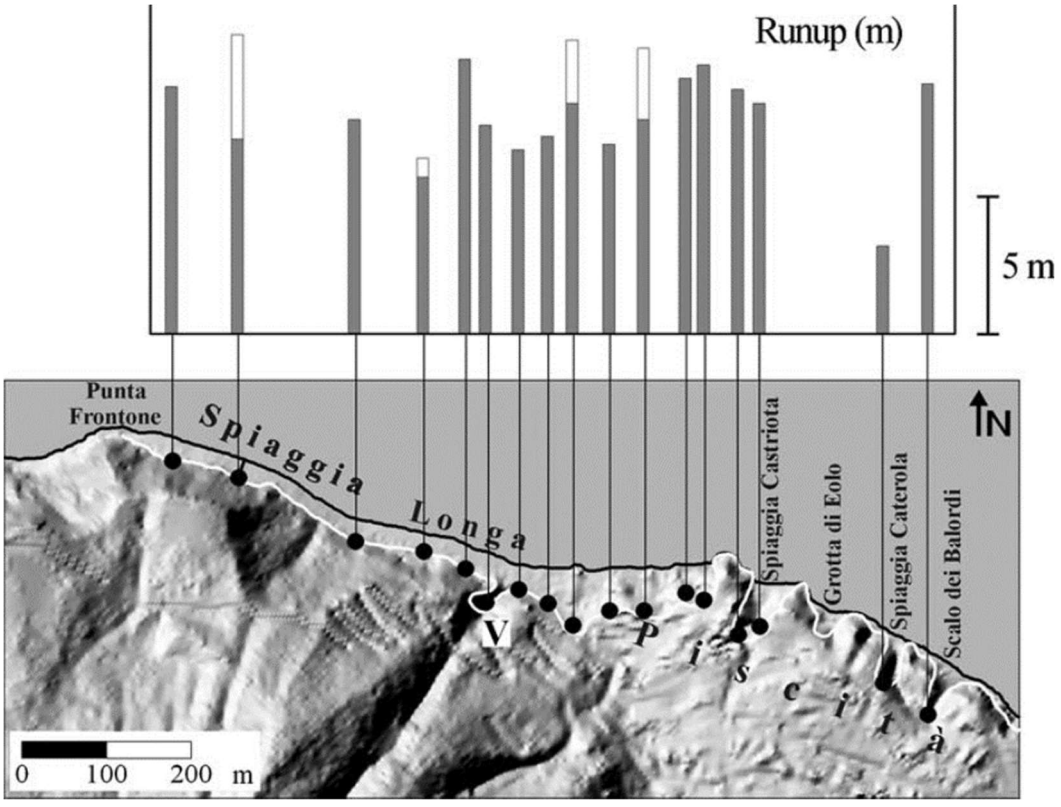

*Figure 3.8 - Example of a sector analysed in the observation campaign. Spieggia Longa, uninhabited beach and Piscità, built-up area. The measurement points of the run-ups are indicated: in the histogram the **grey bars** indicate the smallest run-up recorded at each site and the **white bars** indicate the largest. The **white line** marks the maximum inland tsunami penetration. The **black segment** connecting the shoreline and the second point measured from the northwest indicates the path of the transect in Vallonazzo, the point of maximum ingression. From Tinti et al. (2006).*

3.2.3 The 2020 Aegean Sea tsunami

On 30 October 2020, an earthquake of magnitude was triggered in the eastern part of the Aegean Sea, a few kilometres north of the Greek island of Samos. The earthquake caused severe damage and numerous collapses mainly in the Turkish city of Izmir and triggered a tsunami that affected the coasts of surrounding Greek islands, and the coasts of Turkey.

Along the Turkish Aegean coast, the tsunami damage was more extensive, with run-up values of up to 3.8 m measured at Akarca and there was also a fatality and several injured people (Triantafyllou et al., 2021; Dogan et al., 2021). Along the Greek shores (Figure 3.9), the impact was minor, generally only areas with an elevation less than 2 metres were affected and there were no casualties (Triantafyllou et al., 2021; Kalligeris et al., 2021). Regional and national services issued tsunami warnings about 10 minutes after the earthquake. This tsunami was one of the first to alert and use the Emergency Communications Service for tsunami warning and had a positive impact on the evacuation of the population.

The qualitative, photographic and quantitative descriptions of this tsunami and its effects on the Greek and Turkish coasts are mainly available from three articles, published in the year after the event, which gathered all possible information in detail: Triantafyllou et al. (2021), Dogan et al. (2021), Kalligeris et al. (2021). There are no articles in the scientific literature or databases that provide an intensity assessment for the observation points of this tsunami, so the intensity values at the locations considered were assigned specifically for the purpose of this project, based on the three cited report articles. The adopted approach is equal to the one adopted in the past for the two events described above, i.e. the one adopted by EMTC and ITED (Maramai et al., 2019a, 2019b) and provides a double intensity scale for wave effects on the coast and on human activity. The two reference scales are the 6-grade Sieberg-Ambraseys (Ambraseys, 1962) and the 12-grade Papadopoulos-Imamura (Papadopoulos & Imamura, 2001).

It has been noted that Google Earth's satellite image quality and the correspondence between elevation data and images (coastline elevation 0 m) is considerably reduced in the areas of Greece and Turkey compared to the Italian coasts. In fact, many OPs were excluded from the study in several areas, especially on the island of Samos (reason for exclusion was, for example, a positive elevation at a distance of metres or tens of metres from the coastline). Despite this problem, 48 transects and their points were considered useful for the analysis developed in Chapter 4.

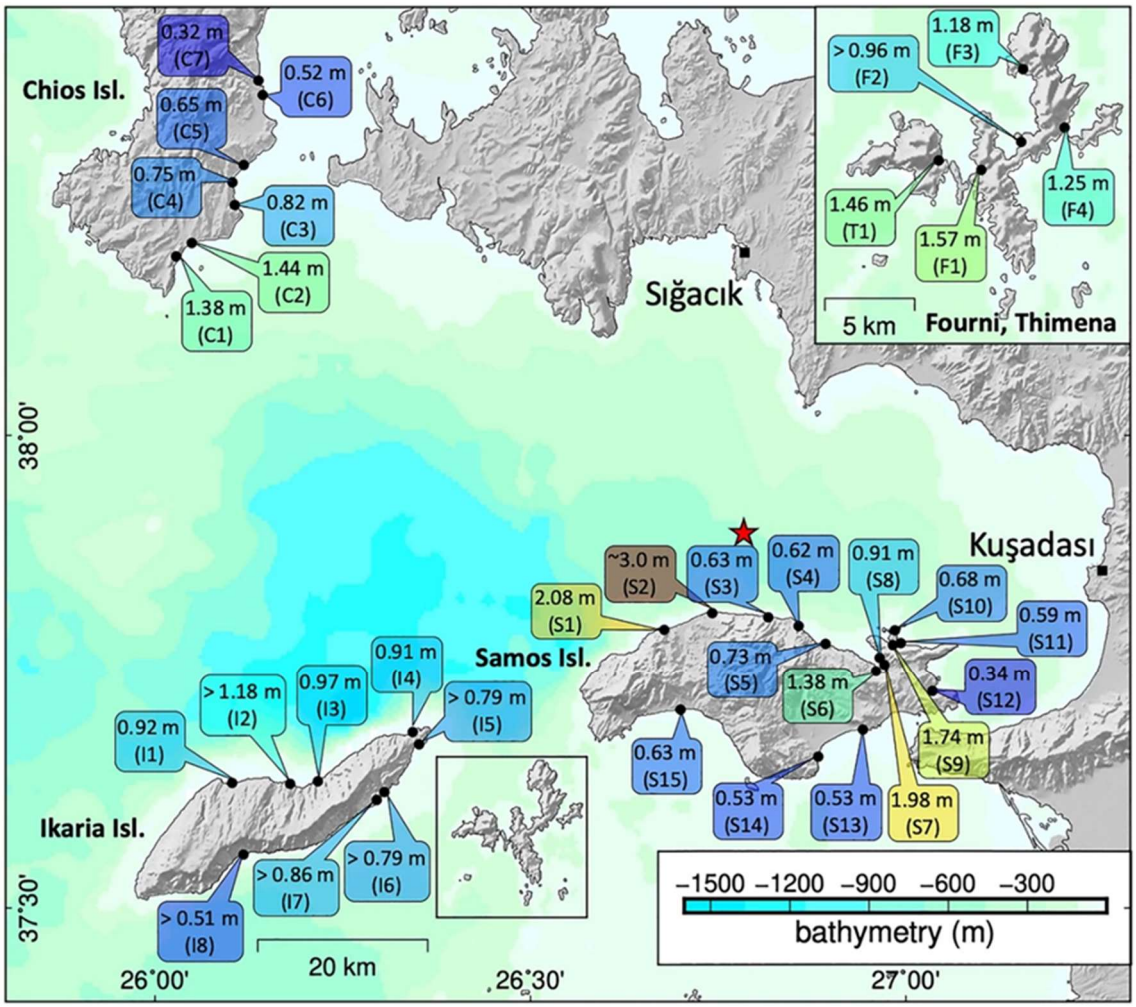

Figure 3.9 - Overview of maximum run-up and/or tsunami elevation measured at all locations visited during post-tsunami reconnaissance missions to the Greek islands. The symbol > refers to the measurement of structures that were submerged, so the water height at that location was higher. Boxes are colour-coded according to their respective value. The coloured background shows the GEBCO bathymetric relief and the red star corresponds to the earthquake epicentre. From Kalligeris et al. (2021).

3.3 Results

By evaluating mean characteristic slope and roughness apertures in all OPs and associated transects, we can complete the observation records with an explicit estimation of all three physical parameters: run-up, ingression and wave height on the shoreline, for all OPs where at least one observation was available. The total number of OPs in this condition is about 170, from which 272 transects were obtained.

The calculation of the wave height along the coastline was performed firstly with a fixed value for each transect a = 100 m and then applying the evaluation for that location according to the 3 values considered descriptive of

the locations analysed (a = 200 m; a = 100 m; a = 50 m; see table in Figure 3.2), based on the best knowledge it was possible to reconstruct for the local settings at the OP at the time of the event.

To evaluate the accuracy of the adopted strategy, initially we focus on the evaluation of the model accuracy at the OPs where both run-up and ingression data were present. Indeed, thanks to the punctual evaluation of the mean characteristic slope of each site (transect) hit by a tsunami wave, it was possible to derive run-ups from the ingression data and vice versa, using formula (3.1) $R = L\,S_0$. Thus, such OPs provide the opportunity to independently test the accuracy of the selected procedure, and specifically of the quantified average slope. Unfortunately, too few data regarding wave height are available, to make a similar comparison for the entire model. Instead, at the OPs where both run-up and ingression data are available, we can compare the physical parameter (run-up or ingression) as measured at site with the value calculated from the application of (equation 3.1) considering the other physical parameter and the local slope. The results are reported in Figures 3.10 to 3.15, demonstrating a good consistency of the results.

The graphs below show a general good correlation for all the events considered, demonstrating that the slope obtained from the transects is sufficiently precise for most of the observation points. In Figures 3.10 and 3.11, referring to the 1908 event, it can be seen that the flags points are the most dispersed, demonstrating that the precise location of the site is a key factor in the accuracy of the output data. Considering that flags were assigned solely on the historical information, it is justified to consider the flagged data as potential outliers due to the incorrect localization of the observations.

The results for the 2020 Aegean Sea tsunami (Figures 3.14 and 3.15) are generally more noisy. This is probably due to the fact that Google data are far more inaccurate in Greece and in Turkey than in Italy. Also, the great detail that is reported on the available field observations, which are also strongly spatially clustered, cannot be fully reproduced by the applied simplified 1D and averaged-along-the-transect model. For example, Figure 3.15 shows the correlation between the measured floods and those calculated from the run-up data for the Aegean Sea event. There are four points that seem to follow a different trend from the one proposed by the relationship. This is due to the fact that they are maximum inundation values along the course of rivers or ditches, where the slope is almost zero and it was not possible to obtain such a small value through the GIS used (slopes less than 0.70 %). Despite this inaccuracy in the slope, the wave heights computed at the shoreline (using roughness a = 200 m inside the

formula (3.13)) provided values comparable to the tsunami elevation (TE) values close to the shoreline reported in those locations by Dogan et al. (2021).

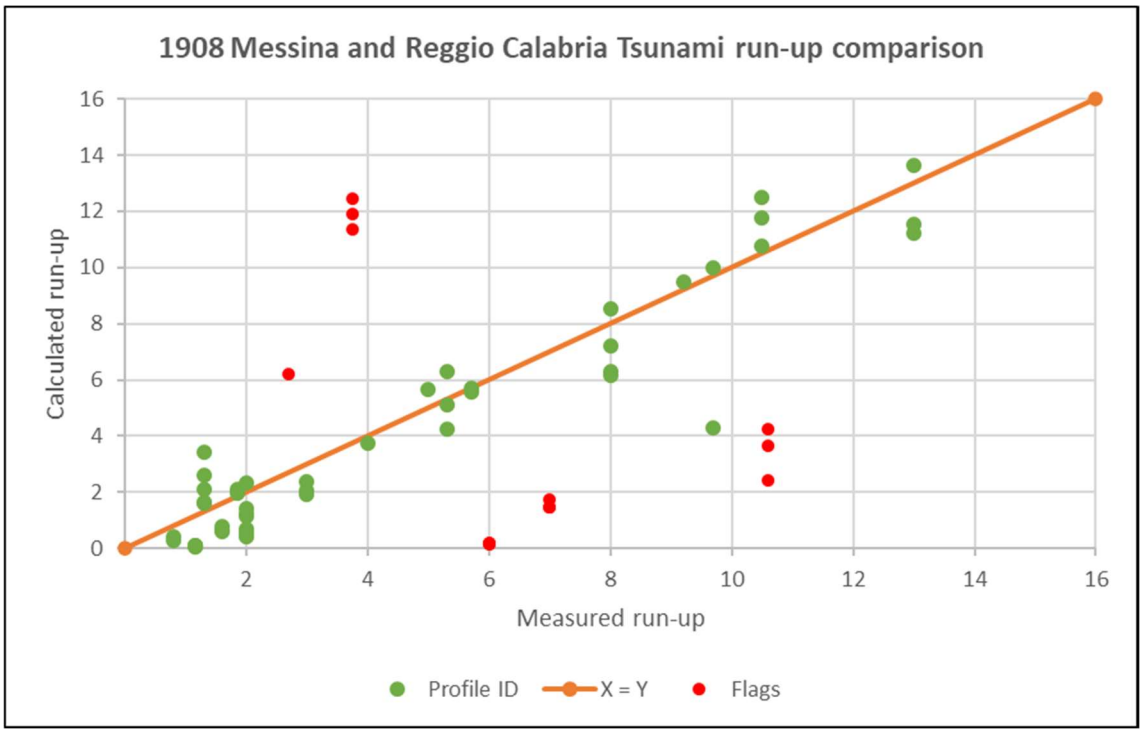

Figure 3.10 - Graph of the run-ups measured and calculated using equation 3.1, for the control of the slopes measured by the transects for the 1908 Tsunami in Messina and Reggio Calabria. Flags in red correspond to places where it was not possible to conduct an effective measurement of the elevations.

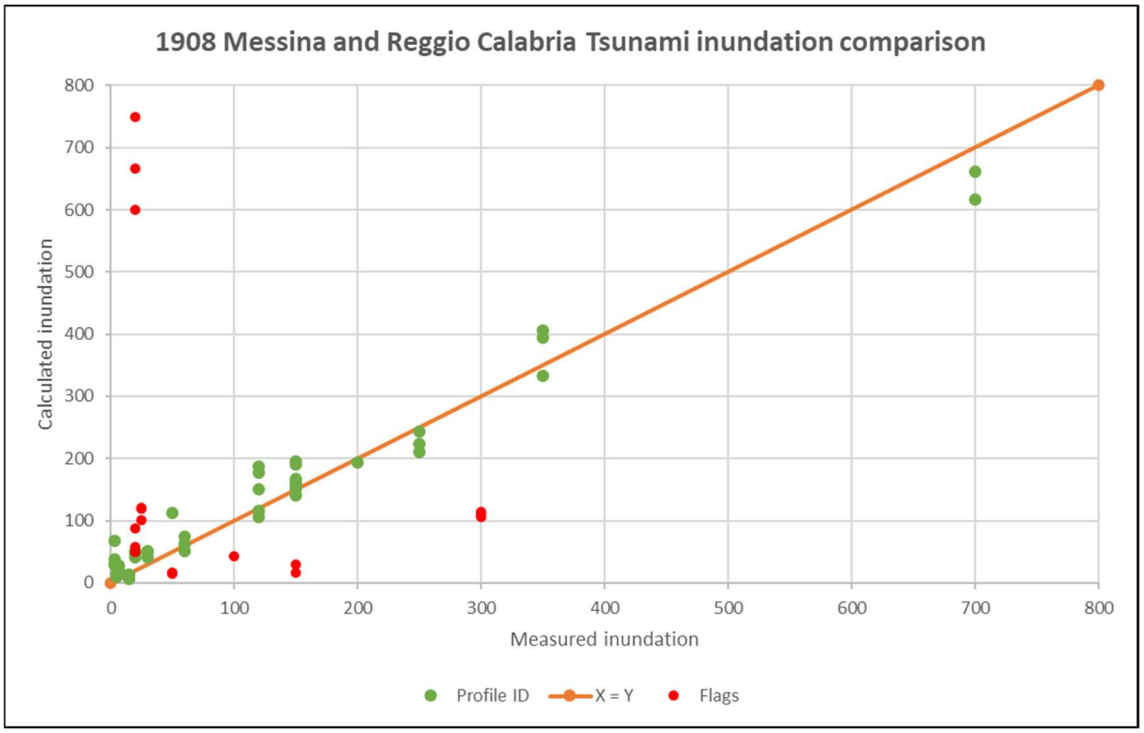

Figure 3.11 - Graph of the inundations measured and calculated using equation 3.1, for the control of the slopes measured by the transects for the 1908 Tsunami in Messina and Reggio Calabria. Flags in red correspond to places where it was not possible to conduct an effective measurement of the elevations

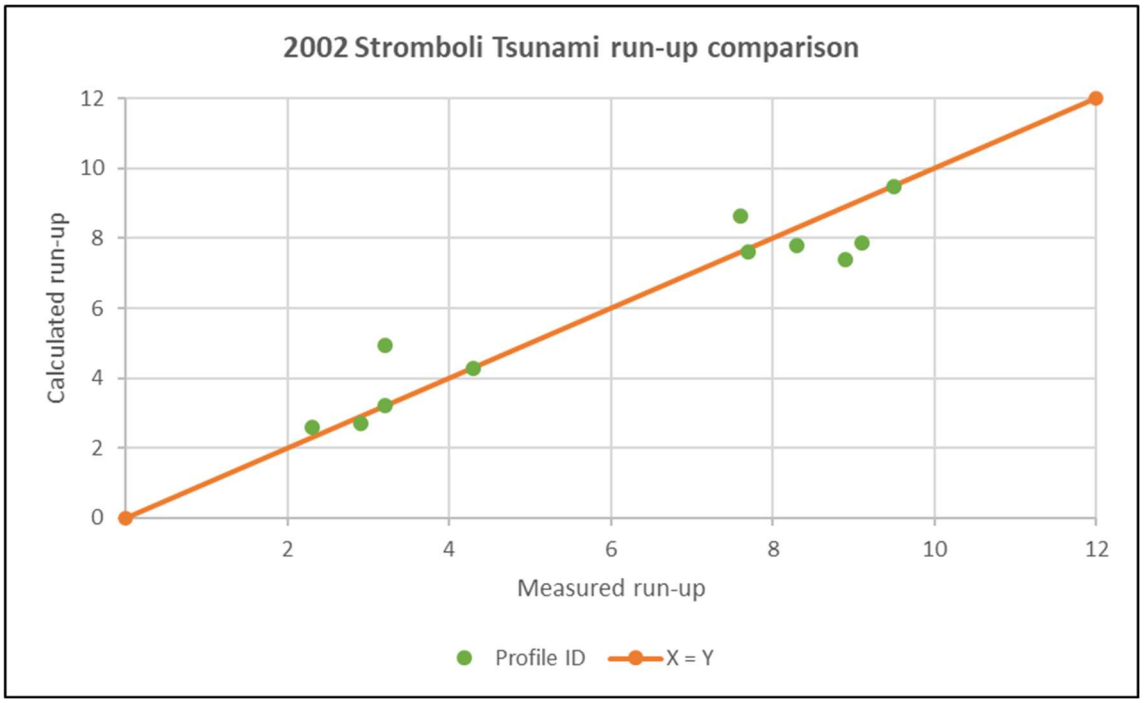

Figure 3.12 - Graph of the run-ups measured and calculated using equation 3.1, for the control of the slopes measured by the transects for the 2002 Stromboli Tsunami.

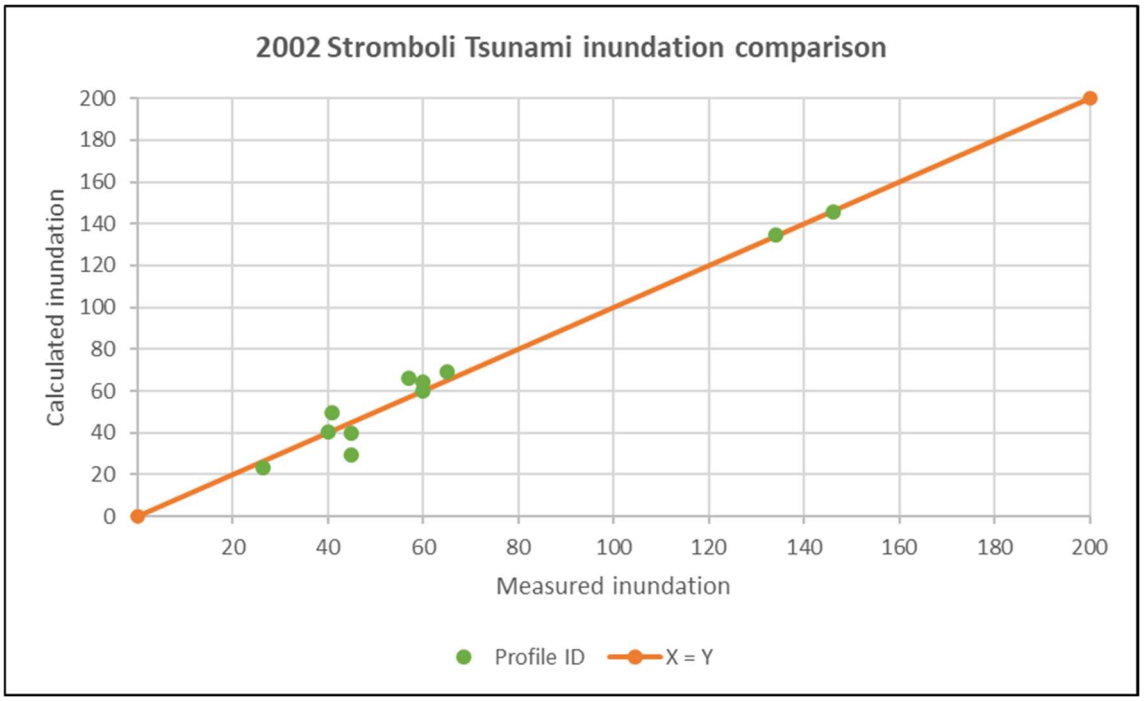

Figure 3.13 - Graph of the inundations measured and calculated using equation 3.1, for the control of the slopes measured by the transects for the 2002 Stromboli Tsunami.

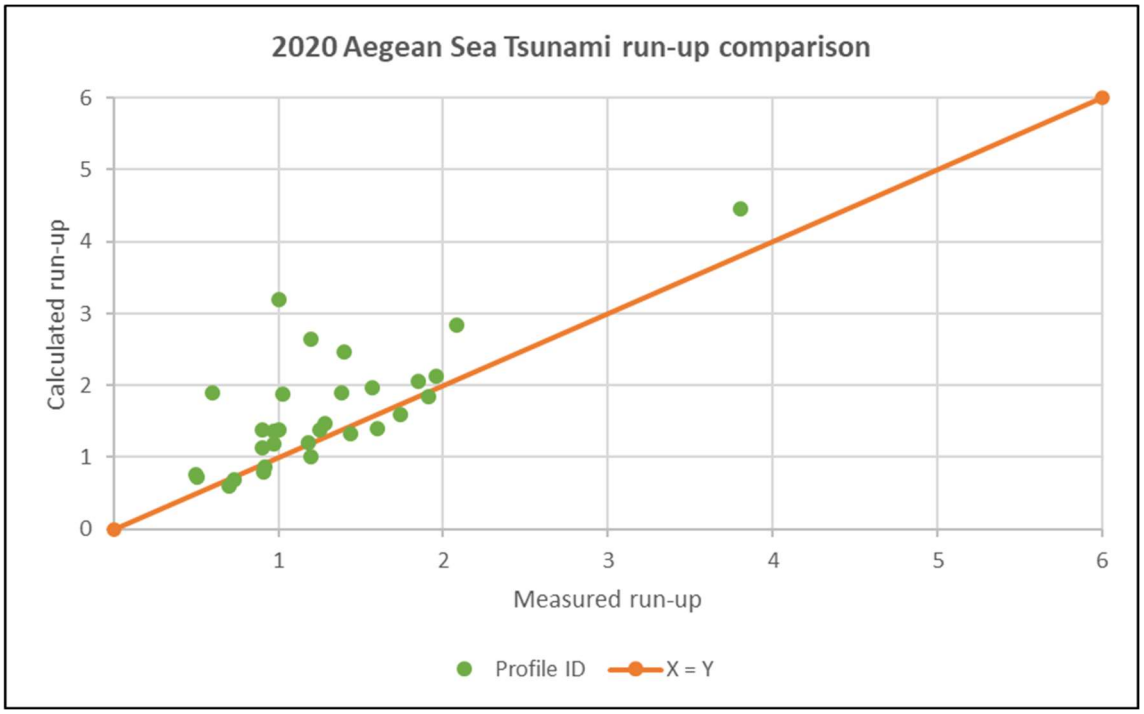

Figure 3.14 - Graph of the run-ups measured and calculated using equation 3.1, for the control of the slopes measured by the transects for the 2020 Aegean Sea Tsunami.

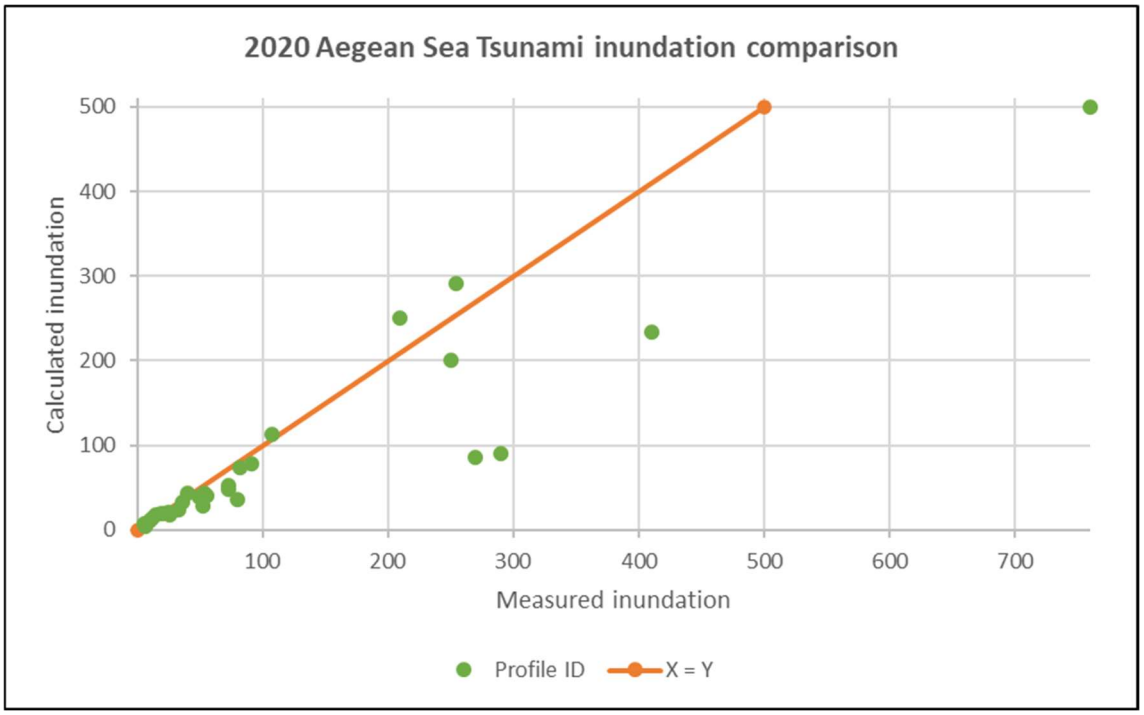

Figure 3.15 - Graph of the inundations measured and calculated using equation 3.1, for the control of the slopes measured by the transects for the 2020 Aegean Sea Tsunami.

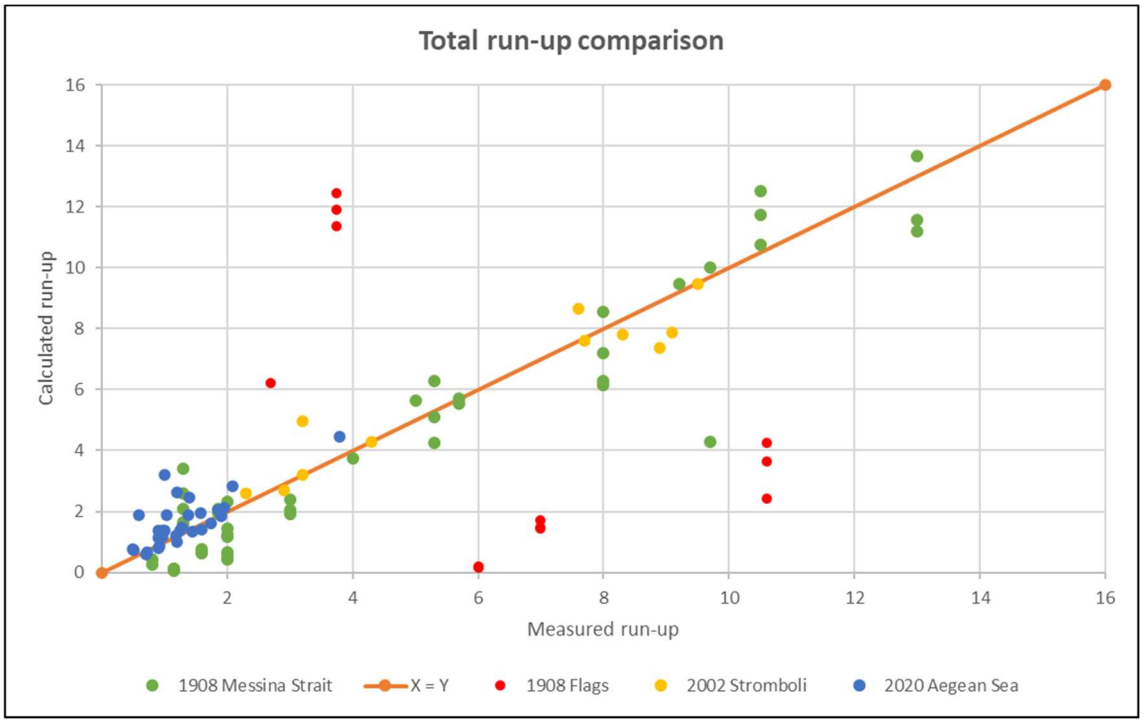

Figure 3.16 - Graph of the inundations measured and calculated using equation 3.1, for the control of the slopes measured by the transects for all the events.

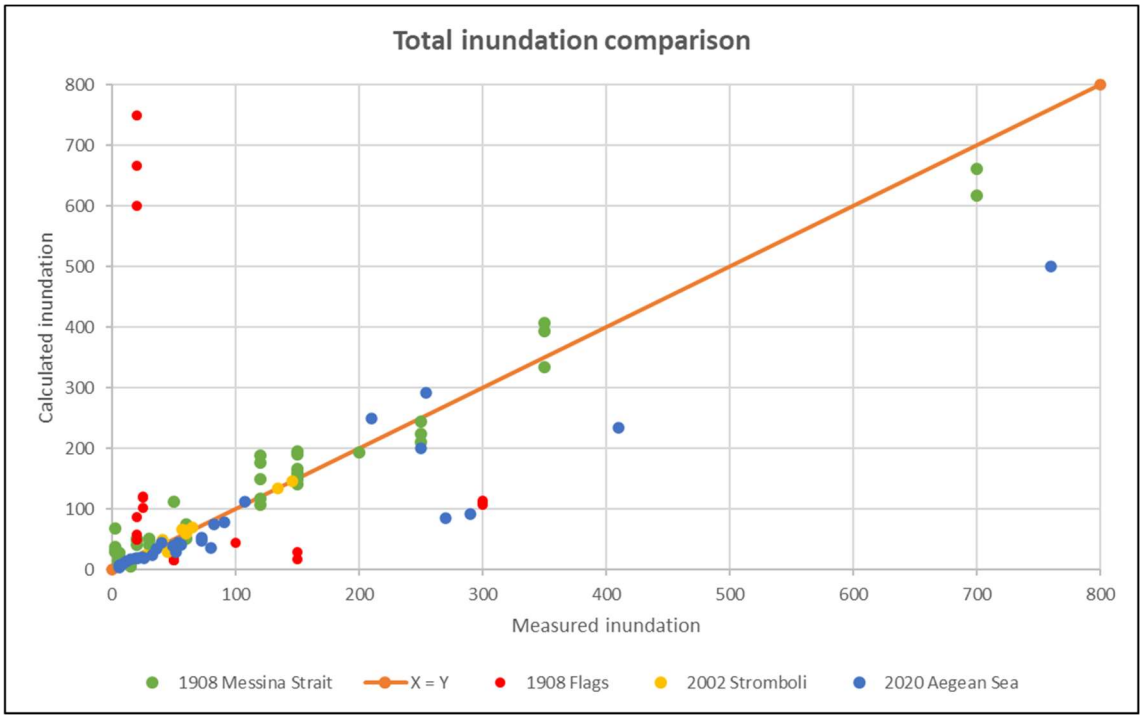

Figure 3.17 - Graph of the inundations measured and calculated using equation 3.1, for the control of the slopes measured by the transects for all the events.

In Figure 3.16 and 3.17, we report all the testing results in the same graph. Overall, the results demonstrate that the computational model provides results generally consistent with observations, even if some specificities due to local

peculiarities may be missed. This was expected, considering that each area is modelled with only two averaged parameters. Since our general goal is to relate macroscopic intensity with overall physical parameters, this level of accuracy is considered sufficient to our aims, and potential uncertainty will simply add uncertainty on the developed regression. Therefore, the complete dataset, without the flags, obtained from the extension of the physical parameters is considered in input to the empirical model to study the correlation between macroscopic intensity of the tsunami and its physical parameters, as discussed in the next Chapter.

4 Developing and testing a relationship between wave height and macroscopic tsunami intensity

4.1 Regression analysis and relative uncertainties – Orthogonal Distance Regression

One of the most common methods for estimating parameters of a model (e.g. a linear regression) to a dataset is the ordinary least-square method (OLS). To use the OLS, some conditions must be fulfilled, including that the uncertainties in the independent variable are negligible with respect to the ones on the dependent variable. In the general case, whenever a clear prevalence of the uncertainty cannot be established, OLS may result not appropriate.

When both the independent and dependent variables are subject to normally and independently distributed measurement errors (errors-in-variables), the estimation of the regression parameters may be based on the so-called generalised orthogonal regression (GOR), also called orthogonal distance regression (ODR) or Deming regression. This statistical approach minimises the weighted distance between the fitting line and each data point along a line that is inclined proportionally to the ratio between the variances of the two variables. It is more complex than OLS and requires to set the ratio between the variances of the measurement errors on the two variables, usually indicated with λ. It is mainly used in clinical chemistry to test equivalence between laboratory instruments, but it has also been applied in geophysics, especially in seismology (Castellaro et al., 2006; Castellaro & Bormann, 2007; Gomez-Capera et al., 2007; Faenza & Michelini, 2010; Lolli & Gasperini, 2012; Das et al., 2013; Cataldi et al., 2021; Pallavi et al, 2022).

A particular case occurs when λ cannot be evaluated and it is arbitrarily set to 1 (Castellaro et al., 2006). This case is sometimes called simple orthogonal regression (SOR) and the orthogonal distance between the line and the points is minimised.

When both variables present uncertainties, a fitting using ODR is more appropriate, indeed the importance of this model lies in the fact that it furnishes an approximation of real-world situations (Fuller, 1987). As demonstrated by Boggs et al. (1988): 'ODR never performs appreciably worse than OLS and often

performs considerably better'. In addition, orthogonal regression allows least-squares data fitting to be extended to problems with independent variables that are not known exactly (Boggs et al., 1988). This is common in geophysics, thus it has been shown that orthogonal regression leads to a better fitting, even in the Simple condition (SOR is equivalent to GOR with $\lambda = 1$) (Castellaro et al., 2006; Castellaro & Bormann, 2007; Gomez-Capera et al., 2007; Faenza & Michelini, 2010; Lolli & Gasperini, 2012). In addition, without making assumptions about the negligibility of the uncertainty of one variable, the relation becomes immediately invertible (Gomez-Capera et al., 2007).

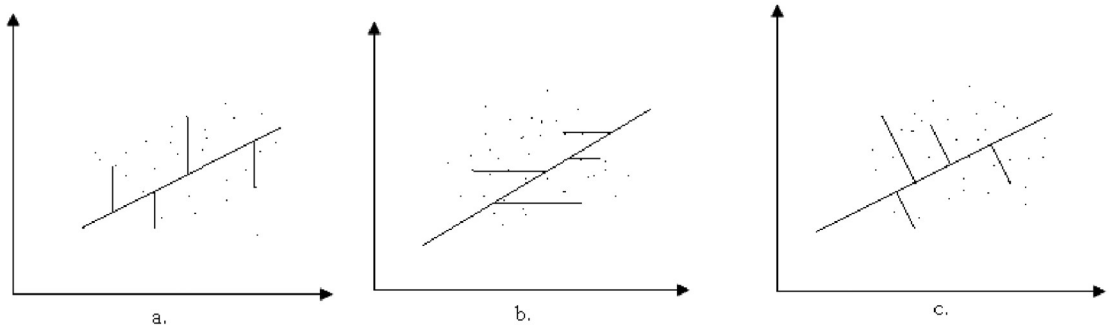

Figure 4.1 – Residuals that are minimised (the square of them) in the
- a.,b.) ordinary least-square (OLS) a.) vertical residuals, dependent variable y, variable x without associated error; b.) horizontal residuals, independent variable y without associated error;
- c.) orthogonal regression (OR). From Leng et al. (2007).

For tsunami intensity as well as for the tsunami physical measures discussed in this thesis, especially for old events like the Messina Strait tsunami that occurred over a century ago, it is impossible to have a precise estimation of the errors on the variables, however it is possible to assume that the ratio between them is constant, since they are both directly proportional to the time elapsed since the event occurred.

For historical tsunamis, intensities are assigned *a posteriori*, sometimes many years or even centuries after the event, relying only on historical documents and photographic evidences or witnesses accounts. Usually, the description of the effects on the human environment is the only available witness. Measures of the physical parameters are extremely rare for historical tsunamis. It is useful to use a cross-referenced approach, if it is possible, but it may happen that they also include eye-witness accounts, in addition to the actual measurements.

For recent tsunamis, intensities can be assigned at the same time as the event and can be reviewed many times using video materials or photographs, reducing significantly the uncertainty. However, also the specific physical

measurements can be better measured, evaluated and discussed by researchers and reporters in the locations.

It should also be taken into account that the resolving power of intensity scales, related to the number of degrees in the scale, allows for overlapping intervals between two adjacent degrees, this results in balanced intensity ratings.

Therefore, it is possible to assume, as first approximation, that the ratio λ may be roughly constant for both historical and more recent events.

This analysis proposes, as its primary objective, the definition of an empirical relationship between the wave height at the coast with local intensities of historical tsunamis. The aim is to make direct use of this regression line to estimate wave height from intensity. Interestingly, the use of orthogonal regression allows the problem to be inverted, that is to estimate the intensity from the wave height. However, this situation is rare in historical documents: it is very unlikely to have a numerical value instead of a qualitative description of the wave impact.

To perform the statistical analysis, the data prepared in Chapter 3 were processed using a specific function for Deming regression provided by Hall (2022), in the MATLAB environment. This computational function is based on the work of Jensen (2007), which provides the derivative of maximum likelihood estimates for the Deming regression model for slope, intercept and variance.

The mathematical model $y_i = \alpha + \beta x_i$ describes a linear relationship between two variables x_i and y_i. In linear regression with observations subject to additive random variation on both x and y and observed values for individuals $(x_i\,,\, y_i)$, $i = 1,\ \ldots, n,$ a model may be written:

$$(Y_i, X_i) = (y_i, x_i) + (e_i, u_i) \tag{4.1}$$

with:

$$X_i = \ x_i + u_i \tag{4.2}$$

$$Y_i = y_i + e_i = \alpha \ + \ \beta x_i + e_i \tag{4.3}$$

where (Y_i, X_i) is observed; (y_i, x_i) are the true values of respectively the dependent variable and the independent variable; e_i and u_i denotes the measurement errors. Measurement errors are assumed independent and normally distributed, with mean zero and with their own variance: $u_i \sim N(0, \sigma_u^2)$, $e_i \sim N(0, \sigma_e^2)$. The initial assumption for Deming regression or general orthogonal regression (GOR) is that λ, the ratio between the variances of the errors in measurements, is known:

$$\lambda = \frac{\sigma_e^2}{\sigma_u^2} \tag{4.4}$$

If the computation is made setting the value of λ to 1, we obtain a simple orthogonal regression (SOR), as previously described.

The differentiation of the log-likelihood function provides:

$$\hat{\alpha} = \underline{Y} - \underline{X}\hat{\beta} \tag{4.5}$$

$$\hat{\beta} = \frac{m_{yy} - \lambda m_{xx} + \sqrt{(m_{yy} - \lambda m_{xx})^2 + 4\lambda m_{xy}^2}}{2m_{xy}} \tag{4.6}$$

$$\hat{x}_i = \frac{\lambda X_i + \hat{\beta}(Y_i - \hat{\alpha})}{\lambda + \hat{\beta}^2} \tag{4.7}$$

where m_{xx} and m_{yy} are the sample variance of x and y and m_{xy} is the sample covariance between x, y and they are the elements of the sample covariance matrix.

$$m_{xx} = \frac{1}{n-1}\sum_{i=1}^{n}\left(X_i - \underline{X}\right)^2 \tag{4.8}$$

$$m_{yy} = \frac{1}{n-1}\sum_{i=1}^{n}\left(Y_i - \underline{Y}\right)^2 \tag{4.9}$$

$$m_{xy} = \frac{1}{n-1}\sum_{i=1}^{n}\left(X_i - \underline{X}\right)\left(Y_i - \underline{Y}\right) \tag{4.10}$$

The variance of the model obtained maximising the log-likelihood function has the form (Jensen, 2007):

$$\hat{\sigma}^2 = \frac{\lambda \sum_{i=1}^{n}(X_i - \hat{x}_i)^2 + \sum_{i=1}^{n}\left(Y_i - \hat{\alpha} - \hat{\beta}\hat{x}_i\right)^2}{2\lambda(n-2)} \tag{4.11}$$

where $(n-2)$ is used for unbiased estimate since there are $(n+2)$ parameters to consider, hence the degrees of freedom are $2n - (n+2) = n - 2$.

The variance of the model can be also calculated following the formulation discussed in Fuller (1987):

$$\hat{\sigma}_F^2 = \frac{\sum_{i=1}^{n}[\,Y_i - \underline{Y} - \hat{\beta}\left(X_i - \underline{X}\right)]^2}{(n-2)} \tag{4.12}$$

obtaining:

$$\hat{\sigma}_F^2 = \frac{(n-1)\left(\lambda + \hat{\beta}^2\right)\hat{\sigma}_u}{(n-2)} \tag{4.13}$$

where:

$$\hat{\sigma}_u = \frac{m_{yy} + \lambda m_{xx} - \sqrt{(m_{yy} - \lambda m_{xx})^2 + 4\lambda m_{xy}^2}}{2\,\lambda} \tag{4.14}$$

In the following, we always quantify the variance with both methods, always obtaining consistent results.

Here, the linear model is built between intensity and the natural logarithm of the wave height. This is similar to the approach followed for the seismological parameters by Faenza and Michelini (2010). In the following subsection, we report first, the 12-grade intensity scale (P-I) proposed by Papadopoulos & Imamura (2001), that we chose as the reference intensity scale. The same results adopting the intensity scale (S-A) proposed by Sieberg (1927) and modified by Ambresys (1962) are reported in Appendix B.

First, we check the effective correlation between the two parameters. In Table 4.1, we report the Pearson correlation coefficient *R* and the relative *p-value*, as evaluated through Matlab's corrcoef() (MathWorks, 2022). In all cases, a strong correlation was found. The p-values are relative to the null hypothesis of no correlation, and show negligible values for both the Messina and Aegean events. The hypothesis of no correlation cannot be rejected only in the case of Stromboli, probably due to the very limited range of intensity covered in this event. Also combining the events, including or excluding the highly uncertainty flagged observations, very high correlation coefficients are found, with very low p-values.

	R	p-value
1908 Messina Strait	0.75	< 0.001
2002 Stromboli	0.32	0.22
2020 Aegean Sea	0.86	< 0.001
With flagged data	0.77	< 0.001
Without flagged data	0.82	< 0.001

Table 4.1 - Values of R, the Pearson correlation coefficient and P the p-value.

The regression lines obtained, specifically for each tsunami event, are shown in the graphs [Intensity, Wave Height] below, comparing SOR with OLS for the three tsunami analysed events separately. To provide a reference to the uncertainty on the model, we also report the lines corresponding to +/- $\hat{\sigma}$ from eq. 4.11 and the lines corresponding to +/- $\widehat{\sigma_F}$ from eq. 4.13, where distance is evaluated orthogonally to the regression line as in Figure 4.1c. In particular:

- the 1908 Messina and Reggio Calabria tsunami results are reported in Figure 4.2,
- the 2002 Stromboli tsunami results are reported in Figure 4.3,
- and the 2020 Aegean Sea tsunami results in Figure 4.4.

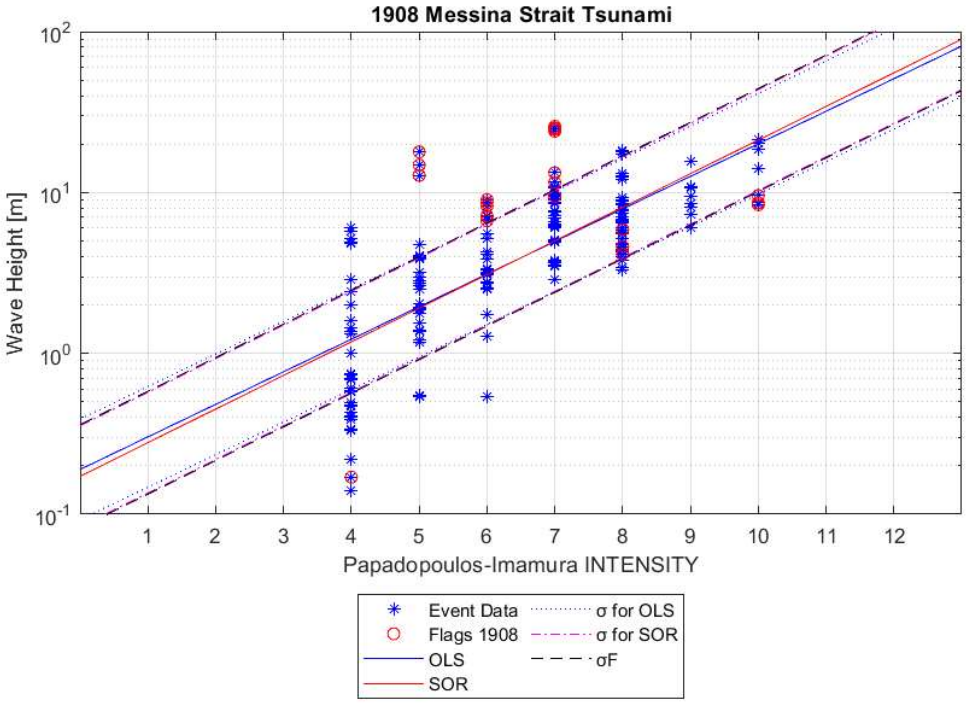

Figure 4.2 - Graph [Intensity - Wave height on shoreline] for comparison of regression methods for the 1908 Messina and Reggio Calabria tsunami.

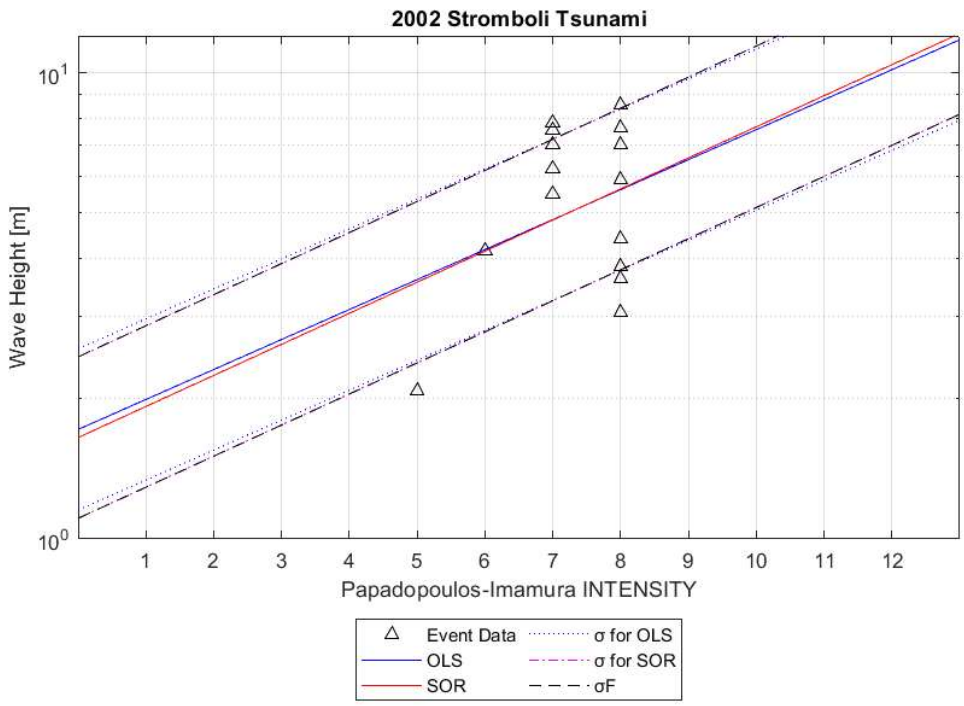

Figure 4.3 - Graph [Intensity - Wave height on shoreline] for comparison of regression methods for the 2002 Stromboli tsunami.

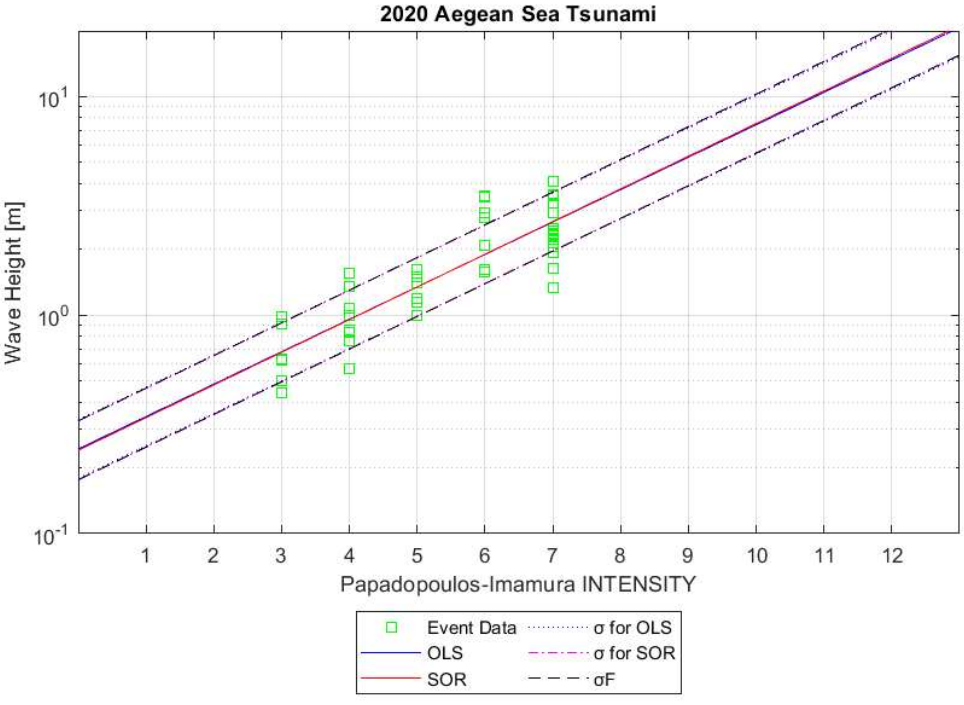

Figure 4.4 - Graph [Intensity - Wave height on shoreline] for comparison of regression methods for the 2020 Aegean Sea tsunami.

The graphs presented show reliable linear regressions. Notably, the results for the recent 2020 Aegean sea tsunami (Figure 4.3) show a small dispersion, demonstrating that the model adopted in Chapter 3 is indeed able to catch the average physical intensity at the target, which well correlates with the macroscopic tsunami intensity. The 1908 Messina Strait event (Figure 4.2) shows a very good correlation too, simply with observations that are more dispersed than for the previous case. There is a point accumulation value for Intensity 4. As in Chapter 3, also here the flagged data are generally at the extremes of the distribution. For the 2002 Stromboli event, the intensity variability is lower (only four intensity levels), but the regression results are adequate. No significant differences are evident between OLS and SOR.

In Figures 4.5 and 4.6 we report the relationship obtained merging all the three datasets. In particular, we present the results:

- Considering the points marked with a flag (Figure 4.5),
- Not considering the flagged points (Figure 4.6).

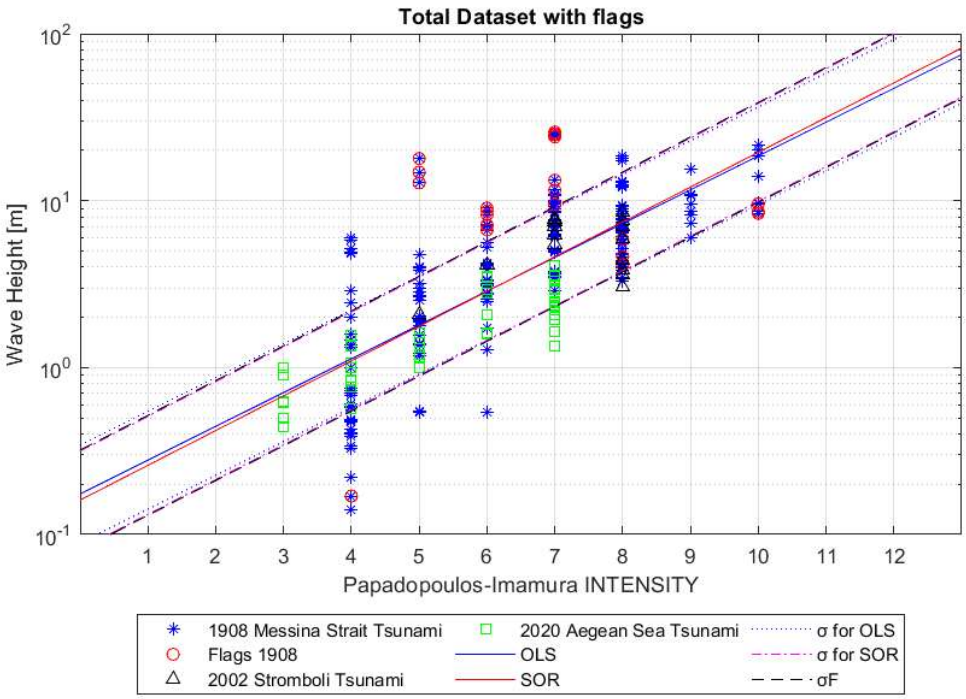

Figure 4.5 - Graph [Intensity - Wave height on shoreline] for comparison of regression methods for the total dataset. In this case, the input values for the calculation of the regression parameters also included the points marked with the Flag.

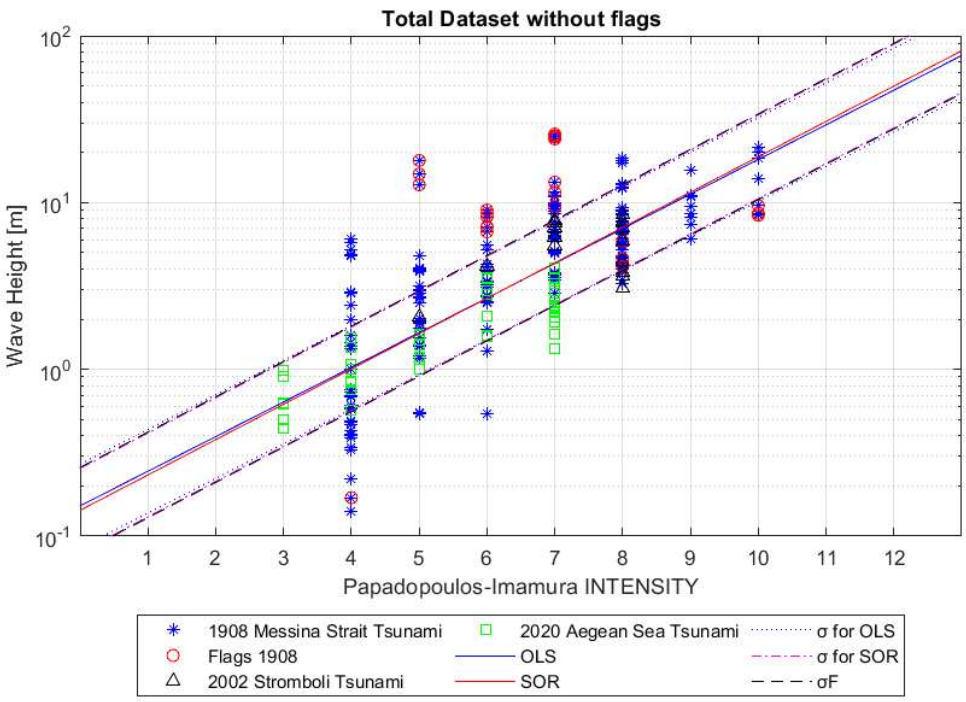

Figure 4.6 - Graph [Intensity - Wave height on shoreline] for comparison of regression methods for the total dataset without considering the points marked with the Flag.

Combining the databases (Figure 4.5 and Figure 4.6) results in a dataset that covers a large range of intensities (3 to 10). No significant differences can be appreciated between ordinary least squares regression (OLS) and orthogonal regression (SOR) for both graphs, nor specific trends related to a specific event with respect to the others. The only exception can be seen observing Figures 4.5 and 4.6, where it can be seen that, at least for intensity 7, the data of the 2020 Aegean Sea event seem slightly smaller than those of the Messina Strait event. However, this may be related to the fact that this intensity is the largest for the Aegean event, and thus a sort of saturation effect is observed.

To produce a more quantitative comparison, in Table 4.2, we report all the numerical results for all the considered cases. It can be seen that the numerical values of each event or dataset considered are very similar between the two types of regressions. The error estimates on the parameters are generally larger for SOR, with the largest relative errors for the Stromboli tsunami. This is probably due to the fact that a jackknife analysis is implemented, consisting in practice in a leave-one-out strategy for the definition of the variance (Hall, 2022). Considering that we expect the existence of a unique relationship, we expect that, within uncertainty, the regression parameters should not be significantly

different. To this end, SOR estimates appear more consistent, as all confidence intervals for both parameters are very close or cross to each other.

Finally, we note that the two approaches to estimate the overall variance on the models discussed in the previous section are always equal to the second decimal place in the two cases (for OR both computed errors).

Database	Type of regression	α			β			σ	σF
1908 Messina Strait Tsunami	OLS	-0.72	±	0.08	0.20	±	0.01	0.31	
	SOR	-0.76	±	0.10	0.21	±	0.01	0.31	0.31
2002 Stromboli Tsunami	OLS	0.23	±	0.37	0.06	±	0.05	0.17	
	SOR	0.22	±	0.84	0.07	±	0.11	0.17	0.17
2020 Aegean Sea Tsunami	OLS	-0.61	±	0.07	0.15	±	0.01	0.13	
	SOR	-0.62	±	0.07	0.15	±	0.01	0.13	0.13
Total Dataset With Flags	OLS	-0.76	±	0.07	0.20	±	0.01	0.29	
	SOR	-0.79	±	0.07	0.21	±	0.01	0.29	0.29
Total Dataset Without Flags	OLS	-0.82	±	0.06	0.21	±	0.01	0.25	
	SOR	-0.84	±	0.07	0.21	±	0.01	0.25	0.25

Table 4.2 - Summary of parameters (α and β) estimated from ordinary least squares regression (OLS) and orthogonal regression (SOR) models, with associated uncertainties, for intercept, slope, and for the entire model (σ). SOR also includes the uncertainty proposed by Fuller (1987) (σ_F).

For the combined datasets, both from the graphs and the summary table, it can be observed that the dominant event for the regression is the 1908 Messina Strait event, even if as a single event it has high errors. This is due to the fact that this event is connected to more observations than the others. It can also be seen that the regression lines with and without flags are almost identical, but the associated error is reduced when they are excluded.

Based on this analysis, we consider the orthogonal regression on the total dataset deprived of flagged data as the best choice. The selected relationship takes the form:

$$log_{10} H = -0.84(\pm 0.07) + 0.21(\pm 0.01)I_{PI} \qquad \sigma = 0.25 \qquad (4.15)$$

The distribution of the residuals (evaluated orthogonally to the linear trend) is reported in Figure 4.7, showing that this relationship is nicely centred on the data, with residuals that are well distributed around 0. In Figure 4.8, we report the residuals as a function of the intensity. Also in this case, no specific trends are observed, showing that the linear regression looks adequate to fit the dataset.

A final stability check of the regression obtained in eq. 4.15 is made by considering the (few) OPs where both the macroscopic intensity and the wave height values were measured, considering all the data in ITED with these characteristics (13 points, 10 of which from Messina) with the addition of Aegean Sea event (4 points). The results are reported in Figure 4.9, which shows that, despite the small amount of data providing the wave height, a good overall consistency between the observations and the relationship is found. The data at intensity 7 is the most remote and refers to the Gioia Tauro OP that occurred in 1783. The OP associated with intensity 7 shows 20 m as the wave height datum, which is significantly shifted from the proposed trend. This point refers to the observation that took place in Gioia Tauro in 1783. The reason for this shift may be due to the fact that the event occurred more than two centuries ago, so the record may not be accurate and the single datum may be less reliable. Another hypothesis is that the day of the observation was erroneously switched because an earthquake-induced landslide occurred the following day, producing a tsunami with devastating effects. The effects of this event are associated with intensities as high as grade 9 and 10 (Papadopoulos-Imamura) (Graziani et al., 2006).

The linear regression of eq. 4.15 is the relationship between macroscopic Papadopoulos-Imamura intensity scale and the physical reference parameter

(wave height along the coast), the main focus of this thesis. It was used in Chapter 5 to estimate wave height values at points in ITED without numerical data and only associated with an intensity.

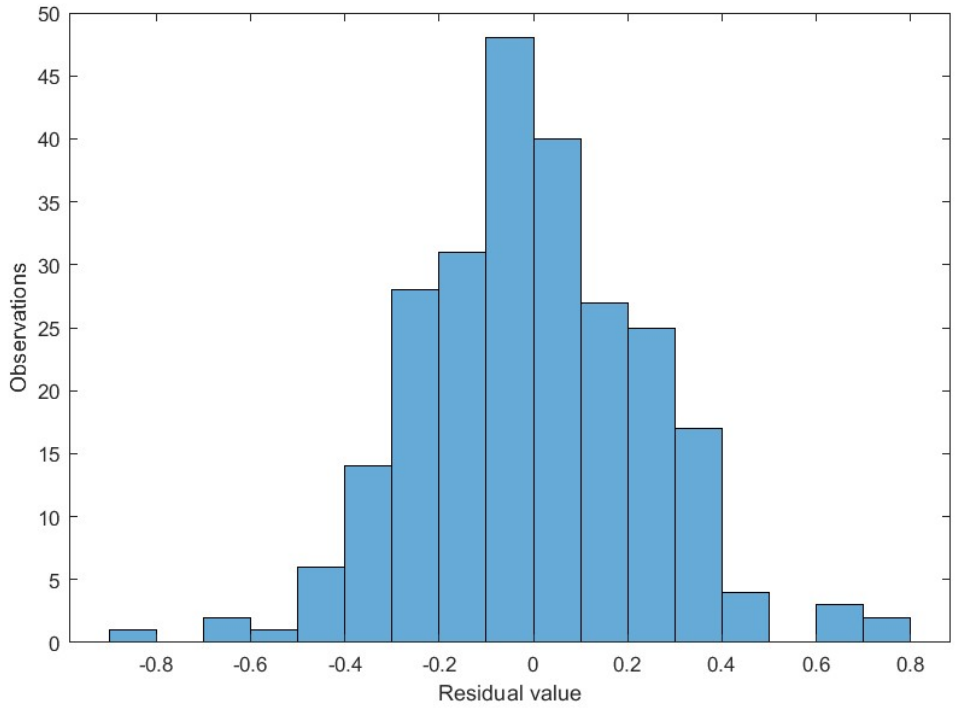

Figure 4.7 - Distribution of the orthogonal residual.

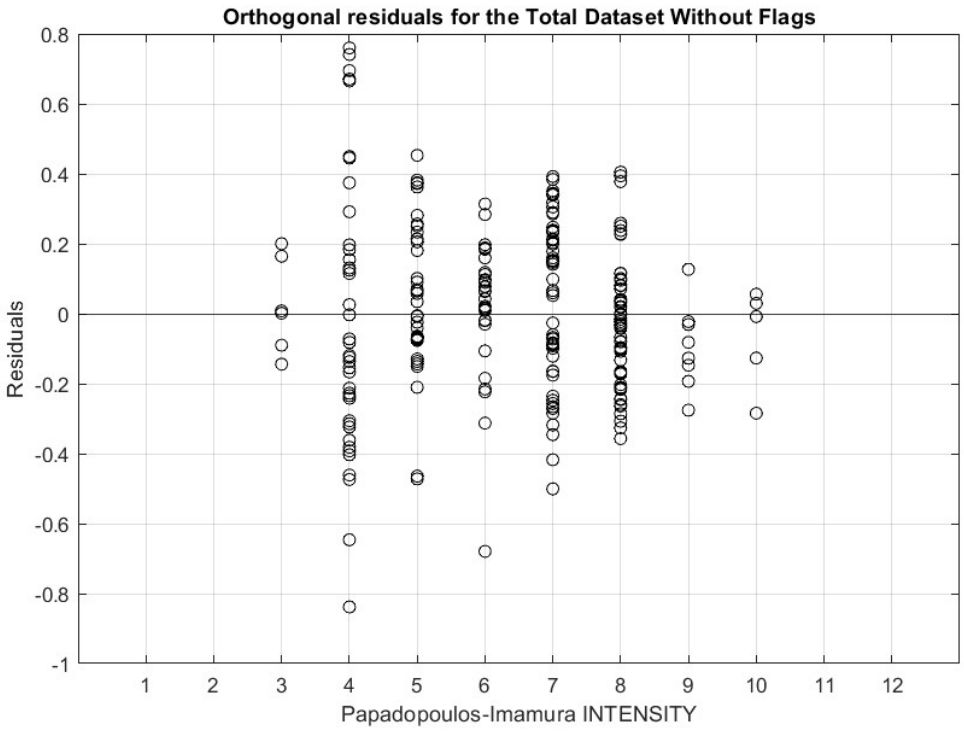

Figure 4.8 - Orthogonal residuals as a function of the macroscopic intensity.

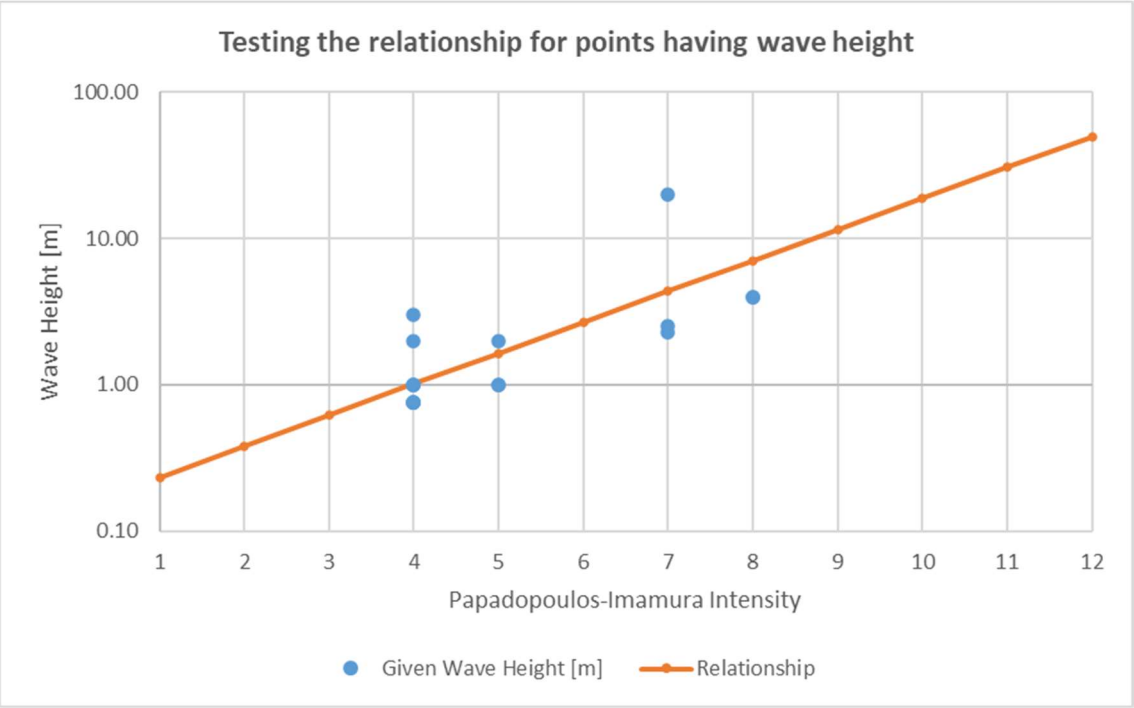

Figure 4.9 - Graph showing the ITED observation points that have wave height as a datum compared with the obtained report.

In Appendix B, graphic and numerical results are provided for the analysis performed considering the intensities of the OPs on the Sieberg-Ambraseys scale. It can be seen that, since the scale has only 6 degrees, the points are distributed over the majority of them (for the total dataset from degree 2 to degree 6. In the case of Stromboli only one intensity value is different from 5, making the results for that single event inconsistent. Also in the case of this intensity, it can be seen that the reference regression considered (SOR for the total dataset without flags) is nicely centred on the data because the residuals are well distributed around 0.

4.2 Stability of the regression to alternative variance ratios

To verify that the choice of variance ratio $\lambda = 1$ (equal variances of the measurement errors) was appropriate, a comparison was made with different values. Introducing Chapter 4, it was explained that the choice of $\lambda = 1$ was adequate to describe the error ratio of both historical and modern events, so the simple orthogonal regression (SOR) model was used with this assumption. By varying this ratio, the general orthogonal regression (GOR) can be used instead,

simulating the impact of assuming a larger/smaller variance of one of the variables.

When considering values less than one, it is assumed that the error on the y (wave height) is smaller than that on the x (intensity). Whereas, when considering a ratio above 1 (error variance on the y larger than that on the x) moving towards the ordinary least-square OLS. Figure 4.10 shows the two cases analysed, considering λ of a lower order of magnitude ($\lambda = 0.1$) and of a higher order of magnitude ($\lambda = 10$).

The most significant difference is found for $\lambda = 0.1$, where the GOR accentuates the deviation from OLS already observed comparing SOR and OLS. In other words, the tendency is to increase the slope. However, this deviation results within the (large) uncertainty bounds of the SOR relationship. Instead, imposing $\lambda = 10$ results in an intermediate case between SOR and OLS, assuming a larger error on wave heights than on intensities but still not negligible. In this case, an almost perfect superposition between GOR and OLS is found for the best regression line. Instead, as observed in the previous section, there is an important difference between the estimated errors.

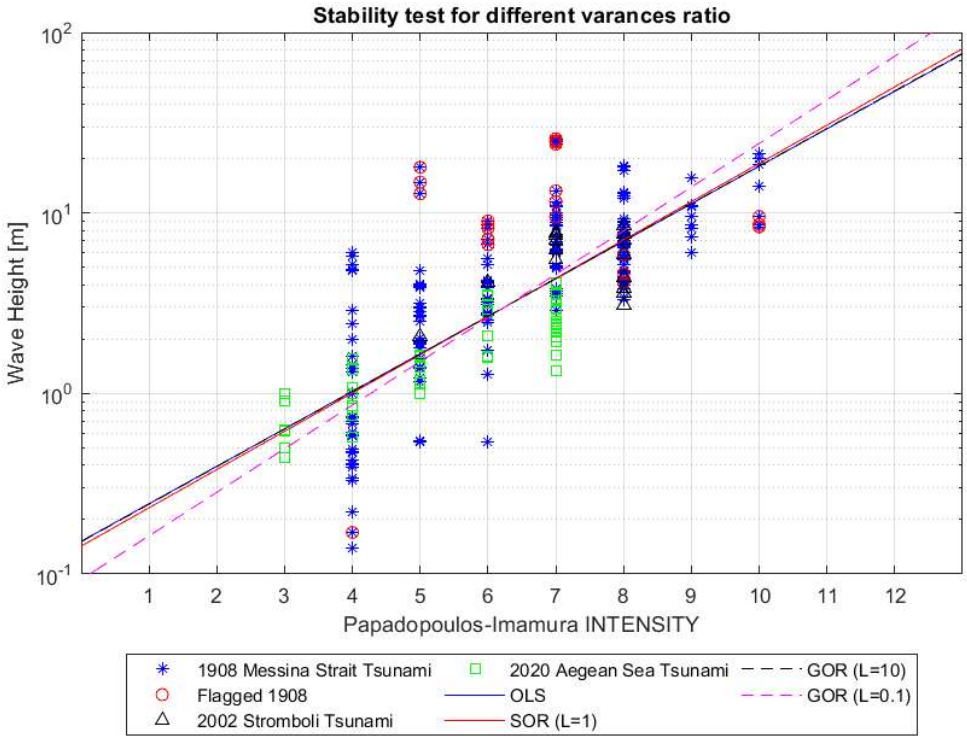

Figure 4.10 - General Orthogonal Regression with error variance ratio λ = 10 black dashed line and λ = 0.1 pink dashed line.

5 Application to the Italian dataset

Thanks to the historical catalogues, it is possible to have a summary of how many tsunamis occurred and where and how strong they impacted. It is possible to identify regions where attention should be focused with a perspective of risk analysis and evaluation of what the tsunamigenic sources might be. For this reason, existing databases are a fundamental tool and the possibility of relating the available data to others can be an additional tool.

Using the empirical relationship developed in this thesis, that is the linear regression reported in equation (4.15), it was possible to produce an explicit estimation of the wave height H for all the observation points in which it has been possible the assessment of the macroscopic intensity. Figure 5.1 shows the direct application of the intensity values and the respective wave heights obtained. In the graph, the points in red correspond to intensities XI and XII and were reported with a different symbol to indicate that they are extrapolated for larger intensity, as such intensities were not present in any of the observation points along the Italian coasts.

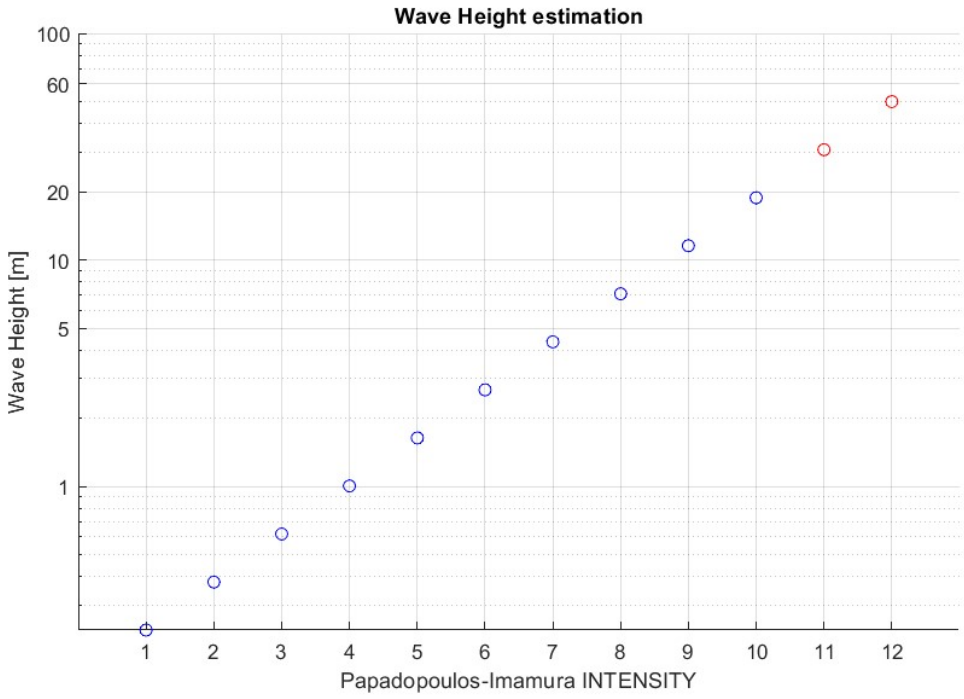

Figure 5.1 – Graph of direct application of the obtained relation to the ITED catalogue (I-X). The points in red (XI-XII) were added manually, as they were not present in the catalogue

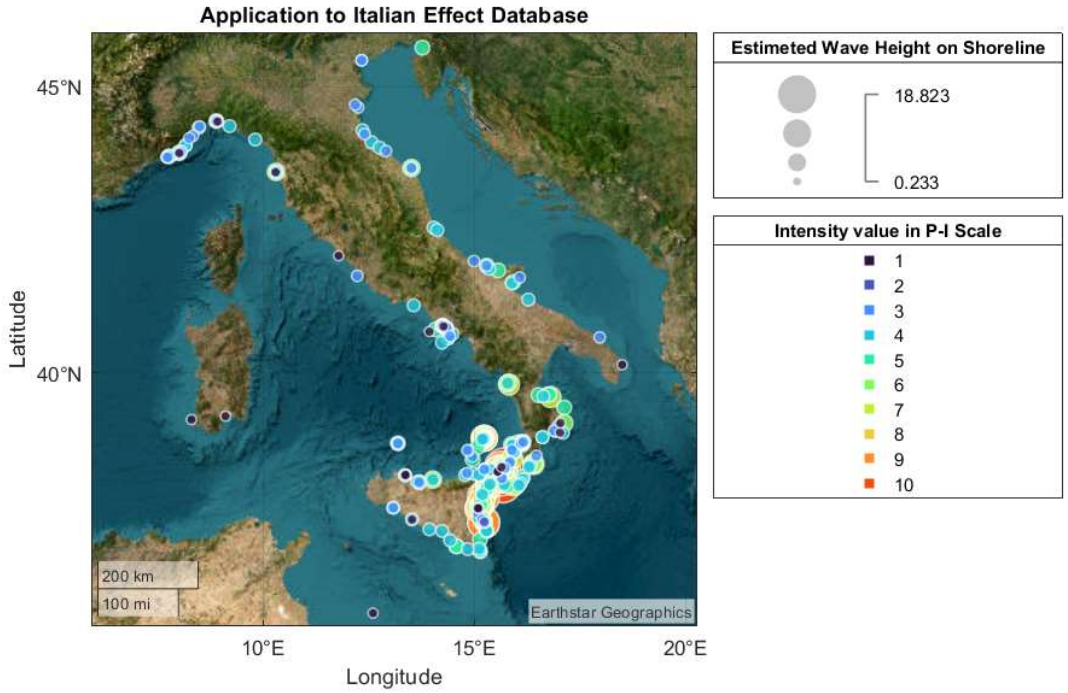

Figure 5.2 - Map displaying the application of equation (4.15) to the entire ITED dataset, converting all the intensity values within. The positions remained unchanged but an estimate of the wave height value obtained from the relationship is shown.

The map of Italy shown in Figures 5.2 displays all historical tsunami impact observation points on the Italian coast. The location and intensity data correspond to that provided by ITED (Maramai et al., 2019b), but the estimated wave height on the coast is also integrated. The distribution of the points is not homogeneous, in fact most of them are concentrated along the coasts of Sicily and Calabria because they are referred to the 1908 Messina Strait event. Multiple estimates for the same OPs are infrequent, since it is rare that multiple tsunami observations at the same location have been made and are catalogued.

Macroseismic studies nowadays are very advanced and allow us to describe the seismic history of a given place on a progressively smaller scale, to the point of assessing the seismic history of individual municipalities. A parallelism can be made to these studies: individual Italian seas have become the target area, producing a 'tsunami history' for each of them, both in terms of intensity and in terms of wave height on the estimated shoreline. The extremely important site specific seismic history produced from macroseismic intensities (Pezzella, 2021) is the reference on which the following tsunami history graphs are based. However, here they are produced at a larger scale, including entire seas. The choice of considering individual seas is made to stack the information from many OPs, as individual OPs generally have too few records. Individual seas have been used for this stacking as they can be considered, in many cases,

approximately isolated to each other. Tsunamis originating in one sea are, in most cases, recorded along the coasts of the same sea. Of course, there are cases where this may not occur, e.g. for 1908 some OPs are also present along the Tyrrhenian coasts of Sicily and Calabria.

The maps in Figures (5.3, 5.6, 5.9, 5.12) show the observation points of historical tsunamis for each Italian sea: Ligurian Sea (Figures 5.3), Tyrrhenian Sea (Figures 5.6), Ionian Sea (Figures 5.9) and Adriatic Sea (Figures 5.12).

Below the maps for each basin, two stem-graphs indicating the history of tsunamis for that sea are reported, respectively with the observed intensities (Figures 5.4, 5.7, 5.10, 5.13) and with the wave heights estimated from the relationship derived in Chapter 4 (Figures 5.5, 5.8, 5.11, 5.14). It can be seen that the historical distribution of tsunamis in the various Italian seas is homogeneous from 1600 to the present day, whereas before that only a few events are present in the Tyrrhenian and Ionian Seas. The intensities and estimated wave heights are low to intermediate for all observations for the Ligurian and Adriatic Seas, while for the Tyrrhenian and Ionian Seas, very high values are also observed, with relative wave heights estimated that reach over 18 m.

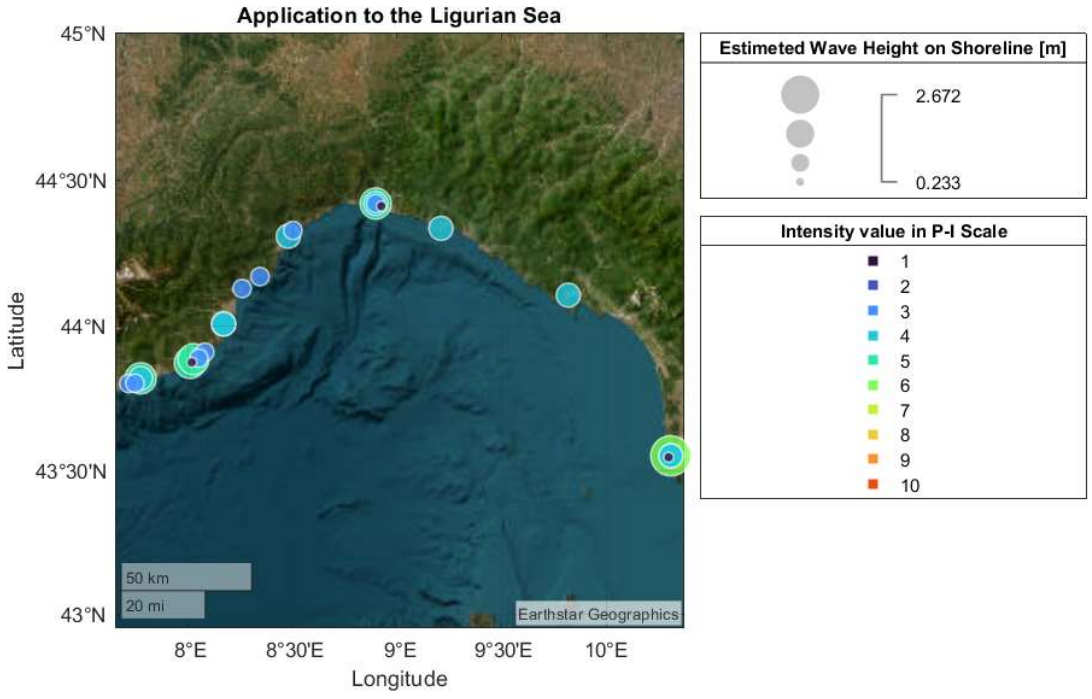

Figure 5.3

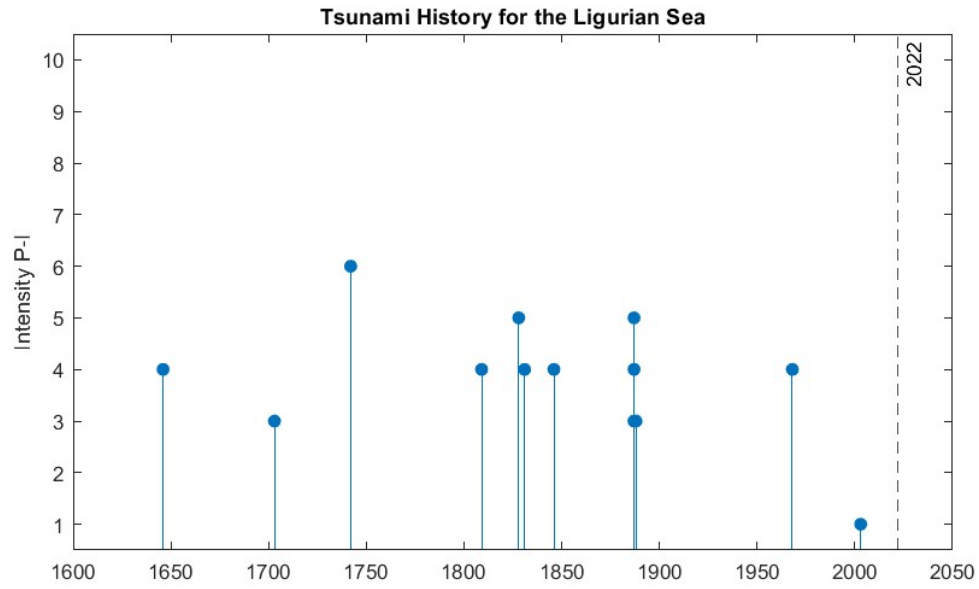

Figure 5.4

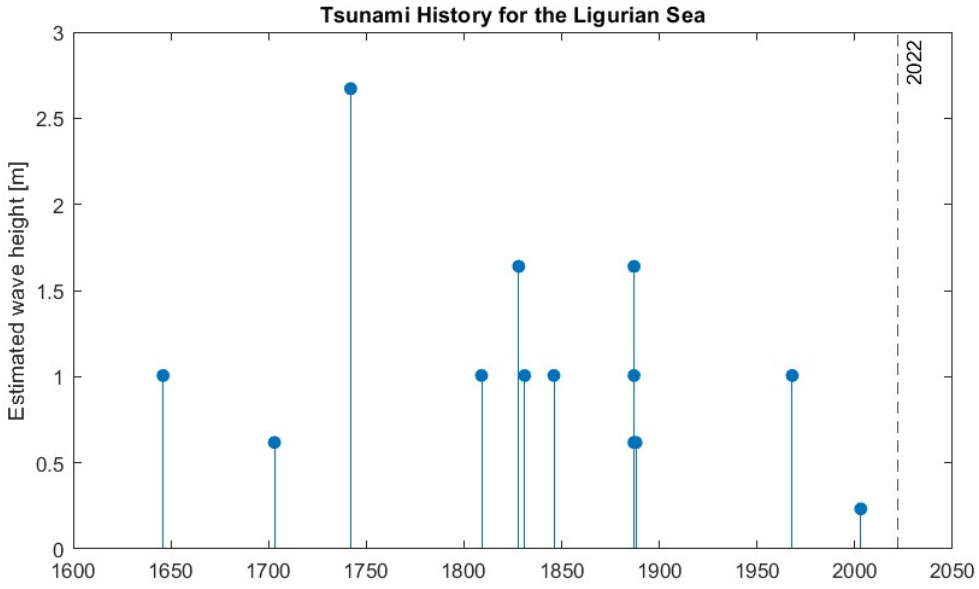

Figure 5.5

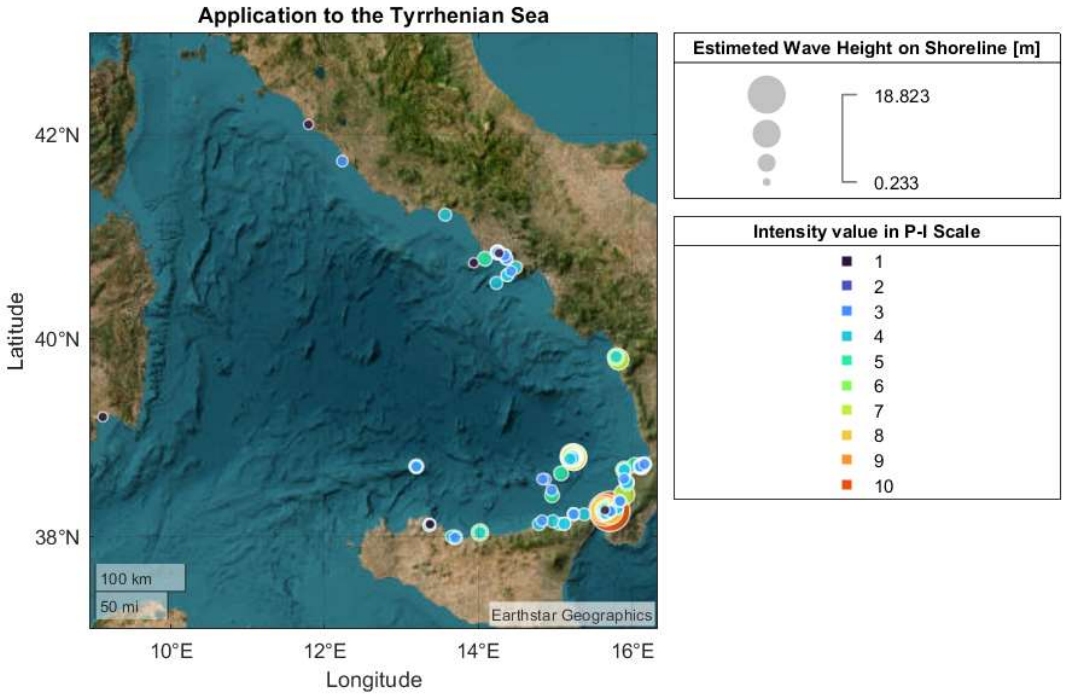

Figure 5.6

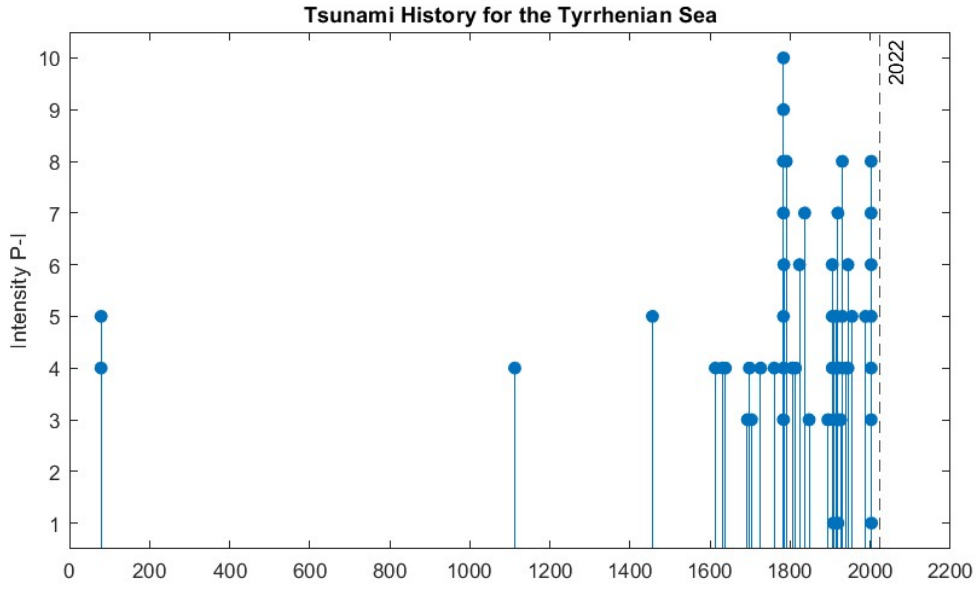

Figure 5.7

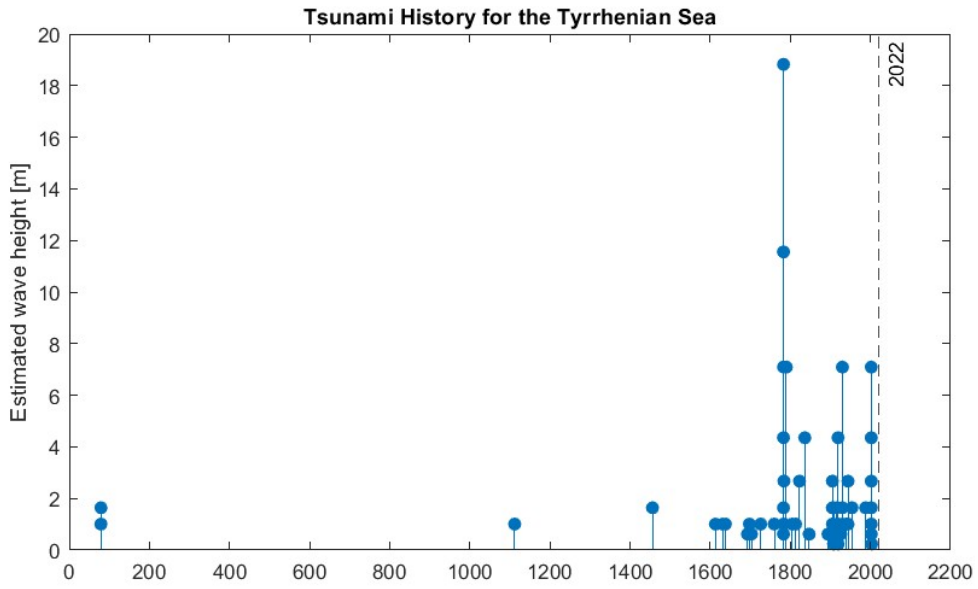

Figure 5.8

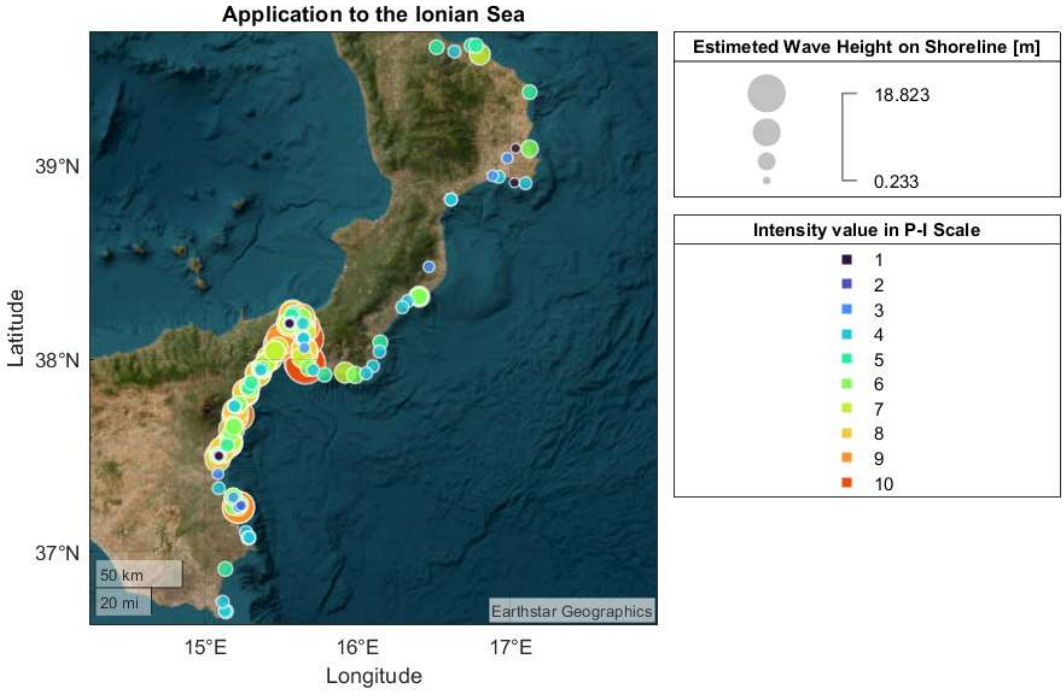

Figure 5.9

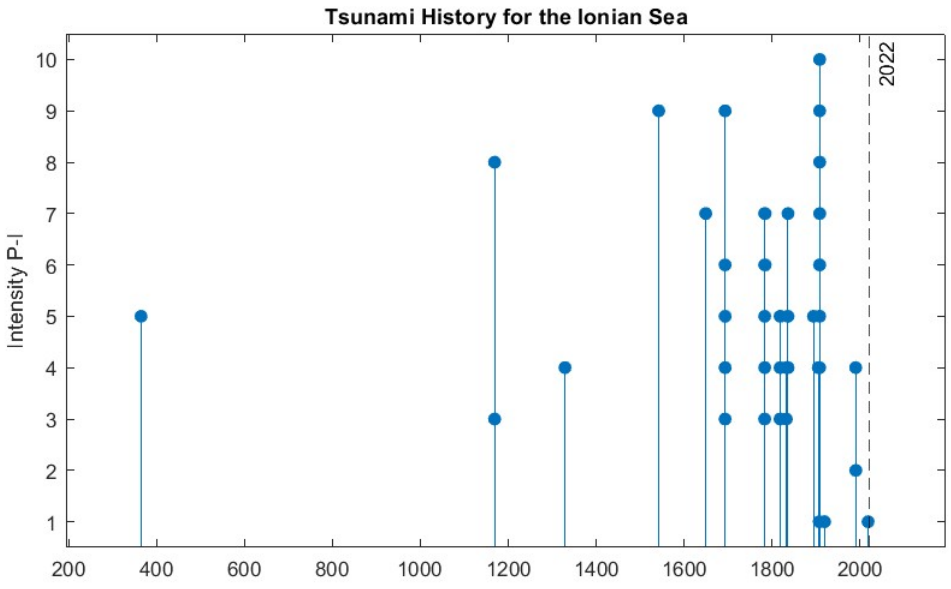

Figure 5.10

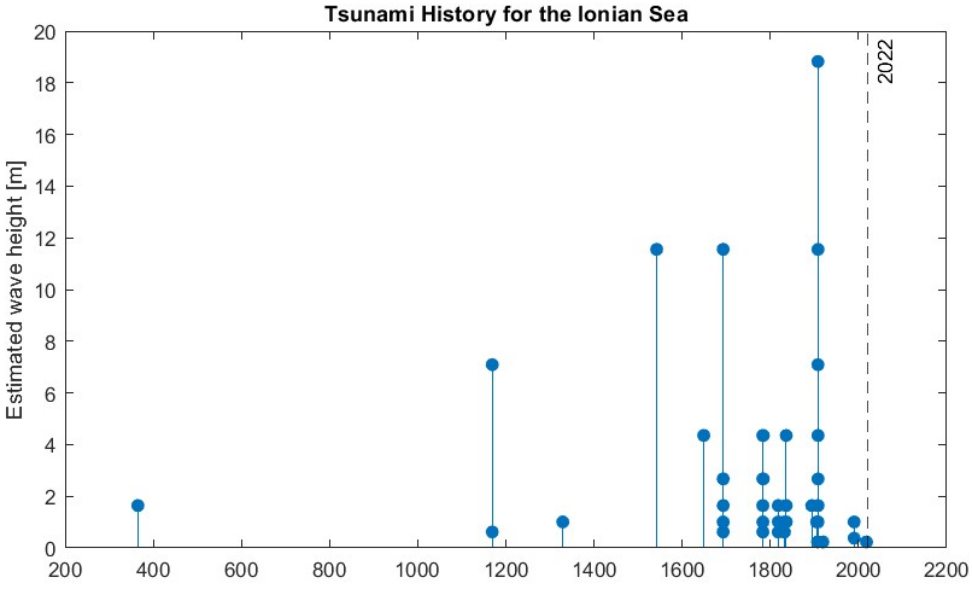

Figure 5.11

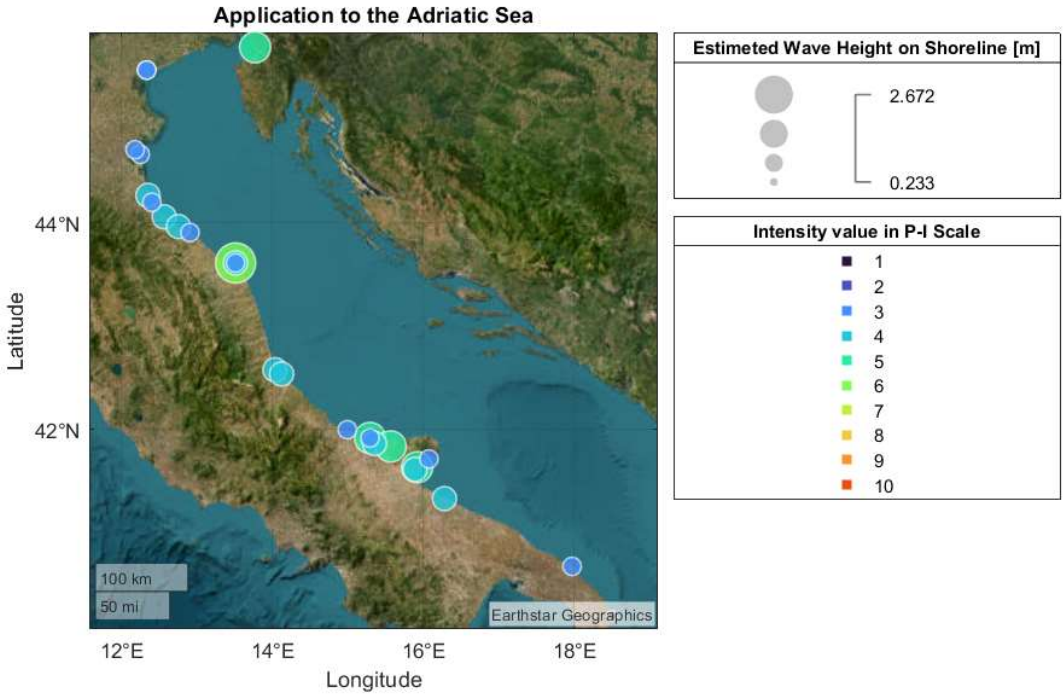

Figure 5.12

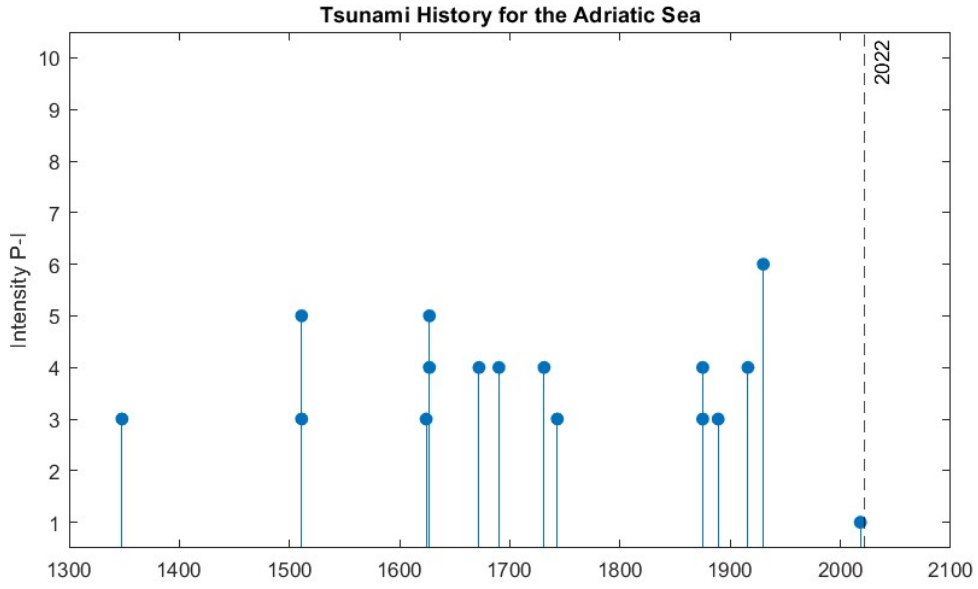

Figure 5.13

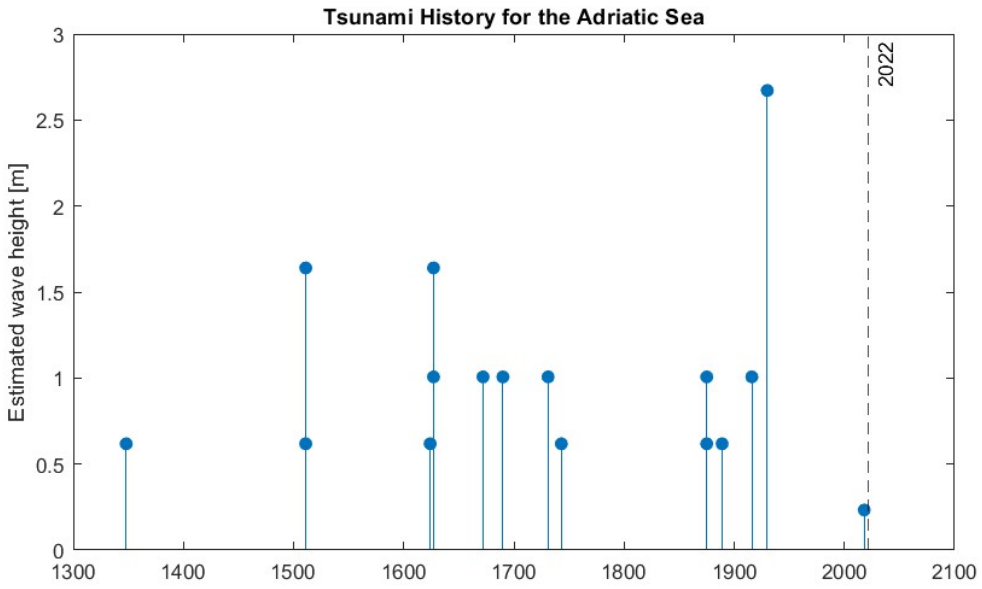
Tsunami History for the Adriatic Sea
Estimated wave height [m]
2022
0
0.5
1
1.5
2
2.5
3
1300
1400
1500
1600
1700
1800
1900
2000
2100

Figure 5.14

6 Conclusions

The primary goal of this thesis has been to derive an empirical relationship between tsunami physical parameters and macroseismic tsunami intensity. To this end, several steps were implemented.

The first step was to build up a sufficiently large dataset for deriving the relationship. We adopted a simple methodology to extend the existing databases by relating to each other the different types of tsunami observables. We selected three events with different sources to be analysed in detail, so that a more complete background could be obtained. The selected events were the 1908 Messina and Reggio Calabria tsunami, the 2002 Stromboli tsunami, and the 2020 Aegean Sea tsunami. Starting from official databases or post-event report papers, each tsunami observation of the selected events was analysed individually, assigning a slope value (where possible) and an average water flow resistance value to each. To this end, we adopted a parameter recently introduced in the literature, to characterise the roughness of the portion of land labelled as inundated: the roughness aperture. The estimation of these two parameters allowed us to derive from the original observation (e.g. inundation length) the other missing tsunami physical measures (e.g. run-up and wave height), completing the original dataset. Interestingly, the adopted procedure is general and it can be applied in a similar manner for any tsunami observation, as long as a quantitative observation of one physical parameter exists, and a sufficiently detailed assessment of mean slope and ground resistance on water can be made.

This extension served mainly to derive, for each observation considered, the wave height at the coastline, which is a stable physical reference parameter since it is independent of local onshore topographic effects and generally uniform for larger stretches of coastline than other inland parameters such as run-up or inundation length. The choice of the wave height on shoreline as the physical reference parameter was made also to match the proposed analysis with regional- or national-scale simulations and hazard quantifications, on which civil protection plans are based, which usually provide wave height or a closely related parameter as an output. Of course, in the future also other reference physical intensity measures may be considered, if this is found useful for some application.

To complete the information, to each observation point we associated a macroscopic tsunami intensity. When possible, the intensities, for each different

event, were obtained through databases, otherwise estimated on the base of field survey reports.

Wave height values were statistically analysed together with the tsunami intensity associated with the same observation points. The aim was to find a correlation between the two variables. At first, we found that intensity and the logarithm of the wave height are significantly correlated. To derive an empirical regression line, the statistical analysis was performed through the simple orthogonal regression model and compared with the ordinary least-square. The orthogonal regression model was chosen to find a robust and invertible relationship between wave height and intensity, following the recent literature dealing with the analogue issue in the seismological field.

The orthogonal regression technique was chosen as it allows for the inversion of variables by taking into account uncertainties on both by estimating the ratio of the variances of the errors. This is fundamental, considering that both wave height and tsunami intensity are affected by large uncertainties. Since information about the uncertainty of all observations was not available, we assumed an equal uncertainty on all data. For simplicity, we selected a ratio between the two variances equal to 1, and we tested the stability of the obtained regression line for alternative choices of the ratios. The analysis of residuals shows no significant trends, with an overall distribution centred and distributed around 0. This means that a linear regression results sufficient to satisfactorily model all the input data. The reliability of the found regression was discussed also for the individual events and in the cumulative graphs, providing consistent results.

Thanks to the relationship obtained, it was possible to derive a numerical estimate of the wave height at coastline in the Italian catalogue at all the observation points, including the ones where there is only an assigned intensity based on macroscopic effects. This made it possible to obtain, for example, a specific assessment of the 'tsunami history' of individual seas. This may represent in the future a very important source of information for the tsunami research, for example for evaluating and testing tsunami hazard analysis.

This study has several limitations. Compared to seismic databases, tsunami catalogues have a very reduced number of records. For Italy, most of the observations refer to events that occurred more than a century ago and are therefore associated with measurement/witness errors in the physical data and ambiguities in the current assignment of intensities, leading to large uncertainties. Furthermore, only a few events in the Italian database contain multiple observations. For these events, our study may allow for improving the

information about the specific sources, for example through inversion studies. However, all the new estimates, including the events with single or a few observations, may bring very relevant information for studies like long-term regional tsunami hazards analyses or for checking existing evacuation areas.

To obtain the relationship described in Chapter 4, only data in the range [3, 10] were used, in fact the highest intensities (11, 12 Papadopoulos-Imamura) are not present in the Italian catalogue and were not associated with the observations of the 2020 event in the Aegean Sea. This lack sets intensity value 10 as the limit of interpretation. The larger intensities are associated with very high wave height values, but there is no criterion to establish whether they are reasonable or not. On the other hand, even in the twelve-degree macroseismic scales, e.g. EMS-98, the 12 degree is defined in such a way as to describe the maximum conceivable effects, which cannot necessarily be observed in an earthquake. Thus the "working range" of all these scales tends usually to be from intensity 3 to intensity 10 (Grunthal, 1998) .

Topographic profiles were derived from Google Earth Pro. Google Earth was a very powerful tool because it quickly provides sufficiently accurate DTM (Digital Terrain Model) data of many geographical areas together with constantly updated satellite photographs. This combination was decisive for the choice of the GIS system over other available sources of information like GEBCO. However, some areas have discrepancies between the terrain model and the image, making it difficult or impossible to interpret the elevations for slope calculation. This problem occurred especially along the coasts of Greece and Turkey for the analysis of the 2020 Aegean Sea tsunami.

Another problem faced in defining topographic profile was the phenomenon of coastal erosion, which significantly influences a posteriori study of the impact of a tsunami as it varies the morphology of the land. For the 1908 event in the Messina Strait, the Calabria coast experienced this phenomenon in several locations.

In the future, it will be possible to improve the wave height estimations by improving the definition of these transects. The transects used here, which locate the observations, are saved and can be queried again on a more precise geographic information system, potentially including multiple local digital terrain models (DTM), which can reach very high resolutions. Another significant improvement may be obtained with a better definition of the roughness aperture parameter. Here, we used typical values at three discrete levels based on the averaged land cover of the area. In the future, a more careful evaluation of the impact of this parameter may be useful. Further research could

lead also to a more extensive tabulation of typical values characterising all types of land use and cover in a more detailed manner.

Finally, we have seen that single events with few data can complement datasets cumulating several events, but by themselves cannot represent a completely reliable and shareable regression, since they may be characterised, for example, by a small range of intensity as in the case of the 2002 Stromboli tsunami, leading to strongly biased results. In the future, there is the possibility of reinforcing the regression obtained by considering a greater number of events, relative to larger geographical areas (e.g. the entire Mediterranean Sea).

Bibliography

Amato, A., Bernardi, F., Cerase, A., Graziani, L., Lorito, S., Mele, F.M., Michelini, A., Perfetti, P., Piatanesi, A., Pintore, S., Romano, F., Selva, J., Stramondo, S., Tonini, R., Valbonesi, C., Volpe, M., Brizuela, B., 2018. Il Centro Allerta Tsunami (CAT) dell'INGV.

Ambraseys, N.N., 1962. Data for the investigation of the seismic sea-waves in the Eastern Mediterranean. Bulletin of the Seismological Society of America 52, 895–913. https://doi.org/10.1785/BSSA0520040895

Armigliato, A., Angeli, C., 2020. Analytical solutions for the run-up of long water waves excited by time-independent and time-dependent forcing.

Bakun, W.H., Wentworth, C.M., 1997. Estimating earthquake location and magnitude from seismic intensity data. Bulletin of the Seismological Society of America 87, 1502–1521. https://doi.org/10.1785/BSSA0870061502

Baptista, M.A., Miranda, J.M., 2009. Revision of the Portuguese catalog of tsunamis. Nat. Hazards Earth Syst. Sci. 9, 25–42. https://doi.org/10.5194/nhess-9-25-2009

Baratta, M., 1910. La catastrofe sismica calabro messinese (28 dicembre 1908). Società geografica italiana, Roma.

Barker, G., 2018. Chapter 18 - Pipe sizing and pressure drop calculations, in: Barker, G. (Ed.), The Engineer's Guide to Plant Layout and Piping Design for the Oil and Gas Industries. Gulf Professional Publishing, pp. 411–472. https://doi.org/10.1016/B978-0-12-814653-8.00018-7

Basili, R., Brizuela, B., Herrero, A., Iqbal, S., Lorito, S., Maesano, F.E., Murphy, S., Perfetti, P., Romano, F., Scala, A., Selva, J., Taroni, M., Tiberti, M.M., Thio, H.-K., Tonini, R., Volpe, M., Glimsdal, S., Harbitz, C.B., Løvholt, F., Baptista, M., Fernando, C., Matias, L., Omira, R., Babeyko, A., Hoechner, A., Gurbuz, M., Pekcan, O., Yalciner, A., Canals, M., Lastras, G., Agalos, A., Papadopoulos, G., Triantafyllou, I., Benchekroun, S., Jaouadi, H.A., Attafi, K., Abdallah, S.B., Bouallegue, A., Hamdi, H., Oueslati, F., 2018. NEAM Tsunami Hazard Model 2018 (NEAMTHM18): online data of the Probabilistic Tsunami Hazard Model for the NEAM Region from the TSUMAPS-NEAM project. https://doi.org/10.13127/tsunami/neamthm18.

Basili, R., Brizuela, B., Herrero, A., Iqbal, S., Lorito, S., Maesano, F.E., Murphy, S., Perfetti, P., Romano, F., Scala, A., Selva, J., Taroni, M., Tiberti, M.M., Thio, H.K., Tonini, R., Volpe, M., Glimsdal, S., Harbitz, C.B., Løvholt, F., Baptista, M.A., Carrilho, F., Matias, L.M., Omira, R., Babeyko, A., Hoechner, A., Gürbüz, M., Pekcan, O., Yalçıner, A., Canals, M., Lastras, G., Agalos, A., Papadopoulos, G., Triantafyllou, I., Benchekroun, S., Agrebi Jaouadi, H., Ben Abdallah, S., Bouallegue, A., Hamdi, H., Oueslati, F., Amato, A., Armigliato, A., Behrens, J., Davies, G., Di Bucci, D., Dolce, M., Geist, E., Gonzalez Vida, J.M., González, M., Macías Sánchez, J., Meletti, C., Ozer Sozdinler, C., Pagani, M., Parsons, T., Polet, J., Power, W., Sørensen, M., Zaytsev, A., 2021. The Making of the NEAM Tsunami Hazard Model 2018 (NEAMTHM18). Front. Earth Sci. 8, 616594. https://doi.org/10.3389/feart.2020.616594

Behrens, J., Dias, F., 2015. New computational methods in tsunami science. Philosophical Transactions of the Royal Society A: Mathematical, Physical and Engineering Sciences 373, 20140382. https://doi.org/10.1098/rsta.2014.0382

Benker, S.C., Langford, R.P., Pavlis, T.L., 2011. Positional accuracy of the Google Earth terrain model derived from stratigraphic unconformities in the Big Bend region, Texas, USA. Geocarto International 26, 291–303. https://doi.org/10.1080/10106049.2011.568125

Billi, A., Funiciello, R., Minelli, L., Faccenna, C., Neri, G., Orecchio, B., Presti, D., 2008. On the cause of the 1908 Messina tsunami, southern Italy. Geophys. Res. Lett. 35, L06301. https://doi.org/10.1029/2008GL033251

Boggs, P.T., Spiegelman, C.H., Donaldson, J.R., Schnabel, R.B., 1988. A computational examination of orthogonal distance regression. Journal of Econometrics 38, 169–201. https://doi.org/10.1016/0304-4076(88)90032-2

Boschetti, L., Ioualalen, M., 2021. Integrated tsunami intensity scale based on maxima of tsunami amplitude and induced current. Natural Hazards 105, 815–839. https://doi.org/10.1007/s11069-020-04338-5

Boschi, E., Gasperini, P., Smriglio, G., Valensise, G., 1995. The new "Catalogue of Strong Italian Earthquakes." Annals of Geophysics 38, 20. https://doi.org/10.4401/ag-4072

Carroll, R.J., Ruppert, D., 1996. The Use and Misuse of Orthogonal Regression in Linear Errors-in-Variables Models. The American Statistician 50, 1–6. https://doi.org/10.2307/2685035

Carveni, P., Benfatto, S., Maniscalco, R., Puntillo, M., Sturiale, G., 2006. La Salsa e la Gurna di Fondachello: evoluzione di un vulcano di fango e di uno stagno costiero all'estrema periferia nord-orientale dell'edificio vulcanico etneo (Sicilia). Il Quaternario 19, 67–76.

Castellaro, S., Bormann, P., 2007. Performance of Different Regression Procedures on the Magnitude Conversion Problem. Bulletin of the Seismological Society of America 97, 1167–1175. https://doi.org/10.1785/0120060102

Castellaro, S., Mulargia, F., Kagan, Y.Y., 2006. Regression problems for magnitudes. Geophysical Journal International 165, 913–930. https://doi.org/10.1111/j.1365-246X.2006.02955.x

Cataldi, L., Tiberi, L., Costa, G., 2021. Estimation of MCS intensity for Italy from high quality accelerometric data, using GMICEs and Gaussian Naïve Bayes Classifiers. Bull Earthquake Eng 19, 2325–2342. https://doi.org/10.1007/s10518-021-01064-6

Catalog of Tsunamis in Japan and Its Neighboring Countries -【津波ディジタルライブラリィ】[WWW Document], n.d. URL https://tsunami-dl.jp/document/111 (accessed 11.17.22).

CAT-INGV, n.d. Centro Allerta Tsunami - Istituto Nazionale di Geofisica e Vulcanologia (INGV) [WWW Document]. URL https://cat.ingv.it/it/

Chiocci, F.L., Romagnoli, C., Tommasi, P., Bosman, A., 2008. The Stromboli 2002 tsunamigenic submarine slide: Characteristics and possible failure mechanisms. J. Geophys. Res. 113, B10102. https://doi.org/10.1029/2007JB005172

Chock Gary Y. K., 2016. Design for Tsunami Loads and Effects in the ASCE 7-16 Standard. Journal of Structural Engineering 142, 04016093. https://doi.org/10.1061/(ASCE)ST.1943-541X.0001565

Chock, G.Y.K., 2016. Design for Tsunami Loads and Effects in the ASCE 7-16 Standard. Journal of Structural Engineering 142, 04016093. https://doi.org/10.1061/(ASCE)ST.1943-541X.0001565

Citrini, D., Noseda, G., 1987. Idraulica. Ambrosiana, Milano, Seconda ed.

Das, R., Wason, H.R., Sharma, M.L., 2013. General Orthogonal Regression Relations between Body-Wave and Moment Magnitudes. Seismological Research Letters 84, 219–224. https://doi.org/10.1785/0220120125

Dipartimento della Protezione Civile, n.d. Rischio maremoto. Le attività [WWW Document]. URL https://rischi.protezionecivile.gov.it/it/maremoto/attivita (accessed 9.22.22).

Dogan, G.G., Yalciner, A.C., Yuksel, Y., Ulutaş, E., Polat, O., Güler, I., Şahin, C., Tarih, A., Kânoğlu, U., 2021. The 30 October 2020 Aegean Sea Tsunami: Post-Event Field Survey Along Turkish Coast. Pure and Applied Geophysics 178, 785–812. https://doi.org/10.1007/s00024-021-02693-3

DPC, 2018. Indicazioni alle Componenti ed alle Strutture operative del Servizio nazionale di protezione civile per l'aggiornamento delle pianificazioni di protezione civile per il rischio maremoto [WWW Document]. URL https://www.protezionecivile.gov.it/it/normativa/indicazioni-alle-componenti-ed-alle-strutture-operative-del-servizio-nazionale-di-protezione-civile-per-l-aggiornamento-delle-pianificazioni-di-protez (accessed 11.23.22).

DPC, Regione Sicilia, 2015. Isola di Stromboli - Piano nazionale di emergenza a fronte di eventi vulcanici di rilevanza nazionale [WWW Document]. URL https://rischi.protezionecivile.gov.it/static/3b89029643532bdb10a49064c0504cc5/pianonazionalestromboli2015.pdf (accessed 11.24.22).

El-Ashmawy, K.L.A., 2016. Investigation of the Accuracy of Google Earth Elevation Data. Artificial Satellites 51, 89–97. https://doi.org/10.1515/arsa-2016-0008

Elbanna, A., Abdelmeguid, M., Ma, X., Amlani, F., Bhat, H.S., Synolakis, C., Rosakis, A.J., 2021. Anatomy of strike-slip fault tsunami genesis. Proceedings of the National Academy of Sciences 118, e2025632118. https://doi.org/10.1073/pnas.2025632118

Faccioli, E., Cauzzi, C., 2006. Macroseismic intensities for seismic scenarios estimated from instrumentally based correlations. https://doi.org/DOI: 10.13140/RG.2.1.3984.2641

Faenza, L., Michelini, A., 2010. Regression analysis of MCS intensity and ground motion parameters in Italy and its application in ShakeMap. Geophysical Journal International 180, 1138–1152. https://doi.org/10.1111/j.1365-246X.2009.04467.x

Favalli, M., Boschi, E., Mazzarini, F., Pareschi, M.T., 2009. Seismic and landslide source of the 1908 Straits of Messina tsunami (Sicily, Italy). Geophysical Research Letters 36. https://doi.org/10.1029/2009GL039135

Fuller, W.A., 1987. Measurement error models. John Wiley & Sons.

Gasperini, P., Bernardini, F., Valensise, G., Boschi, E., 1999. Defining seismogenic sources from historical earthquake felt reports. Bulletin of the Seismological Society of America 89, 94–110. https://doi.org/10.1785/BSSA0890010094

Gayer, G., Leschka, S., Nöhren, I., Larsen, O., Günther, H., 2010. Tsunami inundation modelling based on detailed roughness maps of densely populated areas. Nat. Hazards Earth Syst. Sci. 10, 1679–1687. https://doi.org/10.5194/nhess-10-1679-2010

Gibbons, S.J., Lorito, S., de la Asunción, M., Volpe, M., Selva, J., Macías, J., Sánchez-Linares, C., Brizuela, B., Vöge, M., Tonini, R., Lanucara, P., Glimsdal, S., Romano, F., Meyer, J.C., Løvholt, F., 2022. The Sensitivity of Tsunami Impact to Earthquake Source Parameters and Manning Friction in High-Resolution Inundation Simulations. Front. Earth Sci. 9, 757618. https://doi.org/10.3389/feart.2021.757618

Glimsdal, S., Løvholt, F., Harbitz, C.B., Romano, F., Lorito, S., Orefice, S., Brizuela, B., Selva, J., Hoechner, A., Volpe, M., Babeyko, A., Tonini, R., Wronna, M., Omira, R., 2019. A New Approximate Method for Quantifying Tsunami Maximum Inundation Height Probability. Pure and Applied Geophysics 176, 3227–3246. https://doi.org/10.1007/s00024-019-02091-w

GNS New Zealand Tsunami Database [WWW Document], n.d. URL https://tsunami.gns.cri.nz/#!/db?out=map&map=control&maprecords=1&mapsources=1&colorby=validity&plot=traveltime_firstarrival_lower&sourcecolorby=source_class&view=-40.0108|174.9902|5||768|594 (accessed 11.17.22).

Gomez-Capera, A.A., Albarello, D., Gasperini, P., 2007. Aggiornamento relazioni fra l'intensità macrosismica e PGA. Progetto INGV-DPC S1, Deliverable D11. (report).

Gomez-Capera, A.A., D'Amico, M., Lanzano, G., Locati, M., Santulin, M., 2020. Relationships between ground motion parameters and macroseismic intensity for Italy. Bulletin of Earthquake Engineering 18, 5143–5164. https://doi.org/10.1007/s10518-020-00905-0

Graziani, L., Maramai, A., Tinti, S., 2006. A revision of the 1783–1784 Calabrian (southern Italy) tsunamis. Nat. Hazards Earth Syst. Sci. 6, 1053–1060. https://doi.org/10.5194/nhess-6-1053-2006

Grezio, A., Babeyko, A., Baptista, M.A., Behrens, J., Costa, A., Davies, G., Geist, E.L., Glimsdal, S., González, F.I., Griffin, J., Harbitz, C.B., LeVeque, R.J., Lorito, S., Løvholt, F., Omira, R., Mueller, C., Paris, R., Parsons, T., Polet, J., Power, W., Selva, J., Sørensen, M.B., Thio, H.K., 2017. Probabilistic Tsunami Hazard Analysis: Multiple Sources and Global Applications. Reviews of Geophysics 55, 1158–1198. https://doi.org/10.1002/2017RG000579

Grünthal, G., 1998. European macroseismic scale 1998. European Seismological Commission (ESC).

Guidoboni, E., Ferrari, G., Mariotti, D., Comastri, A., Tarabusi, G., Sgattoni, G., Valensise, G., 2018. CFTI5Med, Catalogo dei Forti Terremoti in Italia (461 aC-1997) e nell'area Mediterranea (760 aC-1500). Istituto Nazionale di Geofisica e Vulcanologia (INGV). https://doi.org/10.6092/ingv.it-cfti5

Guidoboni, E., Ferrari, G., Tarabusi, G., Sgattoni, G., Comastri, A., Mariotti, D., Ciuccarelli, C., Bianchi, M.G., Valensise, G., 2019. CFTI5Med, the new release of the catalogue of strong earthquakes in Italy and in the Mediterranean area. Scientific Data 6, 80. https://doi.org/10.1038/s41597-019-0091-9

Guidoboni, E., Mariotti, D., 2008. Il terremoto e il maremoto del 1908: effetti e parametri sismici, in: Bertolaso, G., Boschi, E., Guidoboni, E., Valensise, G. (Eds.), Il Terremoto e Il Maremoto Del 28 Dicembre 1908 Analisi Sismologica, Impatto, Prospettive. INGV-DPC, pp. 17–136.

Guidoboni, E., Poirier, J.-P., n.d. Storia culturale del terremoto dal mondo antico a oggi.

Gusiakov, V.K., 2011. Relationship of Tsunami Intensity to Source Earthquake Magnitude as Retrieved from Historical Data. Pure and Applied Geophysics 168, 2033–2041. https://doi.org/10.1007/s00024-011-0286-2

Hall, J., 2022. Linear Deming Regression.

Henderson, F.M., 1966. Open channel flow. Macmillan Publishing Co., Inc., New York.

IOC-UNESCO, Intergovernmental Oceanographic Commission, 2019. Fourth Edition. Tsunami glossary. Paris, UNESCO. IOC Technical Series, 85.

Jensen, A.C., 2007. Deming regression, MethComp package.

Jin, D., Lin, J., 2011. Managing tsunamis through early warning systems: A multidisciplinary approach. Ocean & Coastal Management 54, 189–199. https://doi.org/10.1016/j.ocecoaman.2010.10.025

Kaiser, G., Scheele, L., Kortenhaus, A., Løvholt, F., Römer, H., Leschka, S., 2011. The influence of land cover roughness on the results of high resolution tsunami inundation modeling. Nat. Hazards Earth Syst. Sci. 11, 2521–2540. https://doi.org/10.5194/nhess-11-2521-2011

Kajiura, K., 1963. The leading wave of a tsunami. Bulletin Earthquake Research Institute 41, 535–571. https://doi.org/10.1016/0011-7471(65)90572-3

Kalligeris, N., Skanavis, V., Charalampakis, M., Melis, N.S., Voukouvalas, E., Annunziato, A., Synolakis, C.E., 2021. Field survey of the 30 October 2020 Samos (Aegean Sea) tsunami in the Greek islands. Bulletin of Earthquake Engineering. https://doi.org/10.1007/s10518-021-01250-6

Lay, T., Wallace, T.C., 1995. Modern global seismology. Elsevier.

Lekkas, E.L., Andreadakis, E., Kostaki, I., Kapourani, E., 2013. A Proposal for a New Integrated Tsunami Intensity Scale (ITIS-2012). Bulletin of the Seismological Society of America 103, 1493–1502. https://doi.org/10.1785/0120120099

Leng, L., Zhang, T., Kleinman, L., Zhu, W., 2007. Ordinary least square regression, orthogonal regression, geometric mean regression and their applications in aerosol science. J. Phys.: Conf. Ser. 78, 012084. https://doi.org/10.1088/1742-6596/78/1/012084

Leonard, G.S., Power, W.L., Lukovic, B., Smith, W.D., Johnston, D.M., Langridge, R., Downes, G., 2008. Interim tsunami evacuation planning zone boundary mapping for the Wellington and Horizons regions defined by a GIS-calculated attenuation rule. GNS Science report 30, 22.

Levin, B.W., Nosov, M., 2016. Physics of Tsunamis, 2nd ed. Springer Cham.

Lolli, B., Gasperini, P., 2012. A comparison among general orthogonal regression methods applied to earthquake magnitude conversions. Geophysical Journal International 190, 1135–1151. https://doi.org/10.1111/j.1365-246X.2012.05530.x

Lorito, S., Romano, F., Atzori, S., Tong, X., Avallone, A., McCloskey, J., Cocco, M., Boschi, E., Piatanesi, A., 2011. Limited overlap between the seismic gap and coseismic slip of the great 2010 Chile earthquake. Nature Geosci 4, 173–177. https://doi.org/10.1038/ngeo1073

Løvholt, F., Pedersen, G., Harbitz, C.B., Glimsdal, S., Kim, J., 2015. On the characteristics of landslide tsunamis. Philosophical Transactions of the Royal Society A: Mathematical, Physical and Engineering Sciences 373, 20140376. https://doi.org/10.1098/rsta.2014.0376

Lynett, P.J., Borrero, J., Son, S., Wilson, R., Miller, K., 2014. Assessment of the tsunami-induced current hazard. Geophysical Research Letters 41, 2048–2055. https://doi.org/10.1002/2013GL058680

Maramai, A., Brizuela, B., Graziani, L., 2014. The euro-mediterranean tsunami catalogue. Annals of Geophysics 57. https://doi.org/10.4401/ag-6437

Maramai, A., Graziani, L., Alessio, G., Burrato, P., Colini, L., Cucci, L., Nappi, R., Nardi, A., Vilardo, G., 2005. Near- and far-field survey report of the 30 December 2002 Stromboli (Southern Italy) tsunami. Marine Geology 215, 93–106. https://doi.org/10.1016/j.margeo.2004.11.009

Maramai, A., Graziani, L., Brizuela, B., 2021. Italian Tsunami Effects Database (ITED): The First Database of Tsunami Effects Observed Along the Italian Coasts. Frontiers in Earth Science 9.

Maramai, A., Graziani, L., Brizuela, B., 2019a. Euro-Mediterranean Tsunami Catalogue (EMTC), version 2.0. Istituto Nazionale di Geofisica e Vulcanologia (INGV). https://doi.org/10.13127/tsunami/emtc.2.0

Maramai, A., Graziani, L., Brizuela, B., 2019b. Italian Tsunami Effects Database (ITED). Istituto Nazionale di Geofisica e Vulcanologia (INGV). https://doi.org/10.13127/tsunami/ited.1.0

Mariotti, D., 2015. I terremoti del '900: La "catastrofe sismica" del 28 dicembre 1908 – INGVterremoti [WWW Document]. URL https://ingvterremoti.com/2015/12/28/i-terremoti-del-900-la-catastrofe-sismica-del-28-dicembre-1908/ (accessed 11.9.22).

MathWorks, 2022. Correlation coefficients - MATLAB corrcoef - MathWorks Italia [WWW Document]. URL https://it.mathworks.com/help/matlab/ref/corrcoef.html (accessed 11.24.22).

MATLAB, Version R2022a, 2022.

Meletti, C., Marzocchi, W., D'Amico, V., Lanzano, G., Luzi, L., Martinelli, F., Pace, B., Rovida, A., Taroni, M., Visini, F., Group, M.W., 2021. The new Italian seismic hazard model (MPS19). Annals of Geophysics 64, 6. https://doi.org/10.4401/ag-8579

Mercalli, G., 1909. Contributo allo studio del terremoto calabro-messinese del 28 dicembre 1908. Atti del Reale Istituto d'Incoraggiamento di Napoli 7, 249–292.

Michetti, A., Esposito, E., Guerrieri, L., Porfido, S., Serva, L., Tatevossian, R., Vittori, E., Audemard, F., Azuma, T., Clague, J., Comerci, V., Gürpinar, A., McCalpin, J.,

Mohammadioun, B., Mörner, N.-A., Ota, Y., Roghozin, E., 2007. Environmental Seismic Intensity Scale - ESI 2007-. memorie descrittive della carta geologica d'ITALIA.

Murty, T.S., Loomis, H.G., 1980. A new objective tsunami magnitude scale. Marine Geodesy 4, 267–282. https://doi.org/10.1080/15210608009379388

National Geophysical Data Center, n.d. Global Historical Tsunami Database. https://doi.org/10.7289/V5PN93H7

NCEI/WDS National Geophysical Data Center / World Data Service: NCEI/WDS, 2022. Global Historical Tsunami Database.

NEAMTIC, North-Eastern Atlantic, Mediterranean and connected seas Tsunami Information Center [WWW Document], n.d. URL http://neamtic.ioc-unesco.org/ (accessed 11.9.22).

Omira, R., Ramalho, R.S., Kim, J., González, P.J., Kadri, U., Miranda, J.M., Carrilho, F., Baptista, M.A., 2022. Global Tonga tsunami explained by a fast-moving atmospheric source. Nature 609, 734–740. https://doi.org/10.1038/s41586-022-04926-4

Omori, F., 1909. Preliminary Report on the Messina-Reggio Earthquake of Dec. 28, 1908. Bulletin of the Imperial Earthquake Investigation Committee 3, 37–45.

Pallavi, Joshi, S., Singh, D., Kaur, M., Lee, H.-N., 2022. Comprehensive Review of Orthogonal Regression and its Applications in Different Domains. Archives of Computational Methods in Engineering. https://doi.org/10.1007/s11831-021-09696-2

Papadopoulos, G., 2003. Quantification of Tsunamis: A Review. pp. 285–291. https://doi.org/10.1007/978-94-010-0205-9_30

Papadopoulos, G., Imamura, F., 2001. Proposal for a new tsunami intensity scale. ITS 2001 Proceedings 5, 5–1.

Papadopoulos, G., Imamura, F., Nosov, M., Charalampakis, M., 2020b-07-27. Geological Records of Tsunamis and Other Extreme Waves CHAPTER 3: TSUNAMI MAGNITUDE SCALES.

Papadopoulos, G.A., Daskalaki, E., Fokaefs, A., Giraleas, N., 2007. Tsunami hazards in the Eastern Mediterranean: strong earthquakes and tsunamis in the East Hellenic Arc and Trench system. Nat. Hazards Earth Syst. Sci. 7, 57–64. https://doi.org/10.5194/nhess-7-57-2007

Papadopoulos, G.A., Gràcia, E., Urgeles, R., Sallares, V., De Martini, P.M., Pantosti, D., González, M., Yalciner, A.C., Mascle, J., Sakellariou, D., Salamon, A., Tinti, S., Karastathis, V., Fokaefs, A., Camerlenghi, A., Novikova, T., Papageorgiou, A., 2014. Historical and pre-historical tsunamis in the Mediterranean and its connected seas: Geological signatures, generation mechanisms and coastal impacts. Marine Geology 354, 81–109. https://doi.org/10.1016/j.margeo.2014.04.014

Papadopoulos, G.A., Imamura, F., Nosov, M., Charalampakis, M., 2020a-01-01. Chapter 3 - Tsunami magnitude scales, in: Engel, M., Pilarczyk, J., May, S.M., Brill, D., Garrett, E. (Eds.), Geological Records of Tsunamis and Other Extreme Waves. Elsevier, pp. 33–46. https://doi.org/10.1016/B978-0-12-815686-5.00003-1

Paris, R., 2015. Source mechanisms of volcanic tsunamis. Philosophical Transactions of the Royal Society A: Mathematical, Physical and Engineering Sciences 373. https://doi.org/10.1098/rsta.2014.0380

Pezzella, F., 2021. I terremoti del passato nei cataloghi storici e nelle banche dati, preziose fonti di informazioni [WWW Document]. Istituto Nazionale di Geofisica e Vulcanologia. URL https://www.ingv.it/it/newsletter-ingv-n-8-ottobre-2021-anno-xv/i-terremoti-del-passato-nei-cataloghi-storici-e-nelle-banche-dati-preziose-fonti-di-informazioni (accessed 11.24.22).

Piatanesi, A., Lorito, S., Romano, F., Bertolaso, G., Boschi, E., Guidoboni, E., Valensise, G., 2008. Il grande maremoto del 1908: Analisi e modellazione. Il Terremoto e il Maremoto del 28 Dicembre 1908 183–196.

Piatanesi, A., Tinti, S., Bortolucci, E., 1999. Finite-element simulations of the 28 december 1908 Messina Straits (Southern Italy) tsunami. Physics and Chemistry of the Earth, Part A: Solid Earth and Geodesy 24, 145–150. https://doi.org/10.1016/S1464-1895(99)00010-1

Platania, G., 1909. I fenomeni marittimi che accompagnarono il terremoto di Messina del 28 dicembre 1908. Riv. Geogr. Ital 16, 154–161.

Platania, Giovanni, 1909. Il maremoto dello stretto di Messina del 28 dicembre 1908. Bollettino della Società Sismologica Italiana.

Rovida, A., Locati, M., Antonucci, A., Camassi, R., 2017. Archivio Storico Macrosismico Italiano (ASMI) 6000 earthquakes, 670 data sources, 30000 macroseismic intensity data points. https://doi.org/10.13127/ASMI

Rovida, A., Locati, M., Camassi, R., Lolli, B., Gasperini, P., Antonucci, A., 2022. Catalogo Parametrico dei Terremoti Italiani (CPTI15), versione 4.0. https://doi.org/10.13127/CPTI/CPTI15.4

Saito, T., 2019. Tsunami Generation, in: Saito, T. (Ed.), Tsunami Generation and Propagation. Springer Japan, Tokyo, pp. 149–203. https://doi.org/10.1007/978-4-431-56850-6_5

Scala, A., Lorito, S., Romano, F., Murphy, S., Selva, J., Basili, R., Babeyko, A., Herrero, A., Hoechner, A., Løvholt, F., Maesano, F.E., Perfetti, P., Tiberti, M.M., Tonini, R., Volpe, M., Davies, G., Festa, G., Power, W., Piatanesi, A., Cirella, A., 2020. Effect of Shallow Slip Amplification Uncertainty on Probabilistic Tsunami Hazard Analysis in Subduction Zones: Use of Long-Term Balanced Stochastic Slip Models. Pure Appl. Geophys. 177, 1497–1520. https://doi.org/10.1007/s00024-019-02260-x

Schambach, L., Grilli, S.T., Tappin, D.R., Gangemi, M.D., Barbaro, G., 2020. New simulations and understanding of the 1908 Messina tsunami for a dual seismic and deep submarine mass failure source. Marine Geology 421, 106093. https://doi.org/10.1016/j.margeo.2019.106093

Selva, J., Amato, A., Armigliato, A., Basili, R., Bernardi, F., Brizuela, B., Cerminara, M., de' Micheli Vitturi, M., Di Bucci, D., Di Manna, P., Esposti Ongaro, T., Lacanna, G., Lorito, S., Løvholt, F., Mangione, D., Panunzi, E., Piatanesi, A., Ricciardi, A., Ripepe, M., Romano, F., Santini, M., Scalzo, A., Tonini, R., Volpe, M., Zaniboni, F., 2021. Tsunami risk management for crustal earthquakes and non-seismic sources in Italy. La Rivista del Nuovo Cimento 44, 69–144. https://doi.org/10.1007/s40766-021-00016-9

Shuto, N., 1993. Tsunami Intensity and Disasters, in: Tinti, S. (Ed.), Tsunamis in the World: Fifteenth International Tsunami Symposium, 1991. Springer Netherlands, Dordrecht, pp. 197–216. https://doi.org/10.1007/978-94-017-3620-6_15

Sieberg, A.H., 1927. Geologische, physikalische und angewandte Erdbebenkunde. G. Fischer.

Smart, G., Crowley, K., Lane, E., 2016. Estimating tsunami run-up. Natural Hazards 80. https://doi.org/10.1007/s11069-015-2052-8

Soloviev, S.L., Go, C.N., 1974. Catalog of tsunamis in western coast of the Pacific Ocean. Nauka Publishing House, Moscow. Canadian Translation of Fisheries and Aquatic Sciences, 5077, 1984.

Soloviev, S.L., Solovieva, O.N., Go, C.N., Kim, K.S., Shchetnikov, N.A., 2000. Tsunamis in the Mediterranean Sea 2000 B.C.–2000 A.D., Advances in Natural and Technological Hazards Research. Springer Netherlands, Dordrecht. https://doi.org/10.1007/978-94-015-9510-0

Tanioka, Y., Satake, K., 1996. Tsunami generation by horizontal displacement of ocean bottom. Geophysical Research Letters 23, 861–864. https://doi.org/10.1029/96GL00736

Tarabusi, G., Ferrari, G., Ciuccarelli, C., Bianchi, M.G., Sgattoni, G., Comastri, A., Mariotti, D., Valensise, G., Guidoboni, E., 2020. CFTILab - Laboratorio Avanzato di Sismologia Storica. Istituto Nazionale di Geofisica e Vulcanologia (INGV). https://doi.org/10.13127/CFTI/CFTILAB

Tinti, S., Armigliato, A., 2003. The use of scenarios to evaluate the tsunami impact in southern Italy. Marine Geology 199, 221–243. https://doi.org/10.1016/S0025-3227(03)00192-0

Tinti, S., Maramai, A., Armigliato, A., Graziani, L., Manucci, A., Pagnoni, G., Zaniboni, F., 2006. Observations of physical effects from tsunamis of December 30, 2002 at Stromboli volcano, southern Italy. Bull Volcanol 68, 450–461. https://doi.org/10.1007/s00445-005-0021-x

Tinti, S., Maramai, A., Graziani, L., 2004. The New Catalogue of Italian Tsunamis. Natural Hazards 33, 439–465. https://doi.org/10.1023/B:NHAZ.0000048469.51059.65

Tinti, S., Maramai, A., Graziani, L., 2001. A new version of the European tsunami catalogue: updating and revision. Nat. Hazards Earth Syst. Sci. 1, 255–262. https://doi.org/10.5194/nhess-1-255-2001

Tonini, R., Di Manna, P., Lorito, S., Selva, J., Volpe, M., Romano, F., Basili, R., Brizuela, B., Castro, M.J., de la Asunción, M., Di Bucci, D., Dolce, M., Garcia, A., Gibbons, S.J., Glimsdal, S., González-Vida, J.M., Løvholt, F., Macías, J., Piatanesi, A., Pizzimenti, L., Sánchez-Linares, C., Vittori, E., 2021. Testing Tsunami Inundation Maps for Evacuation Planning in Italy. Front. Earth Sci. 9, 628061. https://doi.org/10.3389/feart.2021.628061

Triantafyllou, I., Gogou, M., Mavroulis, S., Lekkas, E., Papadopoulos, G.A., Thravalos, M., 2021. The Tsunami Caused by the 30 October 2020 Samos (Aegean Sea) Mw7.0 Earthquake: Hydrodynamic Features, Source Properties and Impact Assessment from Post-Event Field Survey and Video Records. Journal of Marine Science and Engineering 9. https://doi.org/10.3390/jmse9010068

TSUMAPS-NEAM, Dipartimento della Protezione Civile, Ispra - Istituto Superiore per la protezione e la ricerca ambientale, n.d. Allegato 1 alle Indicazioni operative - Metodologia utilizzata per la definizione delle zone di allertamento [WWW Document]. URL https://rischi.protezionecivile.gov.it/static/ad979b18c9e104b6d3aea330a6cf1b4f/allegato-1-alle-indicazioni-operative.pdf (accessed 9.22.22).

Visini, F., Pace, B., Meletti, C., Marzocchi, W., Akinci, A., Azzaro, R., Barani, S., Barberi, G., Barreca, G., Basili, R., Bird, P., Bonini, M., Burrato, P., Busetti, M., Carafa, M., Cocina, O., Console, R., Corti, G., D'Agostino, N., D'Amico, S., D'Amico, V., Dal Cin, M., Falcone, G., Fracassi, U., Gee, R., Kastelic, V., Lai, C., Langer, H., Maesano, F., Marchesini, A., Martelli, L., Monaco, C., Murru, M., Peruzza, L., Poli, M., Pondrelli, S., Rebez, A., Rotondi, R., Rovida, A., Sani, F., Santulin, M., Scafidi, D., Selva, J., Slejko, D., Spallarossa, D., Tamaro, A., Tarabusi, G., Taroni, M., Tiberti, M., Tusa, G., Tuvè, T., Valensise, G., Vannoli, P., Varini, E., Zanferrari, A., Zuccolo, E., 2021. Earthquake Rupture Forecasts for the MPS19 Seismic Hazard Model of Italy. Annals of Geophysics 64, 3. https://doi.org/10.4401/ag-8608

Wang, Yinsong, Zou, Y., Henrickson, K., Wang, Yinhai, Tang, J., Park, B.-J., 2017. Google Earth elevation data extraction and accuracy assessment for transportation applications. PLOS ONE 12, e0175756. https://doi.org/10.1371/journal.pone.0175756

Appendix A

The following table provides descriptive notes for many OPs and their transects drawn on Google Earth, where difficulties were encountered in an initial approach. The table includes all OPs where it was necessary to supplement the information provided by the summary catalogue ITED. In some cases it was simply sufficient to separate the data provided by the catalogue, other times it was not possible to find a good estimate of the location but an attempt was made. These transects have been marked as Flags. 1st column after the notes. (Flagged in light red).

Points were excluded from the study (Excluded in light purple) if no information was provided for the precise location of the site, or if Google Earth did not provide a good match between satellite images and the elevation terrain model. 2nd column after the notes.

When it was possible to locate the observation points accurately and when an adequate profile could be found to describe the data provided, the transects were included successfully in the analysis (Included in light green). 3rd and last column.

Observation Point	Notes about the OP	F	E	I
ACI TREZZA Casa Monteleone	No evidence for localisation		x	
ACI TREZZA Casa Sorrentino	No evidence for localisation		x	
ACI TREZZA Stabilimento Amenta	No evidence can be found of the cited 'F.lli Amenta' factory.		x	

BRIGA MARINA	Consideration of run-up and ingression on different transects because the run-up reference is to 'casa Pannarello' (Baratta, 1910). The ingression was considered along the Briga stream, immediately next to the San Paolo district.			x
BRUCOLI – CANALE	Data refer to the docking of a military station of the Guardia di Finanza, which does not exist today. This small harbour is inside a fjord-like channel and the measurement of the slope is inaccurate	x		
CATANIA	The port was totally changed during the 20th century, especially in the extension of the quays. An attempt was made to calculate the slope by setting the value at 0 m where the water was still present in 1908, but the measurement is not reliable. (Figura A.1)	x		
CIRO' MARINA	Totally disproportionate run-up data. Great distance from origin (it is in northern Calabria, almost in the Gulf of Taranto). Possibly erroneous data measured in Roccella Ionica and Cirò Marina (Guidoboni & Mariotti, 2008).	x		
COZZO SPADARO - CAPO PASSERO - PORTOPALO DI CAPO PASSERO	ITED datum refers to the Cozzo Spadaro lighthouse, which is at least 500 metres away from the coast. Description by Baratta (1910) without precise indication of the location.		xx	

FORNACE	The ingression value only refers to heavy boulders carried by water, so it is unrelated to the run-up. Furthermore, coastal erosion is probable, as in the testimony of nearby Lazzaro.	x		
GALLICO	Division of transect data by run-up (Silipi) and by ingression (Gallico_Marina) as ingression is indicated as far as a church, while the greatest damage was in the Silipi district with a run-up of 5.4 m (Platania, 1909b, Baratta, 1910).			xx
PALMARA DI GALLICO	No evidence for localisation		x	
GIAMPILIERI MARINA	Run-up measured at Casa Palazzolo 7.20 m (Baratta, 1910; from Platania, 1909a)			x
LA GURNA	La Gurna mud volcano and coastal pond, wetland (Carveni et al., 2006)			x
LAZZARO	Widespread coastal erosion removed a large portion of beach and part of a road (ITED, Maramai et al. 2019b). Many casualties especially along the provincial road in the lower part of the municipality (Baratta 1910).			x

MARZAMENI	Run-up not specified in any location, very variable slope as the old town is located on a rocky promontory, to the north there is a sandy beach and to the south a small harbour.		x	
MESSINA	The Portalegni stream was diverted (it used to flow into the harbour, now to the south). The English Cemetery was completely destroyed because before 1942 it was located in the Zona Falcata, along Via San Ranieri. In 1942 it was moved to the Monumental Cemetery complex. On ITED there are two run-up data in the INFO but only one as numerical data of the OP: (3 m and 6 m) assigned therefore to two different groups of transects, for two of the districts mentioned in the literature (San Ranieri and Torrente Zaera). Messina station was destroyed by the earthquake and is halfway between the port and the SE coast (where the wave came from). So probable influence on city centre data.		x	xx
PACE	The first two of the five transects (Pace_01 and Pace_02) were made in an uninhabited part with a fairly long plain, immediately after the coastline, at a height of 5-6m. Baratta (1910) reports the written witness of Platania (1909b), that the run-up was taken on the house of the municipal delegate	x		x

PELLARO	It is necessary to differentiate the data because a maximum ingression of 350 m is described at Pellaro, which is comparable with the maximum recorded run-up of the entire 1908 tsunami event (13 m). However, the ingression value given by ITED (Maramai et al. 2019b) refers to Punta di Pellaro (500 m), where the transects actually provide a much smaller slope.			xx
REGGIO CALABRIA	Many indications, often difficult to locate due to the changes undergone by the city. Two transects are considered, also thanks to the tables provided by Baratta (1910). Marina di Reggio (Reggio_Lido) and ingression up to via Plutino (Plutino_RC).			x
RIPOSTO	The course of the Jungo torrent in the port of Riposto has been altered by maintenance work and partial canalisation. Run-up measurements in the lighthouse keeper's house and references to the lighthouse (Baratta, 1910), but no information can be found on the 'LANTERNA' present in 1908. The 'Old Lighthouse' (current name) was erected in 1911. Probably in the same place.			x

ROCCALUMERA	Ingression datum of 200 metres, which is very high due to the morphology of the area, even streams and torrents have a slope of ≥ 5%. Coastal erosion? Land subsidence? Google Maps error? (200 m of ingression, with the current morphology, corresponds to about 12 m of run-up that was not observed). Differentiation of this FLAG. From ITED: double run-up data 8 m (north, via Farina), 7 m (Saracen tower).	x		x
ROCCELLA IONICA	Single eye witness, not measurement (Baratta, 1910). Possibly erroneous data measured in Roccella Ionica and Cirò Marina (Guidoboni & Mariotti, 2008).	x		
SALINE MELITO	Salt evaporation pond beyond the railway embankment (H = 6 m). Ingression data (30 m) which does not coincide with the textual description of 'flooding' of the salt evaporation pond, given the essentially zero slope and friction.	x		

SAN GREGORIO - SANT'AGATA STREAM	The fiumara Sant'Agata is north of the Reggio Calabria airport built in 1939 (about 3 km away from the centre of San Gregorio). Descriptive indication of the stretch: many trees uprooted along the shore between Reggio and San Gregorio. The transect was drawn along the fiumara Sant'Agata and the CHARACTERISTIC SLOPE was calculated without considering the height value (8m) relative to the tracks above the bridge included in the DTM. The railway bridge (5.8 m above sea level, probably the bottom) on the S. Agata stream was damaged (Platania, 1909b; from ITED: Maramai et al. 2019b).			x
SANTA TECLA	First two transects taken too far north, on the cliff protecting the village. A closer reading resulted in the two transects to the south, in fact the catalogues state: 'southern beach' (Baratta, 1910) and 'the sea waves came from ESE and caused damage, particularly in the southern part of the village' (Platania, 1909b; from ITED, Maramai et al., 2019b).	x		x
SCALETTA ZANCLEA	Inaccurate ingression data: '200 m and in some places even 300 m' (Baratta 1910). Division of the data because the slope was too steep even on torrents to justify 300 m of ingression. Probable inaccuracy of Google Earth. Used the figure of 8 m run-up on Casa Crimi (Platania 1909a), today Vico Crimi.	x		x

SCILLA	From ITED: double data, one referring to the built-up area to the east of the peninsula (steep); the inlet referring to Marina Grande to the west of the peninsula (shallow beach).			x
VILLA SAN GIOVANNI	Maximum ingression data along Via Garibaldi. Planimetry drawn by Baratta (1910) and reference to the spinning mills as the maximum point of wave extension.			x

Figure A.1 - On the left, from Google Earth, a view of the current port of Catania. On the right, an old 1919 map of the T.C.I. showing the changes made to the port a few years earlier, dividing it into Porto Vecchio and Porto Nuovo. From some photographs of that period, it can be seen that boats were moored under the railway bridge that was elevated in the old part of the harbour.

Appendix B

Graphical and numerical results are provided for the analysis performed considering the intensities of POs on the Sieberg-Ambraseys scale. It can be seen that since the scale has only 6 grades, the points are distributed over the majority of them (for the total dataset from grade 2 to grade 6 in Figures B.4 and Figure B.5). The results are consistent with the ones presented in Chapter 4 for the Papadopoulos-Imamura scale. The only exception is for the 2002 Stromboli event, where the results are distorted by the fact that all intensities except one correspond to grade 5. This leads to a bad constrain of the regression parameters, leading to the impossibility to define the error associated with the parameters.

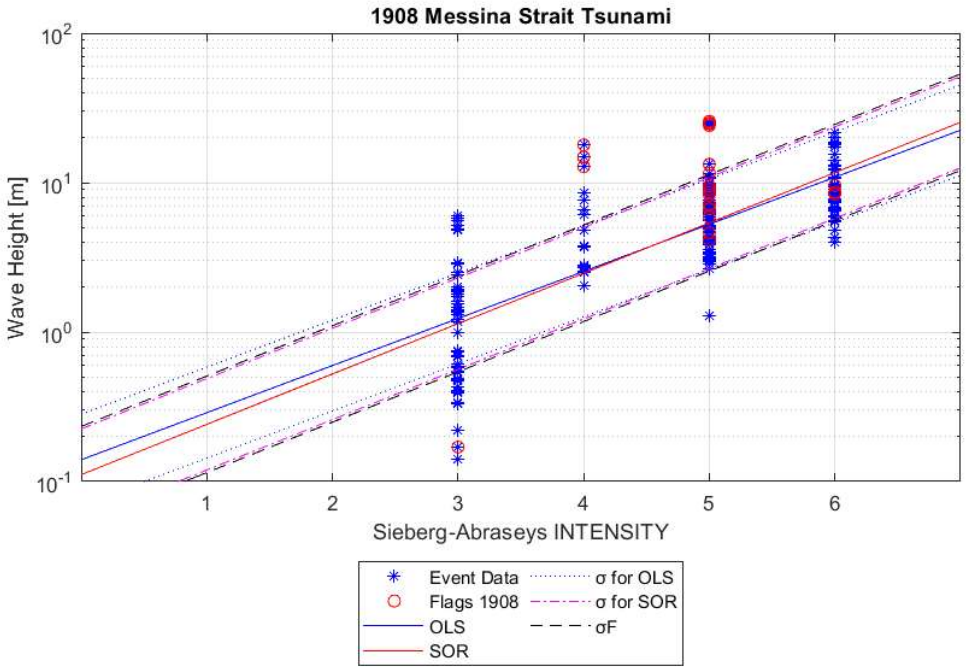

Figure B.1 -

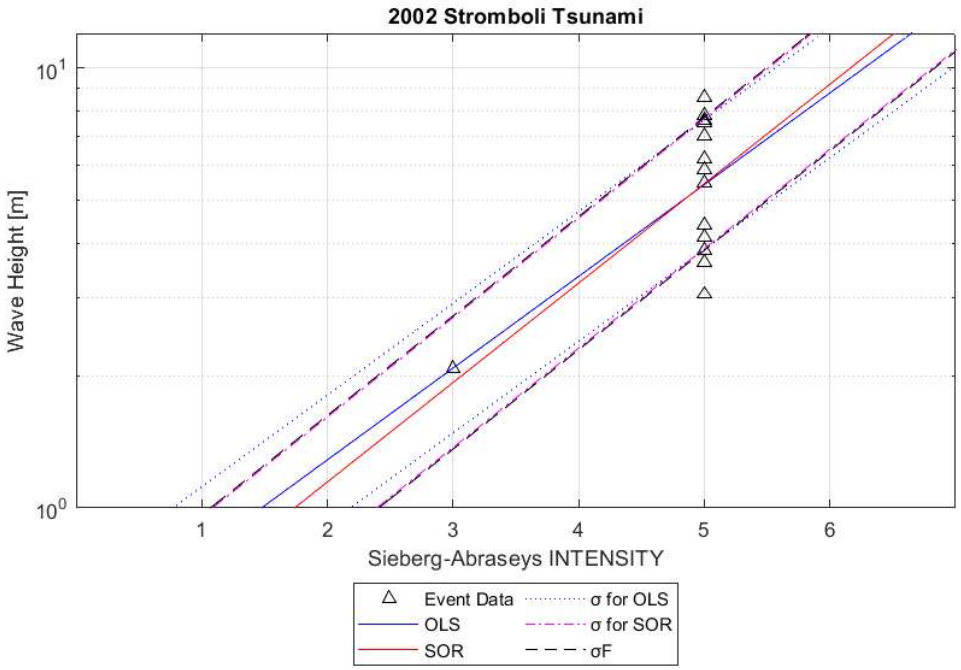

Figure B.2 -

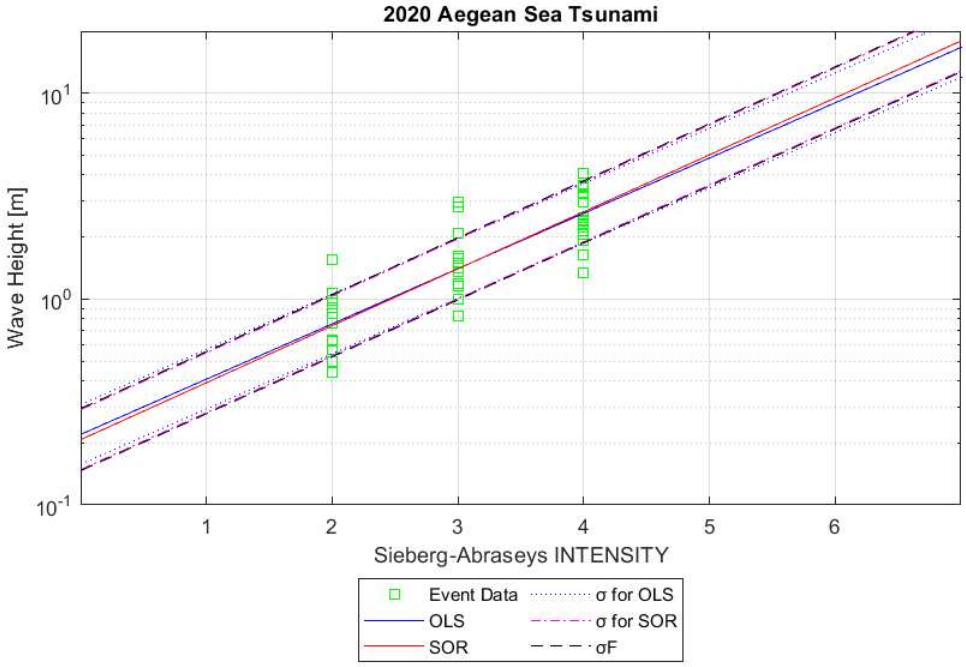

Figure B.3 -

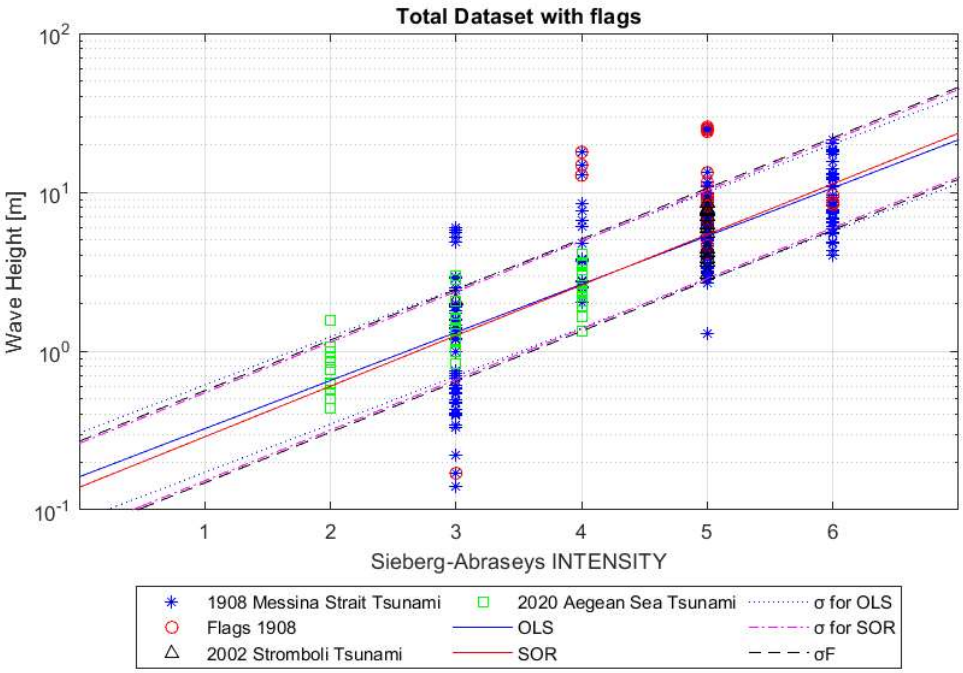

Figure B.4 -

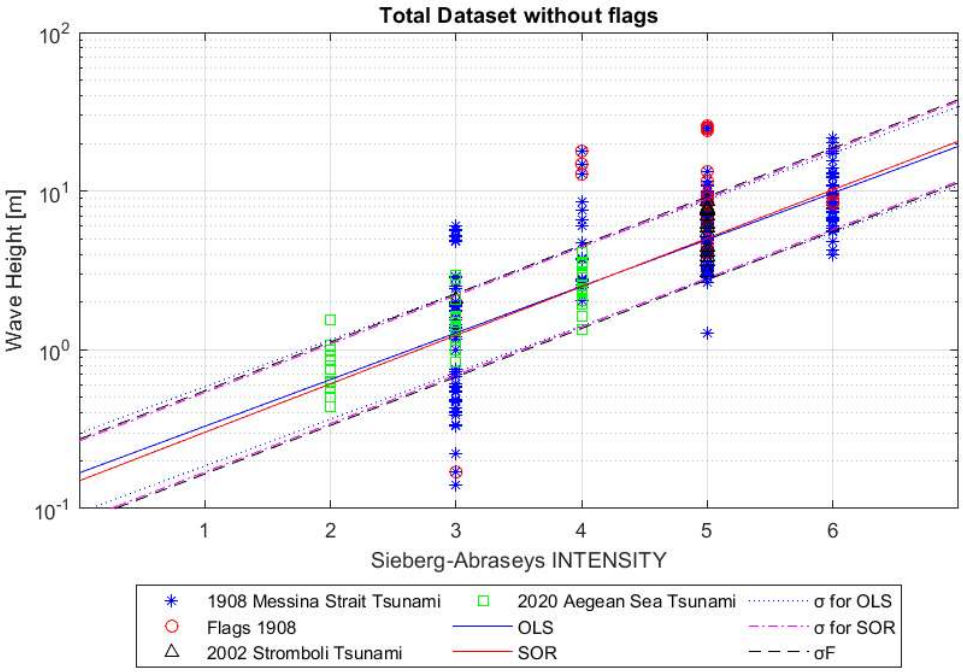

Figure B.5 -

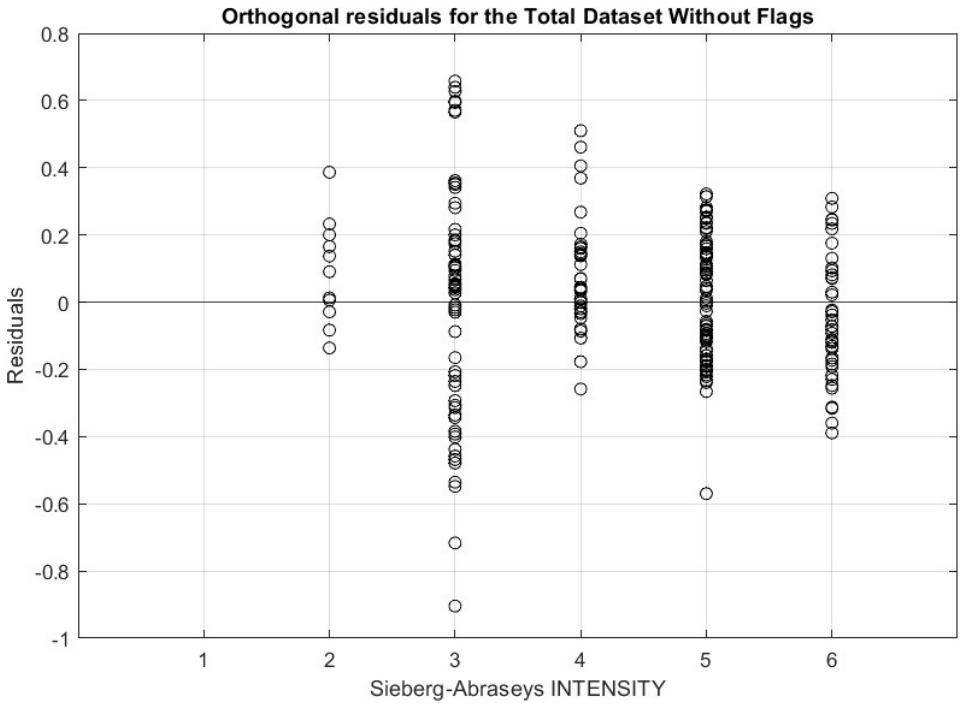

Figure B.6 -

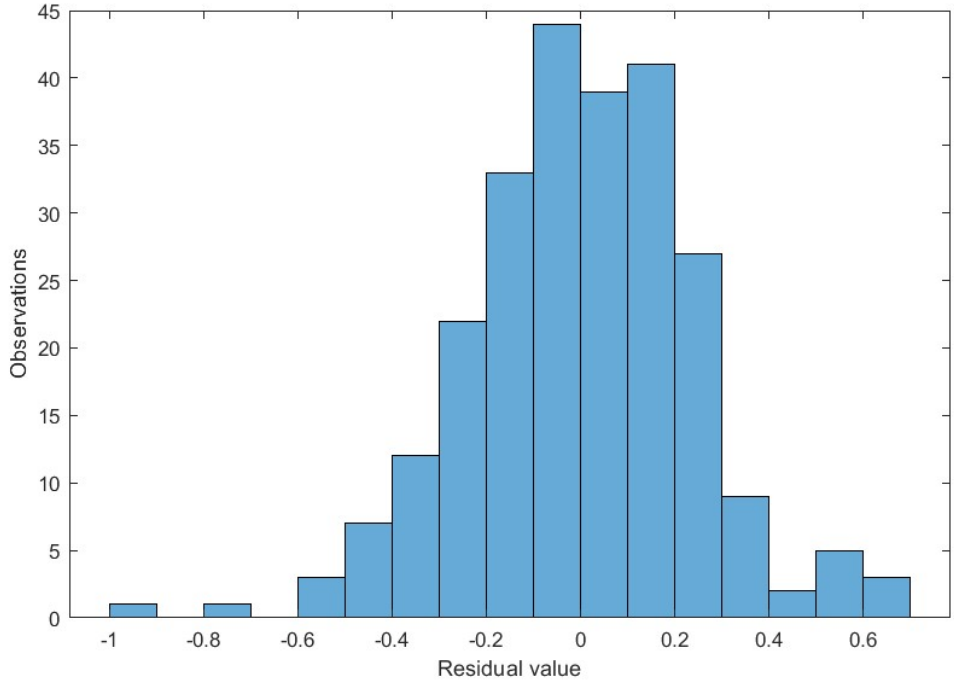

Figure B.7 -

Database	Type of regression	α			β			σ	σF
1908 Messina Strait Tsunami	OLS	-0.85	±	0.09	0.32	±	0.02	0.30	
	SOR	-0.95	±	0.11	0.34	±	0.02	0.29	0.30
2002 Stromboli Tsunami	OLS	-0.31	±	0.37	0.21	±	0.08	0.15	
	SOR	-0.39	±	NaN	0.23	±	Nan	0.14	0.15
2020 Aegean Sea Tsunami	OLS	-0.66	±	0.08	0.27	±	0.03	0.14	
	SOR	-0.68	±	0.09	0.28	±	0.03	0.14	0.15
Total Dataset With Flags	OLS	-0.79	±	0.06	0.30	±	0.01	0.27	
	SOR	-0.86	±	0.07	0.32	±	0.01	0.26	0.28
Total Dataset Without Flags	OLS	-0.78	±	0.06	0.29	±	0.01	0.25	
	SOR	-0.83	±	0.07	0.31	±	0.01	0.24	0.25